MAGNETISM IN AN AMORPHOUS Fe-Pd-P ALLOY SYSTEM

Thesis by

Thomas E. Sharon

In Partial Fulfillment of the Requirements

for the Degree of

Doctor of Philosophy

California Institute of Technology

Pasadena, California

1971

(Submitted May 10, 1971)

To Jerri, Tommy, and Michael

ACKNOWLEDGEMENT

For continuing support and advice throughout the course of this work, the author wishes to convey his deepest appreciation to Professor Pol Duwez and Dr. C. C. Tsuei. The technical assistance of C. Geremia, S. Kotake, and J. A. Wysocki is also gratefully acknowledged.

The author also wishes to thank the National Aeronautics and Space Administration, the International Business Machines Corporation, and the Atomic Energy Commission for financial assistance which made this work possible.

ABSTRACT

Amorphous alloys of composition $Fe_xPd_{80-x}P_{20}$ $(13 \leq x \leq 44)$ have been prepared by rapid quenching from the liquid state. The Mössbauer effect in Fe^{57} has been used to study the magnetic properties of these materials. The hyperfine field distributions have been determined from these experiments, as a function of composition and temperature. The results indicate that the electronic state of Fe in these alloys remains essentially constant throughout the composition range, and that the Pd d band is filled by electron transfer from phosphorus.

The variation of the magnetic transition temperature with composition has been determined by combining the Mössbauer effect results with complementary magnetic measurements. There is a sharp change in slope in this curve at $x \simeq 26$. Below this concentration, the long range magnetic order which prevails in the higher Fe concentration alloys has broken down, giving rise to a more local ordering.

The Mössbauer effect results confirm the existence of weakly coupled Fe atoms in all the amorphous Fe-Pd-P alloys. These atoms reside in low effective fields, and can participate in the spin-flip scattering process which produces a Kondo effect (resistivity

minimum). The large critical concentration observed is also an indication that the spin correlations are greatly reduced in these amorphous alloys.

TABLE OF CONTENTS

INTRODUCTION

One topic of current interest in the field of magnetism is the problem of the magnetization of an amorphous material. Although the concept of an amorphous ferromagnet was introduced by Gubanov[1] over a decade ago, only in the last few years has the subject become an area of active experimental research. The existence of amorphous ferromagnets has been confirmed by conventional magnetic measurements [2-5] and supporting Mössbauer effect data[6]. Thus far the problem of magnetism in an amorphous alloy system (one in which the concentration of the magnetic element can be varied) has received less attention[7, 8]. This is partly due to the fact that success in obtaining an amorphous structure has usually been limited to a rather narrow composition range.

In order to make a meaningful study of the composition dependence of the magnetic properties of an amorphous alloy system, it is essential that a continuity of structure extends throughout the composition range. Although an amorphous material has no long range order (translational symmetry), it does possess definite structural properties based on its short range order. These are reflected in the radial distribution function (RDF) which is obtained from x-ray diffraction analysis, and form the basis for any discussion of the properties of an amorphous alloy. This requirement of

structure continuity parallels that in a crystalline alloy system, where one demands that all the alloys are the same phase.

The structure of an amorphous Fe-Pd-P alloy system has recently been studied by Maitrepierre[9, 10]. It was shown that alloys of composition $Fe_xPd_{80-x}P_{20}$, where $13 \lesssim x \lesssim 44$, can be quenched from the liquid state into an amorphous state using the "piston and anvil" technique[11]. It was found from the radial distribution function data that the short range order in these alloys is continuous with respect to variation in the iron concentration, and that iron and palladium appear to substitute freely in this structure. Maitrepierre has suggested that the short range order in these alloys is based on the kind of structural units found in the metal rich transition metal phosphides (Pd_3P or Fe_3P)[12]. In preliminary magnetization measurements, the saturation moment in a field of 8.4 kOe and at 4.2°K decreased in roughly a linear fashion from $2.1\,\mu_B(Fe_{44}Pd_{36}P_{20})$ to $0.6\,\mu_B(Fe_{13}Pd_{67}P_{20})$. The higher iron concentration alloys were judged to be ferromagnetic by conventional criteria, but the low iron concentration alloys ($x \lesssim 25$) showed a more complex behavior. No Curie point could be defined from the magnetization data, and the effective moment in the paramagnetic region was quite large ($\mu_{eff} \sim 6\,\mu_B$). These observations led Maitrepierre to suggest the existence of "superparamagnetism" in these alloys.

Another somewhat puzzling effect observed in the electrical properties of the amorphous Fe-Pd-P alloys is the existence of a Kondo-type resistivity minimum in even the most iron rich compositions. This is surprising because normally, in a crystalline system, only a few atomic percent of the magnetic impurity causes correlations between the spins which suppress the spin-flip scattering responsible for the Kondo effect. If the phenomenom of the resistivity minimum is really due to this process, this suggests that the correlations between neighboring spins in an amorphous material are significantly reduced compared to the crystalline state.

In the present work, a more detailed study of the magnetism in this amorphous alloy system has been carried out, utilizing the Mössbauer effect and other magnetic measurements. There are several reasons for applying Mössbauer spectroscopy to the study of the magnetic properties of these amorphous alloys. This method permits one to examine the properties of single atoms, rather than complicated assemblages of atoms as in magnetization measurements. The latter results are difficult to interpret if a complicated and perhaps unknown spin arrangement exists. Bulk magnetic measurements also cannot answer the question of whether all the moments are aligned to the same extent, or whether there is a continuous

distribution in the degree of alignment. The Mössbauer effect has proven to be a unique tool for the measurement of such magnetic field distributions[13]. In amorphous alloys this asset should be quite valuable.

A second important reason for applying the Mössbauer technique is that no external field need be applied to the sample. The bulk magnetic properties of a material are greatly influenced by such factors as domain structure, grain size, heat treatment, and many other such effects. At present these factors are poorly understood for amorphous materials. In the Fe-Pd-P alloys, for example, even in the highest field (8.4 kOe) and lowest temperatures (4.2°K) used, the alloys appeared magnetically unsaturated[9]. This means that the conventional techniques[14] used to find the zero field magnetization, which is the quantity of real interest, are either inapplicable or of questionable accuracy. Furthermore, the application of large external fields is undesirable because the microscopic spin ordering may change in response to this perturbing influence.

In the following, it will be shown how a Mössbauer effect study, combined with complementary data from other magnetic measurements, can greatly clarify the nature of the magnetism in this amorphous alloy system.

II. EXPERIMENTAL PROCEDURES

A. Preparation of Alloys

The amorphous Fe-Pd-P alloys were obtained by rapid quenching from the liquid state using the "piston and anvil" technique[11]. Initially, appropriate quantities of iron (99.9% purity), palladium (99.99% purity), and reagent grade red amorphous phosphorus powder were combined into briquets by a sintering process. These were then induction melted in an argon atmosphere and drawn into 2mm rods. The rods were then broken into pieces of appropriate size for use in the quenching process. Full details of the alloy preparation may be found elsewhere[9, 10].

Because actual cooling rates may vary from sample to sample, each sample was carefully checked by a step-scanning diffractometer to ensure that only the broad bands indicative of an amorphous structure were present. If a sample showed any weak Bragg reflections superimposed on this background, it contained some crystalline phase and was rejected for use in further experimental work.

The resulting quenched samples are foils approximately 2 cm in diameter and 40-50μ thick. For use as Mössbauer absorbers, the foils are somewhat thick. This results in high absorption and a relatively small resonant effect. It was thought unwise to thin the foils by mechanical or chemical treatment, however, because of the

unknown effect on their properties. In several cases the brittleness of the foils made such a procedure unfeasible anyway.

Two Fe-Pd-P alloys used by Maitrepierre were subjected to a chemical analysis after sintering[9]. It was found that the actual compositions of all three elements were within 0.5 at.% of the nominal ones. The small weight loss after melting (< .2%) also indicates that it is reasonably accurate to designate the samples by their nominal compositions, hence we do so in any further discussion.

B. Mossbauer Effect Apparatus

The γ-ray resonance absorption spectra were collected using the system illustrated schematically in Fig. 1. Gamma rays are emitted from a radioactive isotope (called the source), which in the present case is 10 mCi of Co^{57} embedded in a Cu matrix. These photons are partially absorbed by any Fe^{57} isotope within the sample (the absorber), and those which pass through are collimated and then detected with a gas filled proportional counter.

A current pulse proportional to the energy of the γ-ray is produced whenever a photon is detected. This pulse is amplified and then analyzed for energy by a single channel analyzer (SCA). Only those photons whose energy corresponds to the 14.4 keV recoil-less transition are of interest for the resonance absorption spectrum.

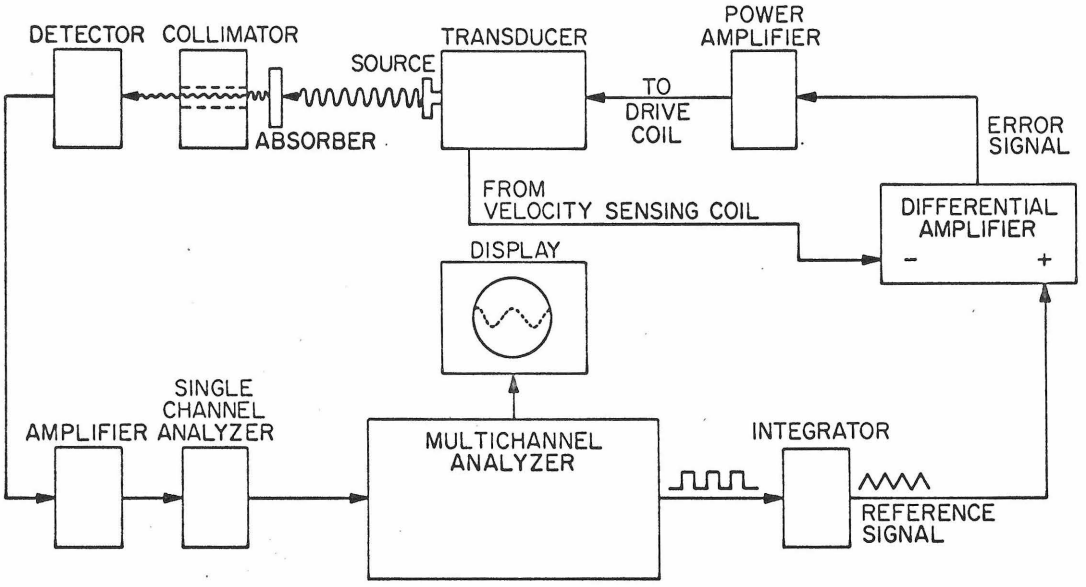

Fig. 1. Schematic diagram of Mössbauer effect apparatus.

A Nuclear Data 512 channel multichannel analyzer is used to collect the counts. A square wave is produced internally by the analyzer with a period of 512 x 100 μ sec. This square wave is integrated by an operational amplifier, and then used as the reference signal to drive the velocity transducer which produces the Doppler shift of the γ-ray. This transducer is of the type described by Kankeleit[15]. While the velocity transducer is producing a parabolic motion of the source (corresponding to a triangular velocity wave), a clock inside the multichannel analyzer opens one channel after the other for 100 μ sec intervals. At the end of 512 x 100 μ sec, the process repeats itself. The actual motion of the source is sensed by a pickup coil which relays the information to a differential amplifier. The reference signal is compared with the actual velocity signal, and an error signal is produced which forces the transducer to accurately follow the triangular velocity wave. The only significant deviation occurs at the turning points of the motion, where the relative error is about 1%.

For use as absorbers in the Mössbauer experiments, the foils were cut into circular discs approximately $\frac{1}{2}$" in diameter. Experiments at room temperature, where a simple two peak spectrum is observed for all but one of the compositions, required data collection

for about 8 hours. In the low temperature apparatus, both source and absorber are cooled. In this case, the increased source to detector distance and absorption from coolants and dewar windows required that data be collected for a longer period. Hence for all but the liquid He experiments data were collected for several days. The statistics for the liquid He experiments are noticeably poorer due to the reduced data collection time.

In order to study the samples at several different temperatures, liquid helium and nitrogen, as well as dry ice-acetone slushes and ice - water solutions, were used. These coolants provided temperatures of 4.2°K, 77°K, 194°K, and 273°K respectively. Room temperature experiments correspond to 295°K. Hence a wide range of temperatures is available to study the effects of temperature on the Mössbauer spectrum. Above room temperature a specially designed oven was used to provide continuous temperature control with a stability of about $\pm$ 0.5°K.

After each set of experiments an Fe foil was used to provide the velocity calibration (Fig. 2). The data wereleast squares fitted to a six peak spectrum and the line splittings of Preston et al[16] were used to calculate the full scale velocity. According to their measurements, the separation of the outer peaks corresponds to 10.657 mm/sec.

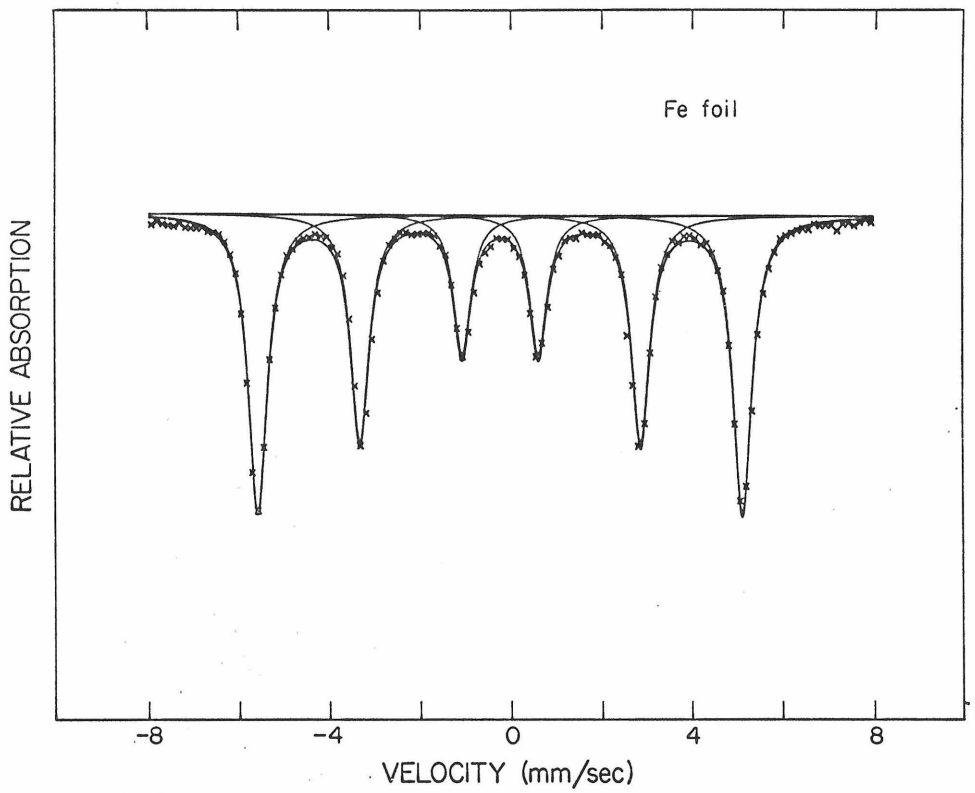

Fig. 2. Example of velocity calibration spectrum taken with a .001" Fe foil.

C. Magnetic Transition Temperature Determination

The present low temperature Mössbauer effect apparatus allows only a series of discrete temperatures to be maintained. Since it is desirable to be able to locate the transition temperatures of samples which may fall in the intermediate temperature ranges, complementary methods were used to detect magnetic transitions.

The two techniques used rely on the drastic change in the bulk magnetic properties of a sample as it undergoes a magnetic ordering. In one method the sample was cut into the shape of a donut and many turns of fine wire wrapped around it to increase its inductance. This toroid was then used as an inductor in an LC oscillator. If the frequency of oscillation is measured as a function of temperature, the magnetic transition can be easily recorded by taking readings from a frequency meter. Only the toroid is in the low temperature dewar, so that the change in frequency reflects only the change in its inductance. In the second method use was made of a very sensitive bridge designed for detecting superconducting transition temperatures[17]. This system is capable of detecting transitions in only a few milligrams of superconducting material. Because the coils in the bridge circuit are balanced at low temperatures, its upward temperature range extends only to about 30°K.

III. STUDY OF MAGNETIC PROPERTIES USING THE MÖSSBAUER EFFECT IN Fe^{57}

A. Hyperfine Interactions

1. General Discussion

The great value of the Mössbauer effect in solid state physics arises from the ability to resolve the very small ($\sim 10^{-8}$ eV) energy differences of nuclear energy levels. These perturbations, known as hyperfine (hf) splittings, are caused by the interaction of the nuclear magnetic and quadrupole moments with the surrounding electronic charge and spin distributions. They are observable only if the linewidth of the recoilless gamma ray is small compared to these characteristic energies.

In Fe^{57}, for example, the decay scheme of the parent isotope Co^{57} is shown in Fig. 3[18]. The isotope Co^{57} has a half life of 270 days, which makes it a very convenient source. It decays through electron capture to one of the higher excited states of Fe^{57}. The Mössbauer transition involves an excited state of spin 3/2 (negative parity) and a ground state of spin 1/2 (also negative parity). The transition is almost completely magnetic dipole in character. Since the excited state has a lifetime of approximately 10^{-7} sec, the linewidth of the emitted gamma is

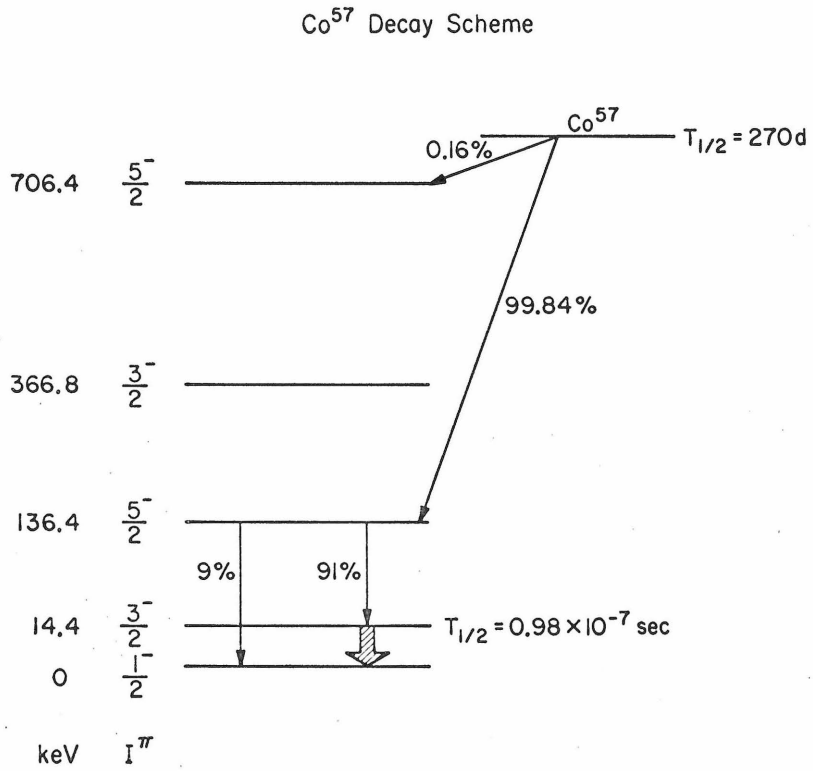

Fig. 3. Decay scheme of Co^{57}. The Mössbauer transition is indicated by the dashed arrow.

$$\Gamma \simeq \frac{\hbar}{\tau} = 4.6 \times 10^{-9}\ \text{eV}$$

This is sufficiently small that the nuclear hyperfine interactions are easily resolved.

In Mössbauer effect studies the energy of emitted photon from the source is Doppler shifted an amount $\frac{v}{c} E_o (E_o = 14.4\ \text{keV})$. To obtain shifts in the range of the hf interactions, velocities in the range 1-10 mm/sec are usually involved. It is customary to express all energies in terms of the velocity required to produce the corresponding Doppler shift. For example, the linewidth of the emitted gamma ray is 0.095 mm/sec in these units. If another Fe^{57} nucleus absorbs this photon, the resulting linewidth when plotted versus velocity will have a theoretical value of $2\Gamma = 0.19$ mm/sec. In practice the observed linewidth is always significantly greater than this due to several broadening mechanisms.

2. Electrostatic Hyperfine Interactions

It is well known that the nucleus is not a point charge but has a finite radius of the order of 10^{-13} cm. If we consider the energy of this nuclear charge distribution $\rho(\bar{x})$ in the electrostatic potential $V(\bar{x})$ produced by the surrounding charges, the expression for its energy is[19]

$$E_{el} = \int \rho(\bar{x})\, V(\bar{x})\, d^3x \qquad (1)$$

The integral extends over the nuclear charge distribution, whose radius is very small compared to any electronic distance of interest. The potential $V(\bar{x})$ includes contributions from the electrons of the parent atom, as well as any surrounding charges external to the atom. Since this energy is expected to be small compared to the nuclear transition energy, we may expand $V(\bar{x})$ in a power series about $\bar{x} = 0$ and insert into Eq. (1)

$$E_{el} = \int \rho(\bar{x}) \left[V(0) + \sum_{i=1}^{3} V_i x_i + \tfrac{1}{2} \sum_{i=1}^{3} \sum_{j=1}^{3} V_{ij} x_i x_j + \ldots \right] d^3x \quad (2)$$

where

$$V_i = \left(\frac{\partial V}{\partial x_i} \right)_{\bar{x}=0}$$

$$V_{ij} = \left(\frac{\partial^2 V}{\partial x_i \partial x_j} \right)_{\bar{x}=0}$$

V_{ij} is known as the electric field gradient (efg). To simplify this expression note that $\int \rho(\bar{x})\, d^3x = Ze$ and that V_{ij} is a symmetric matrix. Hence principal axes for the last term may be chosen such that

$$E_{el} = Z\, eV(0) + \sum_{i=1}^{3} V_i \int \rho(\bar{x})\, x_i\, d^3x + \tfrac{1}{2} \sum_{i=1}^{3} V_{ii} \int \rho(\bar{x}) x_i^2\, d^3x + \ldots \quad (3)$$

In discussing Mössbauer transitions, we are interested only in effects which lead to a net displacement of the transition energy. Hence, the first term is of no consequence. Also, the second term may be neglected because the electric dipole moment of the nucleus is zero (parity is a good quantum number). It can be shown that all terms above the third are also zero[20]. This leaves only

$$E_{el} = \tfrac{1}{2} \sum_{i=1}^{3} V_{ii} \int \rho(\bar{x})\, x_i^2\, d^3x \qquad (4)$$

Rearranging slightly we get

$$E_{el} = \frac{1}{6} \sum_{i=1}^{3} V_{ii} \int \rho(\bar{x})\, r^2 d^3x + \tfrac{1}{2} \sum_{i=1}^{3} V_{ii} \int \rho(\bar{x})\, (x_i^2 - \frac{1}{3} r^2) d^3x \qquad (5)$$

These terms are of great importance to what follows, and lead to the effects known in Mössbauer spectroscopy as the isomer shift and quadrupole splitting, respectively.

a. Isomer shift

The first term of Eq. (5) can be put in a more useful form by applying Laplace's equation,

$$\sum_{i=1}^{3} V_{ii} = -4\pi\rho_{el}(0) = +4\pi e \left|\Psi(0)\right|^2 \qquad (6)$$

$\left|\Psi(0)\right|^2$ is the total electronic density at the nucleus. Thus we have,

$$E_{IS} = \frac{2\pi e}{3} \left|\Psi(0)\right|^2 \int \rho(\bar{x})\, r^2 d^3x \qquad (7)$$

Since $\int \rho(\bar{x}) r^2 d^3x = Ze \langle r^2 \rangle$ we get

$$E_{IS} = \frac{2\pi Ze^2}{3} |\Psi(0)|^2 \langle r^2 \rangle \qquad (8)$$

The net displacement ϵ of the energy levels is therefore

$$\epsilon = \frac{2\pi Ze^2}{3} |\Psi(0)|^2 \left[\langle r^2 \rangle_e - \langle r^2 \rangle_g \right] \qquad (9)$$

where the subscripts e, g refer to the excited and ground states. In Mössbauer experiments we observe the net shift of the absorption line between absorber and source, which is the isomer shift δ :

$$\delta = \frac{2\pi Ze^2}{3} \left[|\Psi_{abs}(0)|^2 - |\Psi_s(0)|^2 \right] \left[\langle r^2 \rangle_e - \langle r^2 \rangle_g \right] \qquad (10)$$

To put Eq. (10) in conventional form we assume a constant nuclear charge density out to the nuclear radius R. Then $\langle r^2 \rangle = \frac{3}{5} R^2$ so that

$$\delta = \frac{2\pi Ze^2}{5} \left[|\Psi_{abs}(0)|^2 - |\Psi_s(0)|^2 \right] \left[R_e^2 - R_g^2 \right] \qquad (11)$$

For Fe^{57}, R_e and R_g are very nearly equal, and $R_e < R_g$. Thus it is customary to write

$$R_e^2 - R_g^2 = \Delta(R^2) \Big|_{R_g}^{R_e} = 2R^2 \left(\frac{\Delta R}{R} \right)$$

Thus the final expression from isomer shift is,

$$\delta = \frac{4\pi Ze^2}{5} R^2 \left(\frac{\Delta R}{R}\right) \left[\left|\Psi_{abs}(0)\right|^2 - \left|\Psi_s(0)\right|^2 \right] \qquad (12)$$

If we keep the source fixed and run a series of absorbers, an increase in the charge density at the nucleus in the absorber will result in a decrease in the isomer shift, since $\Delta R/R$ is negative. The isomer shift is sensitive to the electronic state of the Fe atom. Although $|\Psi(0)|^2$ is due to only s electrons which have nonzero wave function at the nucleus, a change in the number of 3d electrons will also have a large effect on the isomer shift, since the screening of the outer s electrons is affected by this change. Thus the isomer shift is a valuable indication of the chemical or valence state of the Fe atom.

b. Quadrupole splitting

A similar procedure for the second term of Eq. (5) can be carried out. Starting from

$$E_Q = \tfrac{1}{2} \sum_{i=1}^{3} V_{ii} \int \rho(\bar{x}) \left(x_i^2 - \tfrac{1}{3} r^2\right) d^3x \qquad (13)$$

we note that only s electrons have finite densities at the nucleus (in the nonrelativistic limit), and these produce a spherically symmetric potential. Therefore $V_{xx} = V_{yy} = V_{zz}$ for these charges and

$$(E_Q)_{s\ \text{electrons}} = \tfrac{1}{2} V_{zz} \int \rho(\bar{x}) \left[\sum_{i=1}^{3} x_i^2 - r^2 \right] d^3x = 0 \qquad (14)$$

The s electrons therefore make no contribution to the quadrupole interaction. Since $|\Psi(0)|^2 = 0$ for the electrons which do contribute to the electric field gradient causing the quadrupole interaction,

$$V_{xx} + V_{yy} + V_{zz} = 0 \qquad (15)$$

For cubic symmetry, we have the immediate result that there is no quadrupole splitting, since $V_{xx} = V_{yy} = V_{zz} = 0$ from Eq. (15).

For the case of axial symmetry ($V_{xx} = V_{yy}$), Eq. (13) reduces to

$$E_Q = \frac{1}{4} V_{zz} \int \rho(\bar{x}) (3z^2 - r^2) d^3x \qquad (16)$$

The quantum mechanical expression for Eq. (16) follows from the fact that [20]

$$\int \rho(\bar{x}) (3z^2 - r^2) d^3x = eQ \frac{3m^2 - I(I+1)}{3I^2 - I(I+1)} \qquad (17)$$

where $Q = \frac{1}{e} \int \Psi_{II}^* \left[\sum_{i=1}^{A} r_i^2 (3 \cos^2 \theta_i - 1) \right] \Psi_{II}\, d\bar{r}_1\, d\bar{r}_2 \ldots d\bar{r}_A$

is the expression for the quadrupole moment of the nucleus of A nucleons and spin I, and m is the quantum number for I_z. Ψ_{II} is the wave function corresponding to the maximum projection

of spin I on the z axis. Thus the final expression for the quadrupole splitting in an axially symmetric efg is

$$E_Q(m) = \frac{1}{4} e^2 q Q \frac{3m^2 - I(I+1)}{3I^2 - I(I+1)} \qquad (18)$$

where $eq = V_{zz}$ is the conventional definition for the electric field gradient.

For the case of Fe^{57} where $I_e = 3/2$, Eq. (18) gives two energy levels

$$E_Q(\pm 3/2) = +\frac{1}{4} e^2 q Q$$

$$E_Q(\pm 1/2) = -\frac{1}{4} e^2 q Q$$

Fig. 4a illustrates this case for $q > 0$. The resulting Mössbauer spectrum consists of two peaks (of equal intensity for a powdered absorber) with separation $\left|\frac{1}{2} e^2 q Q\right|$.

For the general case of nonaxial symmetry, the quadrupole Hamiltonian becomes

$$\hat{H}_Q = \frac{e^2 q Q}{4I(2I-1)} \left[3I_z^2 - I(I+1) + \frac{\eta}{2} (I_+^2 + I_-^2)\right] \qquad (19)$$

where $$\eta = \frac{V_{xx} - V_{yy}}{V_{zz}}$$

$$I_\pm = I_x \pm i I_y$$

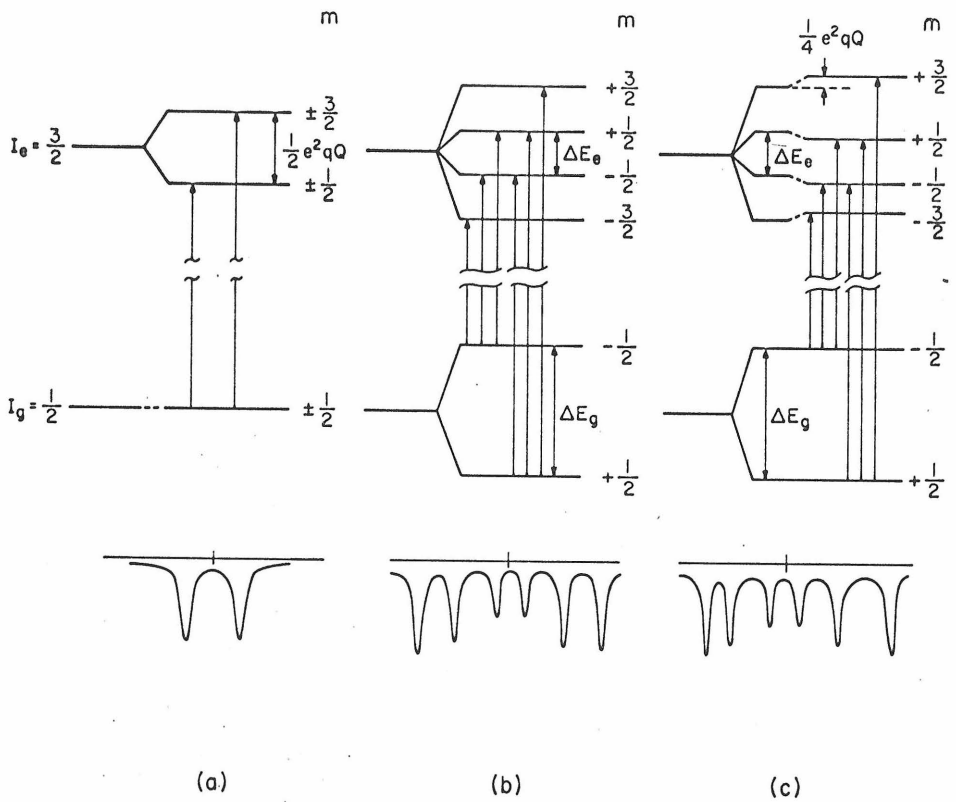

Fig. 4. Nuclear energy levels of Fe^{57} and resulting Mössbauer spectra: (a) Electric quadrupole interaction. (b) Magnetic hyperfine interaction. (c) Combined magnetic and electric quadrupole interactions with efg principal axis parallel to H.

and axes are chosen such that $|V_{zz}| > |V_{xx}|, |V_{yy}|$. For $I_e = 3/2$ (as in Fe^{57}) diagonalizing the Hamiltonian still produces only two sublevels, just as in the axially symmetric case. Now, however, the splitting is $\left|\frac{1}{2}e^2qQ\right|[1 + \eta^2/3]^{\frac{1}{2}}$ and the eigenstates of $\hat{H}_Q$ are no longer eigenstates of I_z[21]. The intensity of the two lines remains equal for a powdered sample, however, so the appearance of the Mössbauer spectrum is just as in Fig. 4a.

A measurement of the quadrupole splitting provides information about the electronic state of the Fe atom, as well as the effects of the local environment. Since there are two major sources of the electric field gradient - the charges on neighboring ions and the electrons in incompletely filled shells (3d for Fe), the two contributions must somehow be separated if a useful interpretation is to be made. This is sometimes possible by studying the temperature dependence of the quadrupole splitting. If the efg arises mainly from internal electrons in unfilled shells, the temperature dependence is often quite pronounced because of the change in population of the crystal field states. In a metal, however, the quadrupole splitting is usually insensitive to temperature and arises mainly from the deviation of the local environment from cubic symmetry[22].

3. Magnetic Hyperfine Interactions

a. Pure magnetic coupling

If there exists a magnetic field $\bar{H}$ at the nucleus whose magnetic moment is nonzero, then there is an additional term in the Hamiltonian representing this interaction

$$\hat{H}_M = -\bar{\mu} \cdot \bar{H} \tag{20}$$

Since $\bar{\mu} = g\mu_N \bar{I}$ (μ_N is nuclear magneton)

$$\hat{H}_M = -g\mu_N \bar{I} \cdot \bar{H} \tag{21}$$

This simple Hamiltonian has the eigenvalues

$$E_M(m) = -g\mu_N H m \tag{22}$$

where m is the quantum number corresponding to I_z. A good example of pure magnetic coupling is the spectrum of an ordinary Fe foil. Because of the cubic symmetry, the quadrupole interaction is zero and the energy levels are given by Eq. (22). Since $g_g/g_e = -1.715$ for Fe^{57}, the six line spectrum illustrated in Fig. 4b results. (See also Fig. 2).

b. Combined electric and magnetic coupling

In noncubic magnetic materials there exist in general both electric quadrupole and magnetic interactions. The resulting

Hamiltonian is a sum of the two Hamiltonians discussed earlier. They have the special forms shown in Eqs. (19) and (21) only if the principle axis of the efg and the magnetic field are collinear, however. In the most general case it is best to express each in terms of its own favored axes, and then by using appropriate rotation operators to express both in a common set of axes. This greatly complicates the analysis, since the eigenvalues and eigenvectors are no longer expressible in closed form. Only for special cases are closed form solutions available. One such case, which will be of great importance to follow, is the problem of the axially symmetric efg with principal axis at an angle θ with respect to the magnetic field direction[23]. Then

$$E(m) = - g\mu_N Hm + (-1)^{|m|+\frac{1}{2}} \frac{e^2qQ}{4}\left[\frac{3\cos^2\theta - 1}{2}\right] \qquad (23)$$

provided $\mu H \gg \left|\frac{e^2qQ}{4}\right|$.

For $\theta = 0$, Eq. (23) reduces to the simple expression for collinear axes of the magnetic field and axially symmetric efg. In this case all four sublevels of the excited state are shifted by a magnitude $\left|\frac{e^2qQ}{4}\right|$ with the resulting spectrum illustrated in Fig. 4c. The more general case described by Eq. (23) has exactly the same appearance, provided the replacement of q by $q' = q\left(\frac{3\cos^2\theta - 1}{2}\right)$ is

made.

B. Interpretation of Effective Magnetic Field at the Nucleus

1. Contributions to the Hyperfine Field

The magnetic field at the nucleus is due to several factors. According to Marshall[24], it can be expressed as

$$H = H_{int} + H_{dipolar} + H_{orbital} + H_c \qquad (24)$$

where

$$H_{int} = H_{applied} - DM_s + \frac{4\pi}{3} M_s + H'$$

DM_s is the demagnetizing field, and H' is the correction term to the Lorentz field $\frac{4\pi}{3} M_s$ for non-cubic symmetry. When the external field is zero, the contributions from H_{int} are usually small and can generally be neglected.

The second term in Eq. (24) arises from the dipole interaction between the electronic and nuclear spins and is usually of the order of 1-10 kOe.[23]

The orbital term arises from the circulating current due to a nonzero angular momentum. If the angular momentum is quenched ($\vec{L} = 0$), this term is zero. In metallic iron, however, this term has been estimated to be +70 kOe[25].

The last term in Eq. (24), known as the Fermi contact term, has been shown to be the main contribution to the magnetic field at the Fe nucleus. This field results from the polarization of the core s electrons and 4s conduction electrons by the 3d magnetic electrons. The contribution from the core electrons is directed in the opposite direction to the magnetic moment of the atom, while the contribution of the 4s conduction electron polarization at the nucleus and the orbital contributions are positive. For metallic Fe the polarization of the core electrons is estimated to give a contribution of -(400-500)kOe. The expression for H_c is[26]

$$H_c = - \frac{8\pi \mu_B}{3} \sum_s \left\{ \left| \Psi_{s\uparrow}(0) \right|^2 - \left| \Psi_{s\downarrow}(0) \right|^2 \right\} \qquad (25)$$

Marshall[27] and others have shown that all the factors contributing to the magnetic field at the nucleus should be proportional to the magnetic moment of the parent atom. Hence a plot of the hyperfine field and magnetization should have identical variation in temperature. Experimentally it has been shown that for pure Fe[28] and for Fe Pd[29] alloys this is true to an excellent approximation. When the reduced hf field deviates considerably from the reduced magnetization, it usually occurs when Fe is being used as a magnetic probe in a different magnetic host, for example Ni. Then the variations in exchange interaction between host-host pairs

and host-probe pairs may cause the difference[25].

2. Relaxation Effects

At the Fe nucleus in a solid, the effective magnetic field may be considered to be parallel (or antiparallel) to the moment of the atom. This moment is not a static quantity, however, because of various relaxation processes (mainly spin-lattice and spin-spin) the electronic moment is in a constant "flipping" process as it changes its state. If the frequency of flipping is much larger than the Larmor frequency of the nuclear spin in its internal field, the nucleus will see only the average of this hyperfine field. For paramagnetic materials, this should be zero. If on the other hand, the spin flip frequency is comparable to or smaller than the nuclear Larmor frequency, a hyperfine field may be observed even in a material with no magnetic order. For this to be possible in practice requires very dilute magnetic impurities to minimize spin-spin interaction.

To minimize spin lattice relaxation, the ion should be in a S state to eliminate any coupling to the lattice through the spin-orbit interaction. Also the material should be non-metallic, to eliminate relaxation processes involving conduction electrons. These conditions are met in very dilute Fe: Al_2O_3, where a hyperfine splitting is observed at low temperatures in the paramagnetic state[30]. In a metallic non-dilute magnetic host, however, relaxation

times are so short it is quite safe to assume that $\tau_{relax} \ll \tau_{Larmor}$ Hence

$$H \propto \langle S_z \rangle$$

Another slightly different relaxation effect occurs in "superparamagnetic" materials. These are substances in which there exist small clusters of magnetically coupled atoms. This could refer to a very fine Fe or Fe_2O_3 powder (~ 100 Å diameter particles), or perhaps to a magnetic phase precipitated out of a nonmagnetic matrix. In any case one requirement for "superparamagnetism" is that the particles are small enough to ensure that each is a single domain. In these materials the magnetization vector in each particle undergoes a kind of Brownian motion due to thermal energy in which it is continuously changing its direction among the various possible easy directions of magnetization. This ensures that no hysteresis effects such as remanence or coercive force exist in superparamagnetic materials[31].

It can be shown that the frequency corresponding to this process can be described by a relaxation time

$$\tau = \tau_0 \exp \frac{KV}{kT} \qquad (26)$$

where $\tau_0 \cong 10^{-9}$ sec, K is the anisotropy energy per unit volume,

and V is the volume of the particle[32]. If τ becomes comparable to or less than the nuclear Larmor period ($\sim 10^{-7}$ sec for Fe), then the hyperfine field will disappear even though the single domain particles maintain their magnetic alignment internally. These effects have been observed in many superparamagnetic systems[33-36].

IV. EXPERIMENTAL RESULTS AND DATA ANALYSIS

A. Mössbauer Effect

1. Room Temperature Results

Typical Mössbauer spectra for the amorphous Fe-Pd-P alloys at room temperature (295°K) are shown in Fig. 5. As explained in Section III, a sufficient condition for the absence of quadrupole splitting is cubic symmetry at each Fe site. Since the amorphous alloys obviously do not satisfy this criterion, the two peak spectrum is expected. At this temperature only the highest Fe concentration alloy ($Fe_{44}Pd_{36}P_{20}$) shows evidence of magnetic splitting. The experimental data were fitted to two Lorentzian peaks of equal areas. The widths were allowed to vary to allow for some correlation between isomer shift and quadrupole splitting, which would produce an asymmetrical spectrum. The width difference for almost all the samples was found to be quite small (< .01 mm/sec), thus the spectra are nearly symmetric.

Figures 6-8 show the parameters obtained by a least squares fitting using this approach. The large broadening observed (a line-width of 0.28mm/sec is obtained with the same source and a thin Fe foil) is characteristic of the large scatter in isomer shifts and field gradients which exist in the amorphous material. The values

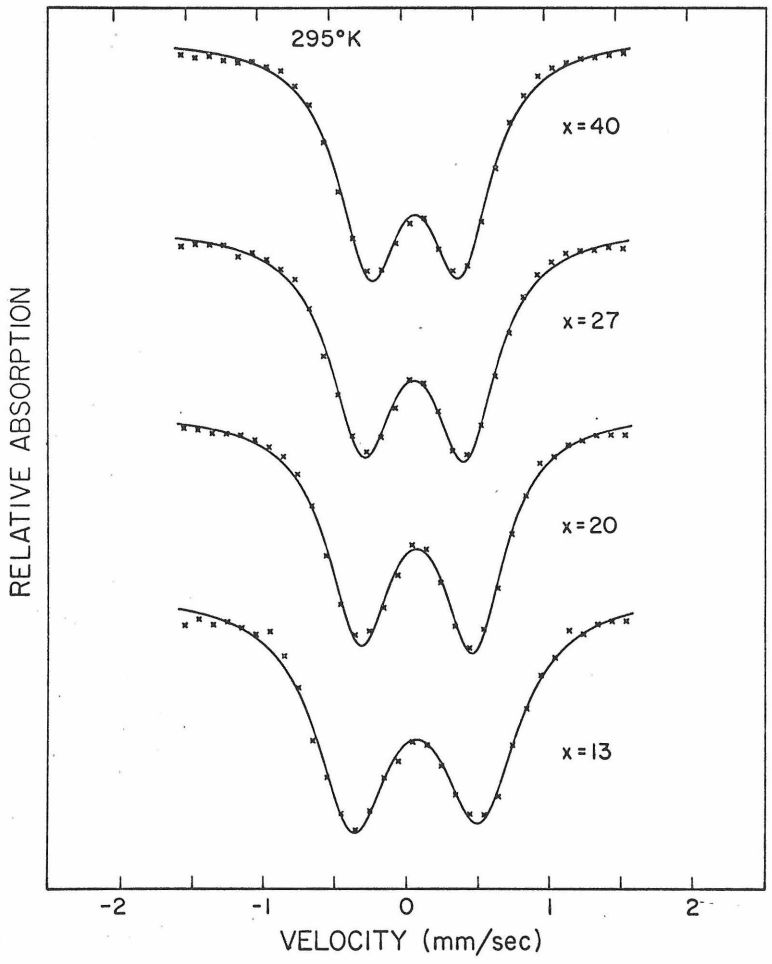

Fig. 5. Typical Mössbauer spectra for the amorphous $Fe_xPd_{80-x}P_{20}$ alloys at room temperature (295°K).

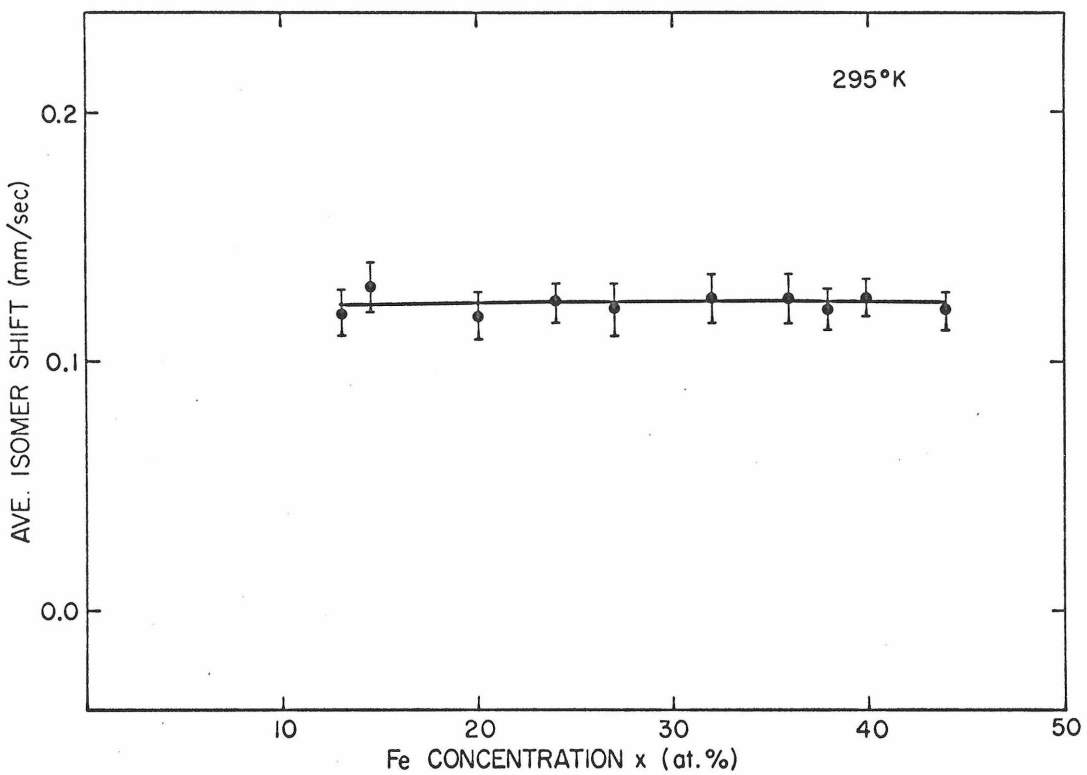

Fig. 6. Isomer shift vs. iron concentration for the amorphous $Fe_xPd_{80-x}P_{20}$ alloys.

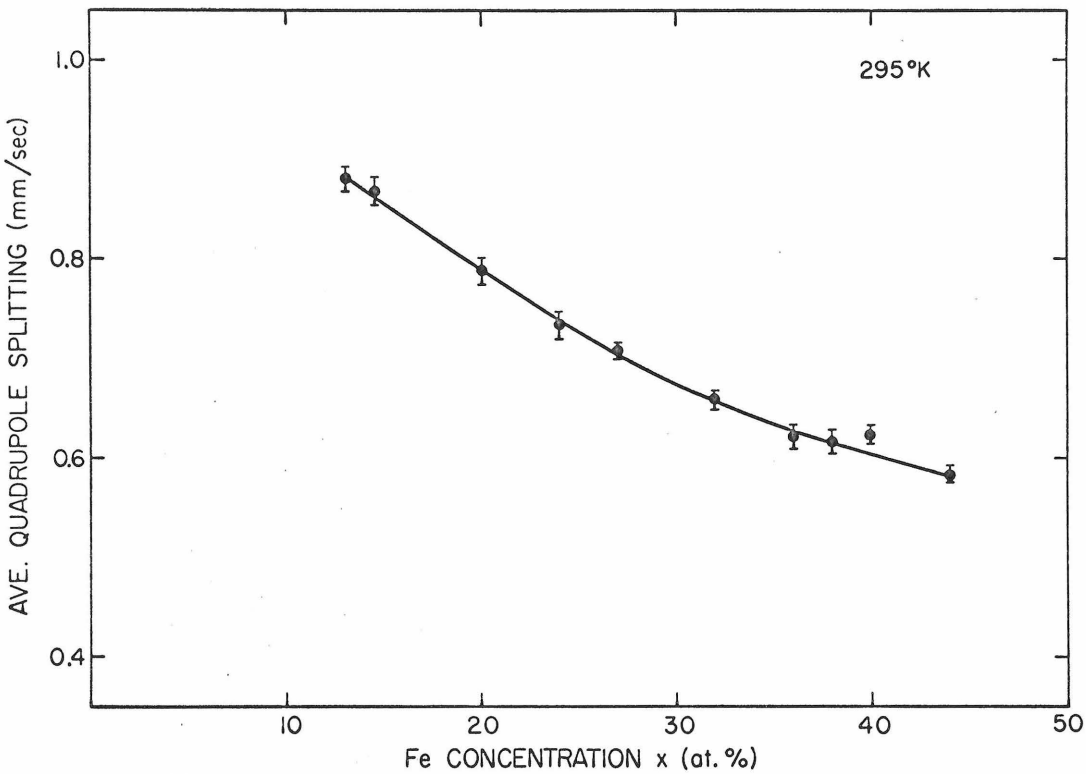

Fig. 7. Quadrupole splitting vs. iron concentration for the amorphous $Fe_xPd_{80-x}P_{20}$ alloys.

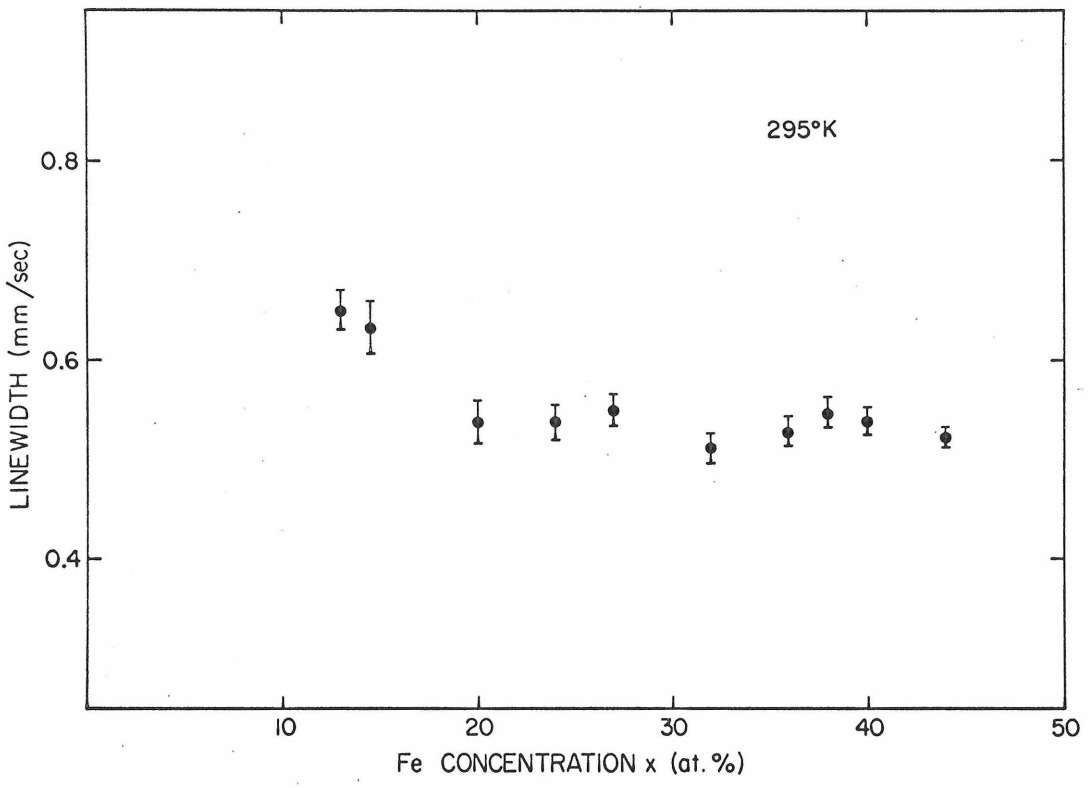

Fig. 8. Linewidth vs. iron concentration for the amorphous $Fe_xPd_{80-x}P_{20}$ alloys.

obtained for the $Fe_{44}Pd_{36}P_{20}$ alloy are extrapolations from experiments just above the Curie point (321°K).

In Fig. 8 no attempt is made to draw a smooth line through the data, since the linewidth depends on such factors as foil thickness and vibrational broadening which are not easily controlled.

2. Low Temperature Results

The problem of analyzing the Mössbauer spectrum of a magnetic material is greatly simplified by a knowledge of its structure. From this information one obtains the number of inequivalent Fe sites (hence components in the spectrum). In the crystalline case, one also obtains the point symmetries at each Fe site. This information is important because of the constraints imposed on the parameters used to fit the experimental data. Even with this knowledge, the problem of analyzing the absorption spectrum of a magnetic material with several sites per unit cell can be quite complicated, since a nonlinear least squares procedure with many parameters must be used. For a disordered alloy, the difficulty of the calculation increases immensely since the number of inequivalent sites actually becomes infinite. In the amorphous case, the difficulties may be expected to be even greater. Therefore, before discussing the analysis of the Fe-Pd-P Mössbauer spectra at low temperatures it may be helpful to briefly discuss two different approaches to the

disordered alloy problem which have been moderately successful.

An example of the first approach is represented by the study of Wertheim et al[37] of various 3d transition metals (Ti, V, Cr, ... Ni) in body centered cubic (bcc) Fe. These alloys may be denoted by the form Fe X (the underscored element is the solvent or host material), where X represents one of the other transition metals in the 3d series. In the bcc structure, there are eight nearest neighbors (nn) and six next nearest neighbors (nnn). Since the two components form a random solid solution for low X concentration, one can calculate the probabilities for various nearest and next nearest neighbor configurations. It was then assumed that the magnitude of the hyperfine field at a given Fe site depends only on the number of these impurity neighbors in the following fashion:

$$H(n,m) = H'(1 - \alpha n - \beta m) \qquad (27)$$

where H' is the hyperfine field of pure Fe(330 kOe), and n, m are the number of nn and nnn impurities. A corresponding expression is used for the isomer shift. One then calculates the Mössbauer spectrum corresponding to each set of (n, m) values, weights it with the appropriate probability, and sums over the 63 possible configurations.

It was found that the ratio of β to α which yields the best

agreement with the experimental data is about 0.8, largely independent of the nature of the impurity. The hyperfine field also tends to decrease for Fe atoms with impurity neighbors (approximately 8% for one nn, 6% for one nnn). Again these values do not depend greatly on the nature of the impurity.

The analysis is greatly simplified by the fact that there is no need to consider the quadrupole coupling. This fortuitous circumstance stems from the fact that the introduction of one nn impurity produces a field gradient with its principal axis along the [111] direction. Thus even though the quadrupole interaction is not absent, the factor $[3\cos^2\theta - 1]$ in Eq. (23) is zero because the spins are aligned along a [100] direction. Next nearest neighbor effects are significantly smaller because of the screening of electrostatic effects in a metallic host such as Fe. It is evident that this approach begins to break down when there is an appreciable probability of two or more nn impurities. This limits the approach to dilute impurities ($\lesssim$ 10% X).

The other disordered alloy problem which is easily treated is the case of dilute Fe impurities in a cubic host. Here the best example is Fe Pd[29, 38]. These alloys, which have the face centered cubic (fcc) structure, become ferromagnetic at exceeding low Fe concentrations ($\sim$.1% Fe). The environment around each

Fe atom is fcc Pd, and thus a simple six line spectrum (as in Fig. 2) is observed.

For the amorphous Fe-Pd-P alloys to be discussed here, both of these methods are clearly inapplicable because of the concentration range involved and the lack of symmetry. Therefore, a combined magnetic and electric quadrupole interaction of the most general kind discussed in section III must exist. The only a priori structural information is the averaged radial distribution function, which gives no information about the angular distribution about any given Fe atom.

In light of these difficulties, the approach to be followed must rely heavily on the experimental results for clues in interpreting the observed spectra. A typical low temperature Mössbauer absorption spectrum for the Fe-Pd-P alloys is shown in Fig. 9. There are several observations of significance to be made. First, it is possible to distinguish six peaks, although they are greatly broadened compared to the Fe foil spectrum of Fig. 2. A check of the line positions shows that they are in roughly the same ratio as observed for pure Fe. The inner peaks are noticeably sharper than the outer peaks. Finally, aside from the small differences in shape of the outermost peaks, the spectrum is nearly symmetric about its center. This last feature is quite surprising in view of the

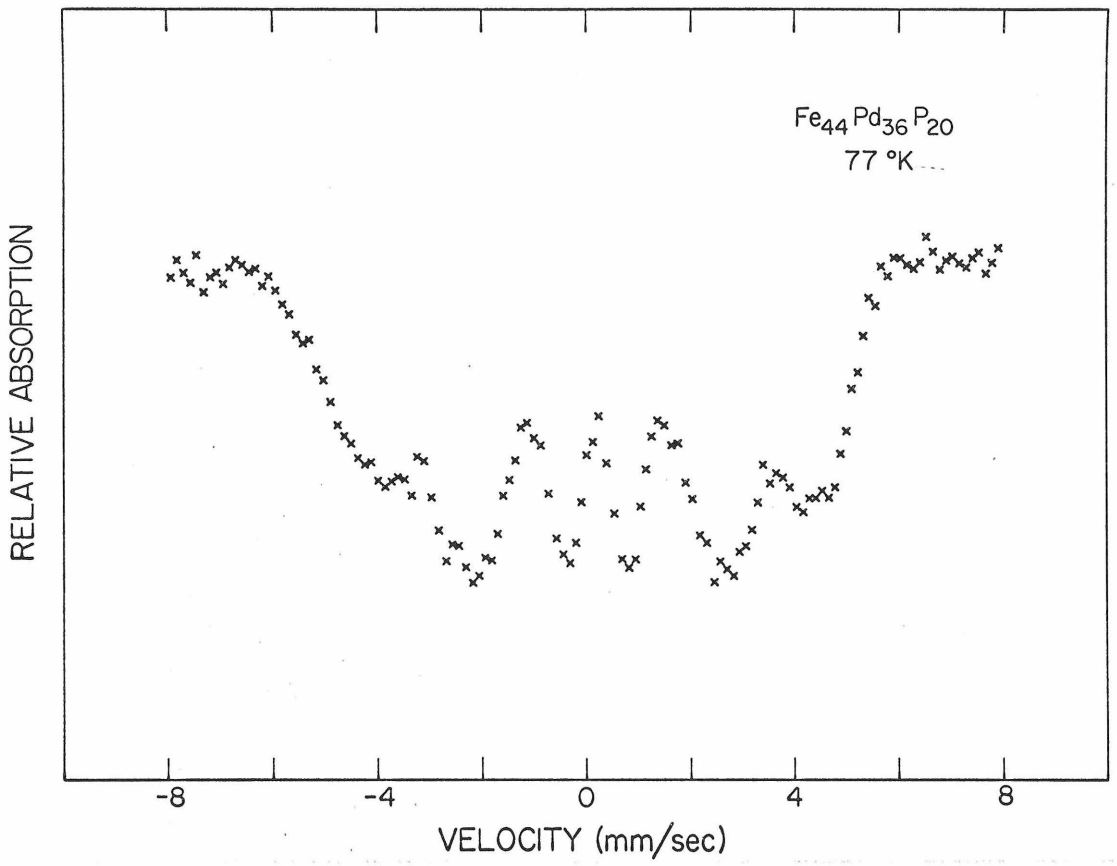

Fig. 9. Low temperature Mössbauer spectrum for the $Fe_{44}Pd_{36}P_{20}$ alloy.

combined electric and magnetic interactions present, and was also noted in an amorphous $Fe_{80}P_{12.5}C_{7.5}$ alloy[6]. For this alloy Tsuei et al. suggested that the quadrupole interaction merely broadens the peaks, rather than changing their positions. No further explanation was suggested for this effect, however.

If we also momentarily neglect the quadrupole interaction, the experimental data are consistent with a distribution of hyperfine fields in the alloy. The increased broadening from inner to outer peaks is consistent with this assumption, since each line would be broadened roughly in proportion to its displacement from the centroid of the pattern (see Fig. 4b). From an approach based on Eq. (27), it is possible to see how a range of hyperfine fields could exist in an amorphous material. From the RDF, we know that in an amorphous material the nearest neighbor atoms are not at one precise separation, but rather a shell of atoms exists whose width may be roughly $0.5\,\text{Å}$[10]. The second shell is less well defined. In Eq. (27), therefore, α and β take on a range of values, depending on the exact positions of the atom in the shells. In the amorphous Fe-Pd-P alloys, one of the dominant mechanisms affecting the hyperfine field at an Fe atom is expected to be electron transfer from neighboring phosphorus atoms. By donating electrons to the 3d shell of the Fe atoms, their moment and hyperfine field will be reduced[6]. We can

illustrate this effect by a simple example in which n in Eq. (27) is associated with the number of nearest neighbor P atoms. To simulate conditions in the amorphous Fe-Pd-P alloys, we assume rather close packing (approximately 12 nearest neighbors) with 20% of the sites randomly occupied by phosphorus. We then write

$$\bar{H}(n) = H'(1 - \alpha n) \tag{28}$$

where only nearest neighbor effects are considered for simplicity, in view of the fact that in amorphous materials short range effects are expected to be dominant. The value for H' is taken to be 300 kOe (appropriate to Fe Pd alloys), and $\alpha H' = 18$ kOe (a 6% decrease for 1 nn P atom). The probabilities of the various hyperfine fields are then given by the binomial distribution:

$$P_n = \binom{12}{n} (.2)^n (.8)^{12-n} \tag{29}$$

These values and their corresponding hyperfine fields are represented by the vertical bars in Fig. 10. To allow for the amorphous nature of the alloy, we now allow α to take on a range of values. This distribution may be assumed to be due to fluctuations in interatomic distances and next nearest neighbor effects. This is illustrated in Fig. 10 for $\sqrt{(\Delta\alpha)^2}/\alpha = 0.66$, where $(\Delta\alpha)^2$ is the mean square

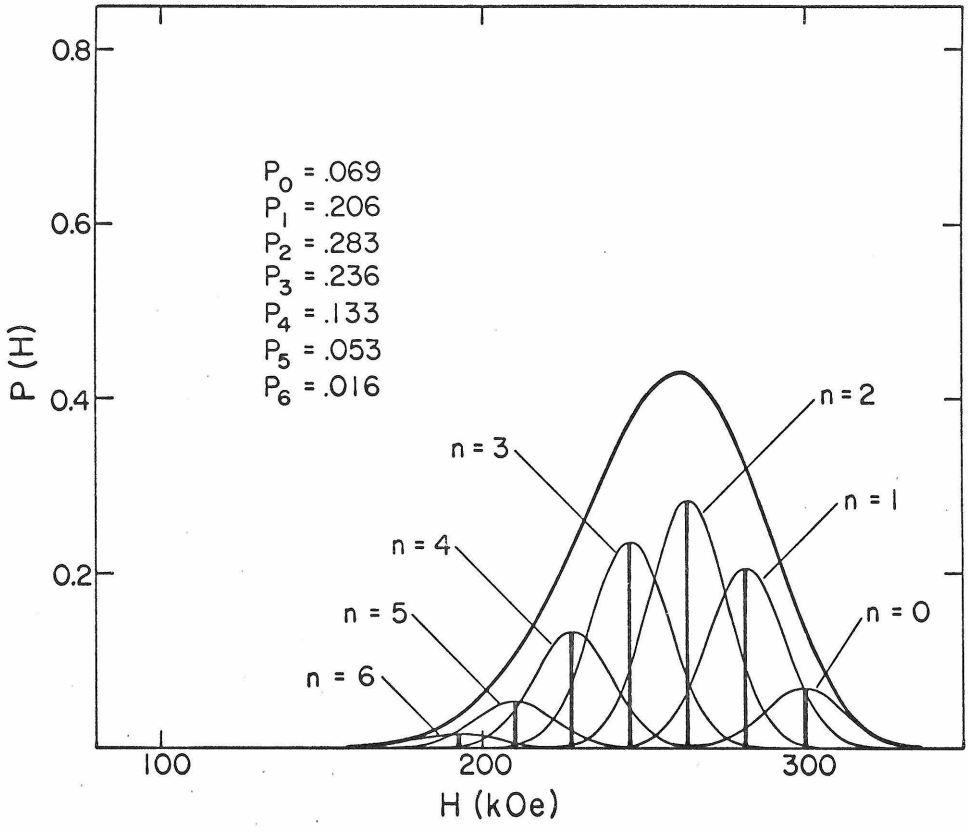

Fig. 10. Illustration of possible hyperfine field distribution in an amorphous material.

deviation from the average value. If the distribution about the average a is assumed to be Lorentzian in shape, the broadening of each six peak pattern can be simply handled by introducing a parameter λ such that the width of the peaks is given by

$$\Gamma_i = \Gamma_0 [\, 1 + \lambda \, |E_i| \,] \qquad (30)$$

where $|E_i|$ is the displacement of the ith peak from the centroid of the absorption pattern (isomer shift). This is the approach followed by Tsuei et al[6] in discussing the amorphous Fe-P-C alloy. They used five sets of six peak patterns, and achieved a good fit of the experimental data.

For the amorphous Fe-Pd-P alloys, this approach was considered but not used for several reasons. First, the number of variable parameters is quite large and these parameters often vary unpredictably. In particular, the intensities for the different six peak components do not always agree well with a binomial distribution. The large number of parameters (31 for five sites) makes the numerical analysis quite lengthy and very expensive in computer time. Secondly, the lack of detailed structure in the spectra of the Fe-Pd-P alloys makes it unlikely that a unique fitting based on a certain number of sites can be achieved. In fact, the most that can probably

be learned about the hyperfine field distribution is its shape, average value, and width. Actually this information is quite sufficient for the discussion of the magnetic properties.

It was decided, therefore, to base the analysis of the Mössbauer spectra on a distribution of hyperfine fields. As a first attempt, a Gaussian distribution of fields was assumed. This is equivalent in the simple model illustrated in Fig. 10 to replacing the top curve representing the sum of the components by a Gaussian curve of appropriate average value and width. This would appear to be a quite good approximation. Thus it was assumed that

$$P(H) = \frac{1}{\sqrt{2\pi\Delta^2}} \exp\left[-\frac{(H-\bar{H})^2}{2\Delta^2}\right] \qquad (31)$$

was the probability density function for hyperfine fields. A computer program was written to calculate the corresponding Mössbauer absorption spectrum, and a nonlinear least squares analysis was used to adjust $\bar{H}$ and Δ to best fit the experimental data. Using this approach it was found that the outer peaks could be fitted quite well, but the absorption in the central part of the spectrum was much greater than predicted by this simple model. This implies that there are significant contributions to the absorption coming from Fe sites with small hyperfine fields. In other words, the distri-

bution function has a "tail" on the low field side, while on the high field side it falls quite rapidly and its shape can be approximated well by a Gaussian curve. To take into account this "tail" effect in the calculation, it is convenient to have an analytical form for P(H). It was found that the form of P(H) can be well represented by the following empirical formula:

$$P(H) \propto \begin{cases} \dfrac{1}{(H-H_o)^2 + \Delta_o^2/4} & 0 < H \leq H_o \\ \exp - \dfrac{(H-H_o)^2}{2\Delta_1^2} & H > H_o \end{cases} \qquad (32)$$

The two forms are matched in value at $H = H_o$ and P(H) is then normalized numerically so that $\int_0^\infty P(H)\, dH = 1$.

Typical fittings achieved with this model are shown in Figs. 11-16, along with the hyperfine field distributions, and are quite good considering that only 3 parameters are involved in the analysis. This means that the actual P(H) distribution is quite well approximated by Eq. (32). In Tables I-III the actual values for the parameters and their estimated standard deviations are shown. In Table IV we present the average value $\bar{H} = \int_0^\infty P(H)\, H\, d\, H$ and the standard deviation ΔH for the distributions at 4.2°K. ΔH is defined by

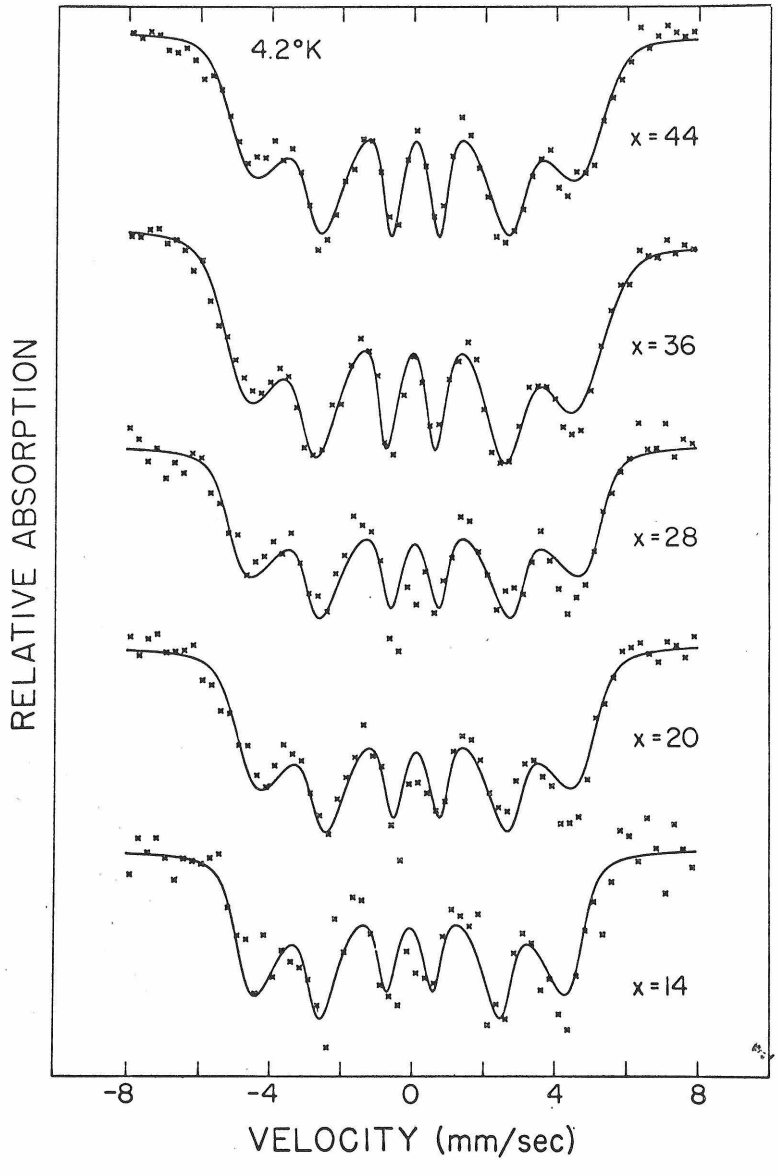

Fig. 11. Mössbauer spectra of the amorphous $Fe_xPd_{80-x}P_{20}$ alloys at 4.2°K. The experimental points are shown and the fitting based on Eq. (32).

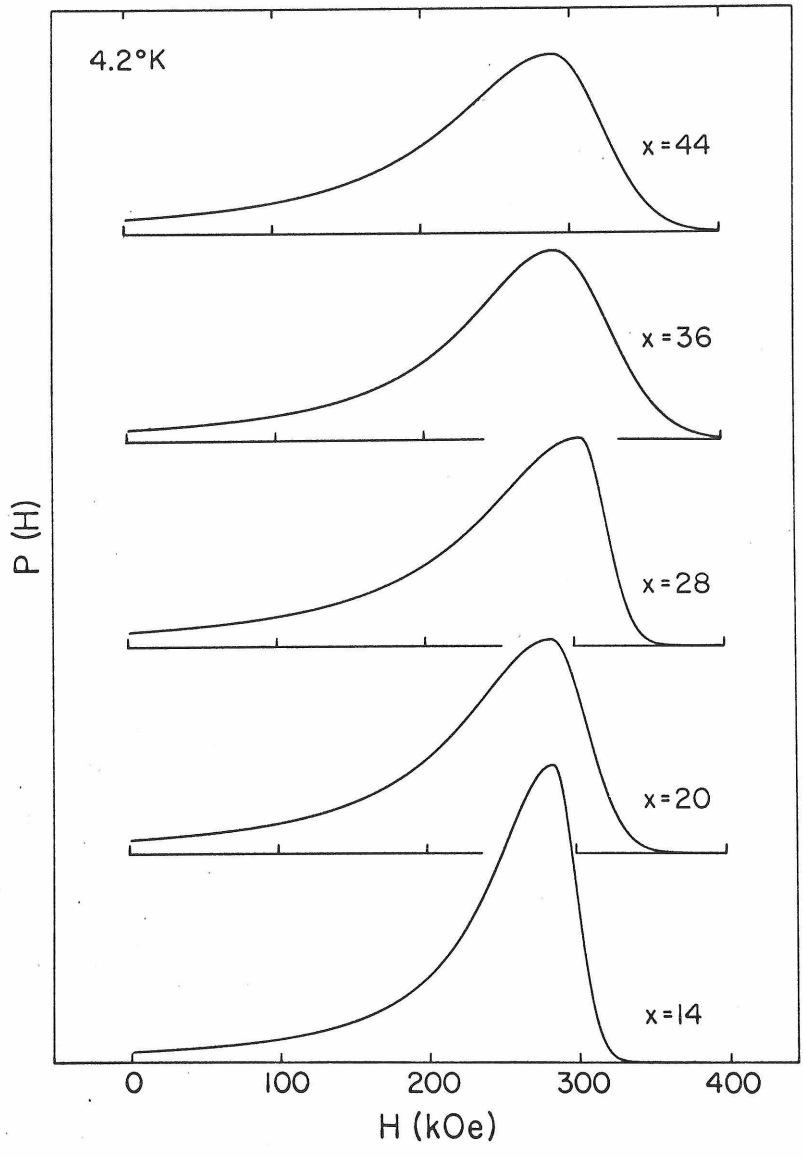

Fig. 12. Hyperfine field distributions corresponding to the fittings of Fig. 11. The vertical scale is the same for all the curves.

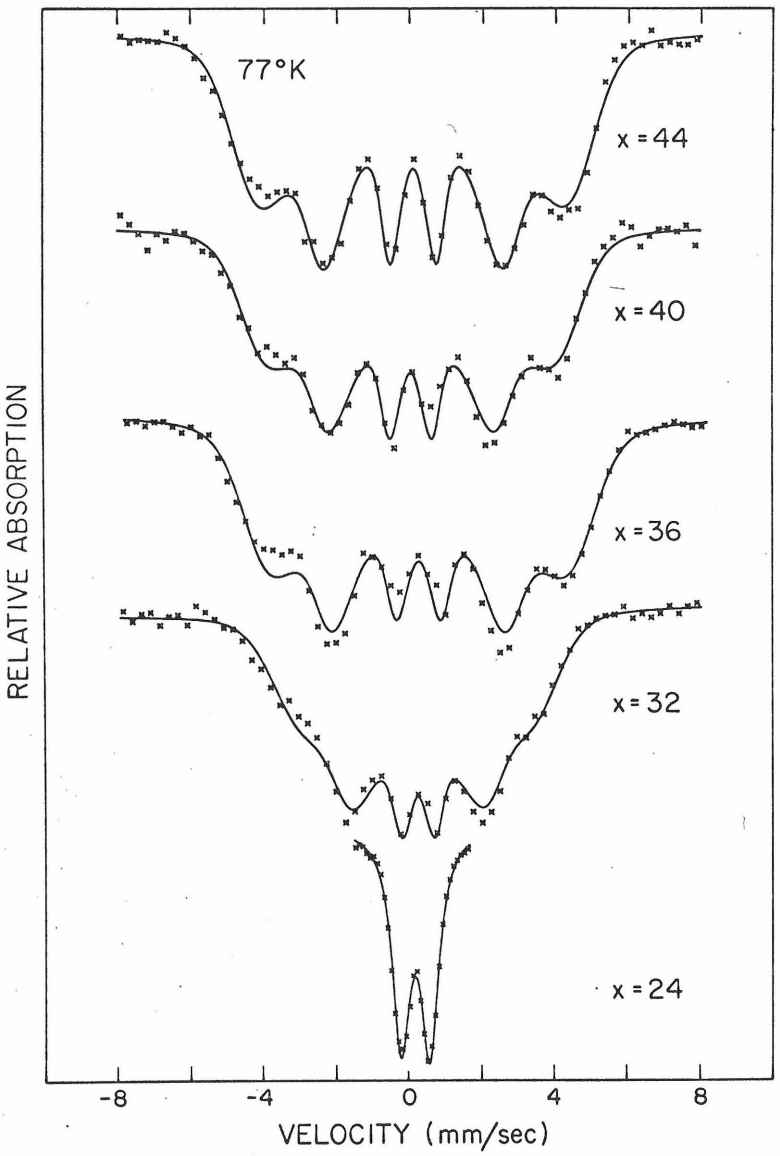

Fig. 13. Mössbauer spectra of the amorphous $Fe_xPd_{80-x}P_{20}$ alloys at 77°K.

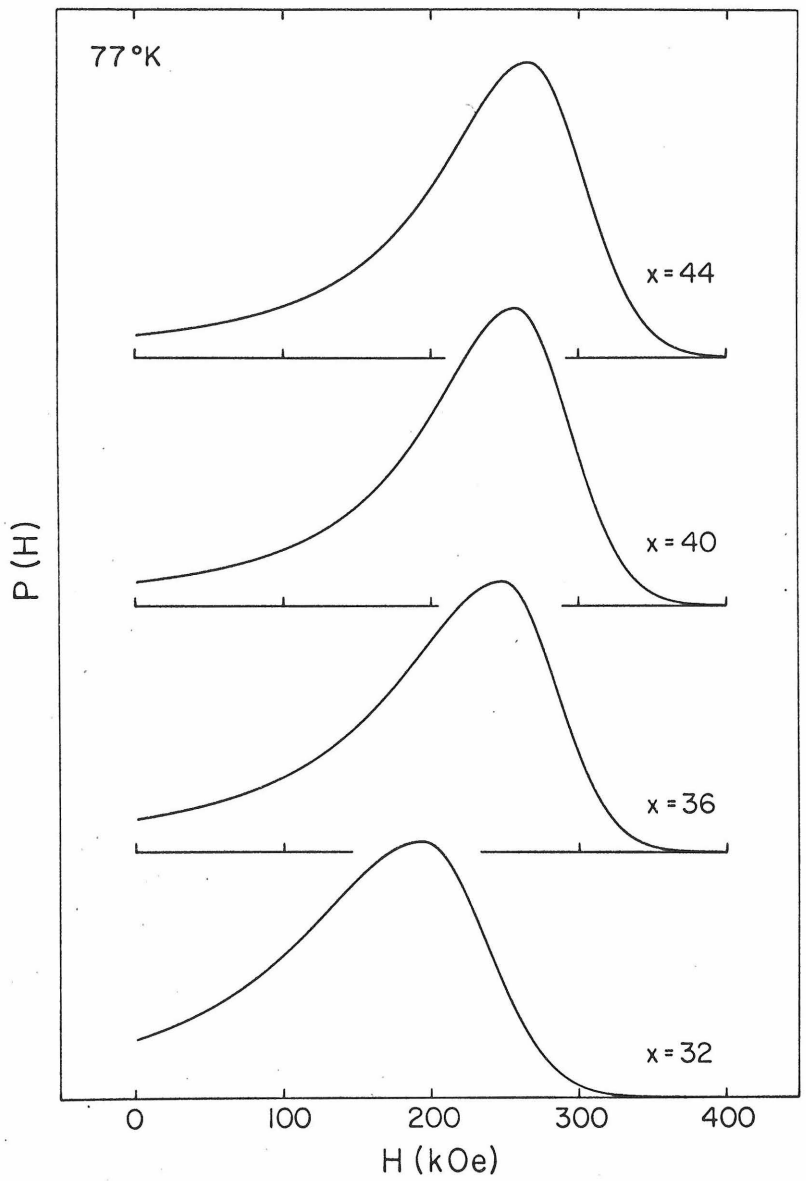

Fig. 14. Hyperfine field distributions corresponding to the fittings of Fig. 13.

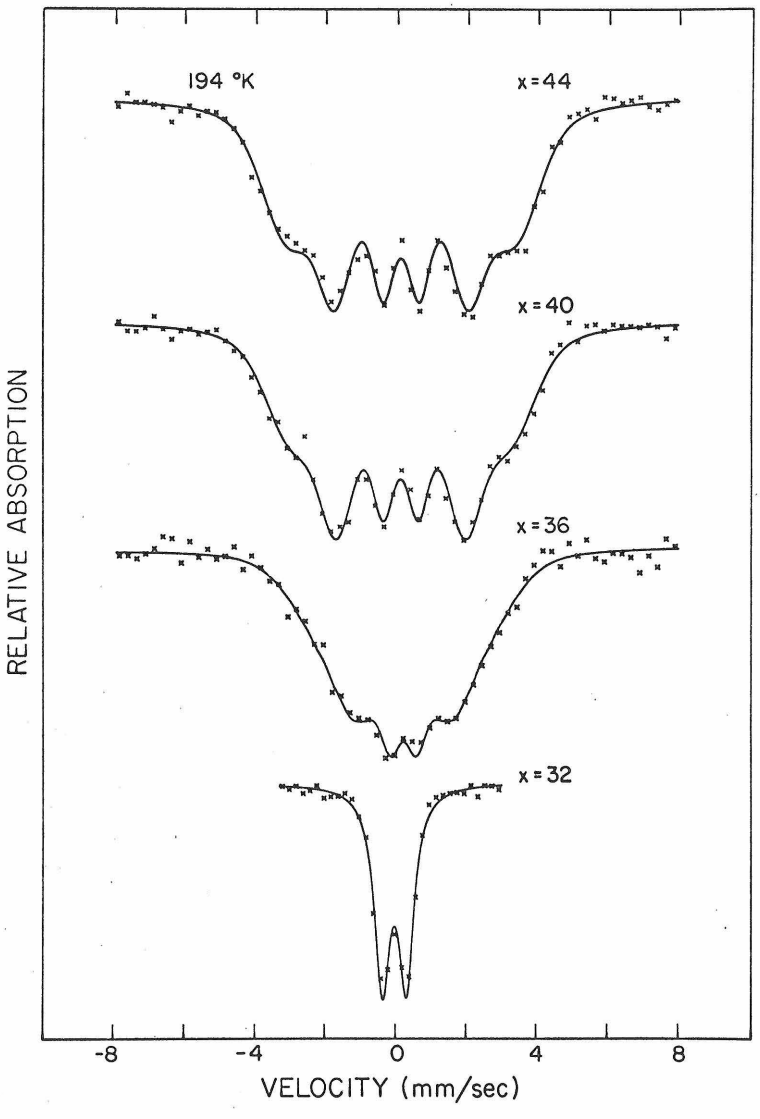

Fig. 15. Mössbauer spectra of the amorphous $Fe_xPd_{80-x}P_{20}$ alloys at 194°K.

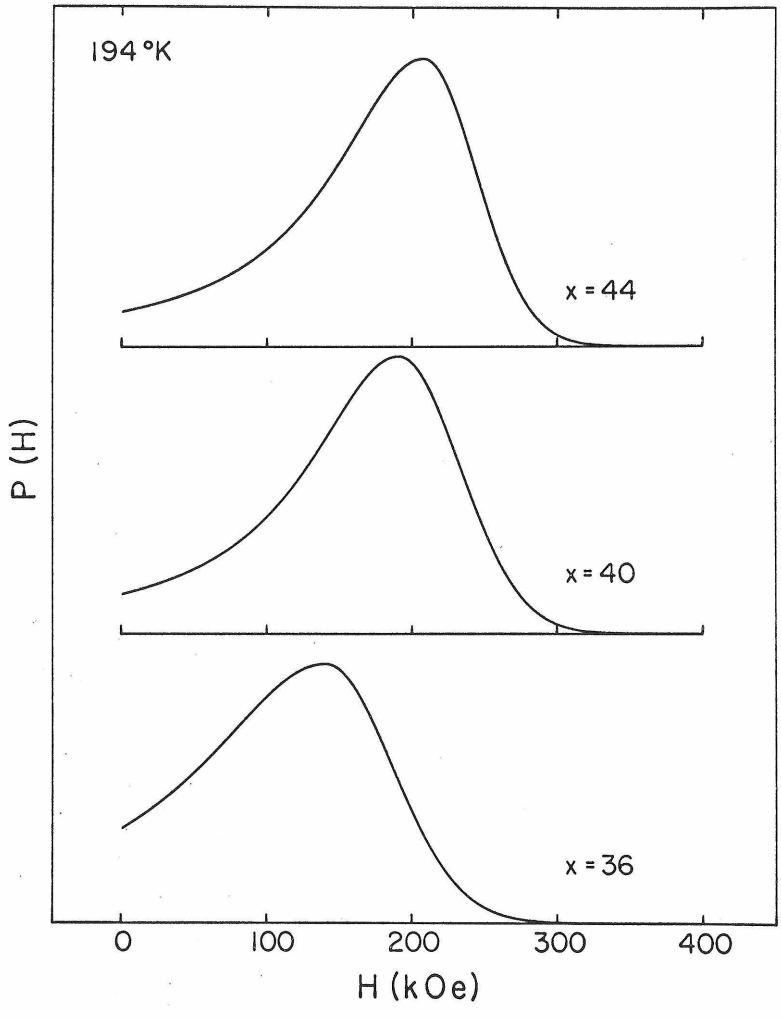

Fig. 16. Hyperfine field distributions corresponding to the fittings of Fig. 15.

TABLE I

Parameters obtained from analysis of Mössbauer Effect data at 4.2°K based on Eq. (32). Estimated standard deviations are shown in parentheses. The symbols δ and Γ refer to the average isomer shift and linewidth, respectively.

Composition	δ(mm/sec)	Γ (mm/sec)	H_o(kOe)	Δ_0(kOe)	Δ_1(kOe)
$Fe_{44}Pd_{36}P_{20}$	0.102 (.017)	0.447 (.047)	288.4 (4.5)	171.8 (11.0)	33.3 (2.9)
$Fe_{36}Pd_{44}P_{20}$	0.108 (.016)	0.523 (.046)	287.7 (3.8)	146.6 (8.3)	36.8 (2.9)
$Fe_{28}Pd_{52}P_{20}$	0.085 (.030)	0.553 (.095)	304.9 (13.7)	167.0 (17.1)	16.8 (11.3)
$Fe_{24}Pd_{56}P_{20}$	0.076 (.020)	0.444 (.055)	296.6 (4.8)	167.6 (12.5)	20.0 (3.4)
$Fe_{20}Pd_{60}P_{20}$	0.080 (.021)	0.570 (.069)	284.2 (6.7)	148.5 (11.1)	23.2 (6.3)
$Fe_{14}Pd_{66}P_{20}$	-0.043 (.052)	0.554 (.181)	283.2 (21.4)	106.0 (26.2)	14.6 (19.9)

TABLE II

Parameters obtained from analysis of Mössbauer Effect data at 77°K based on Eq. (32).

Composition	δ (mm/sec)	Γ (mm/sec)	H_o(kOe)	Δ_0(kOe)	Δ_1(kOe)
$Fe_{44}Pd_{36}P_{20}$	0.098 (.009)	0.500 (.027)	265.9 (2.4)	152.0 (5.24)	38.5 (1.8)
$Fe_{40}Pd_{40}P_{20}$	0.133 (.005)	0.643 (.017)	257.4 (1.7)	151.8 (2.5)	36.9 (1.5)
$Fe_{36}Pd_{44}P_{20}$	0.070 (.011)	0.511 (.032)	248.0 (3.3)	183.7 (6.9)	36.5 (2.7)
$Fe_{32}Pd_{48}P_{20}$	0.111 (.018)	0.495 (.046)	194.2 (6.6)	210.4 (4.6)	42.9 (5.4)

TABLE III

Parameters obtained from analysis of Mössbauer Effect data at 194°K, 273°K, and 295°K based on Eq. (32).

Composition	δ(mm/sec)	Γ (mm/sec)	H_o(kOe)	Δ_0(kOe)	Δ_1(kOe)
$Fe_{44}Pd_{36}P_{20}$(194°K)	0.091(.015)	0.470(.039)	207.9(3.3)	154.1(8.8)	36.4(3.6)
$Fe_{40}Pd_{40}P_{20}$(194°K)	0.092(.004)	0.464(.009)	191.5(1.0)	155.4(2.2)	41.8(0.8)
$Fe_{36}Pd_{44}P_{20}$(194°K)	0.125(.037)	0.583(.145)	140.7(16.6)	211.6(38.7)	46.0(14.1)
$Fe_{44}Pd_{36}P_{20}$(273°K)	0.138(.022)	0.560(.095)	133.4(9.1)	165.0(19.4)	38.2(8.1)
$Fe_{44}Pd_{36}P_{20}$(295°K)	0.129(.013)	0.511(.080)	87.3(7.5)	142.1(21.8)	54.1(6.8)

TABLE IV

Characteristics of the hyperfine field distributions at 4.2°K

Composition	$\bar{H}$ (kOe)	ΔH (kOe)	$\Delta_{\frac{1}{2}}$ (kOe)
$Fe_{44}Pd_{36}P_{20}$	234.9	78.0	125.5
$Fe_{36}Pd_{44}P_{20}$	244.5	75.7	119.8
$Fe_{28}Pd_{52}P_{20}$	235.7	75.9	102.2
$Fe_{24}Pd_{56}P_{20}$	228.6	74.7	107.4
$Fe_{20}Pd_{60}P_{20}$	228.7	71.7	100.0
$Fe_{14}Pd_{66}P_{20}$	233.7	63.3	70.1

$$(\Delta H)^2 = \langle (H-\bar{H})^2 \rangle = \int_0^\infty P(H)(H-\bar{H})^2 \, dH$$

Also given is the full width at half-maximum $\Delta_{\frac{1}{2}}$ of the distributions.

Despite the good agreement between observed and calculated spectra, the validity of this approach seems questionable at this point, since no provision has been made for the electric quadrupole interaction. The justification for this is closely related to the amorphous nature of the alloys. In the magnetically ordered state which prevails at low temperature, the magnetic moments of the iron atoms are ordered over a range considerably larger than an interatomic distance. The electric field gradient, on the other hand, is primarily determined by only the neighbors within a few interatomic distances. The metallic nature of these alloys prevents the existence of longer range electrostatic effects. This means that on the average over the region of magnetic ordering, structural fluctuations in the amorphous alloy will lead to a completely random angle between the efg principal axis and the magnetic field direction. There should be a uniform distribution of polar and azimuthal angles between these two directions. This is equivalent to saying that the anisotropy energy constant K in an amorphous ferromagnet is very small.

At any given Fe site there is in general no axial symmetry. Nevertheless, since there is no preferred direction on the average

in an amorphous structure, the most probable value of $\eta = \frac{V_{xx}-V_{yy}}{V_{zz}}$ must be zero. A value of $\eta = 1$ (V_{xx} or $V_{xx} = 0$) would imply a very definite local order of atoms, and would be extremely unlikely in an amorphous material.

Using Eq. (23), we can then justify our treatment of the experimental data in terms of a hyperfine field distribution alone. For any given sublevel of the excited state, the energy shift due to the quadrupole interaction is

$$\Delta E_Q = \frac{e^2qQ}{4}\left[\frac{3\cos^2\theta-1}{2}\right] \tag{33}$$

where θ is the angle between $\bar{H}$ and the efg principal axis. The average value of this shift is therefore

$$\langle \Delta E_Q \rangle = \frac{1}{4\pi}\int_0^{2\pi}\int_0^{\pi} \frac{e^2qQ}{4}\left[\frac{3\cos^2\theta-1}{2}\right]\sin\theta\, d\theta\, d\varphi \tag{34}$$

Since $\langle \cos^2\theta \rangle_\Omega = 1/3$, $\langle \Delta E_Q \rangle = 0$. Therefore the average line positions in the Mössbauer spectrum are unaffected. The only effect is a broadening of the six peaks.

Using this model we can calculate the lineshape resulting from this quadrupole broadening. From the data of Fig. 7 we can estimate $\left|\frac{e^2qQ}{4}\right|$, and use the linewidth Γ_o of Fig. 8 to estimate the linewidth from other factors. The resulting absorption lineshape

A(V) should be

$$A(V) = A_o \int_o^{\pi} \frac{1}{\left[V - \frac{e^2qQ}{4} \left(\frac{3\cos^2\theta - 1}{2} \right) \right]^2 + \Gamma_o^2/4} \sin\theta d\theta \quad (35)$$

Actually since the quadrupole splitting from Fig. 7 measures only the magnitude of q, the expression on the right in Eq. (35) should be summed over positive and negative values of this quantity.

The lineshape was calculated for several values of $e^2qQ/4$ and Γ_o corresponding to various compositions. Fig. 17 shows the calculated lineshape for the $Fe_{44}Pd_{36}P_{20}$ alloy: $\Gamma_o = 0.53$ mm/sec, $\left| \frac{e^2qQ}{4} \right| = 0.28$ mm/sec. As can be seen from the figure, the lineshape remains approximately Lorentzian with an increased linewidth $\Gamma = 0.63$ mm/sec. This compares experimentally with a value 0.45 - 0.56 mm/sec for this alloy determined from the data analysis. The reason for this discrepancy is that Γ_o taken from Fig. 7 includes the broadening effects arising from the scatter in electric field gradients, whereas in the broadening effect observed in the combined electric and magnetic interaction, the largest values of q are most effective. The value chosen for Γ_o should reflect mainly the broadening due to the scatter in isomer shifts. If we choose Γ_o in the range 0.35 - 0.40 mm/sec, we obtain reasonable agreement with the magnitudes for linewidth reported in Tables I-III.

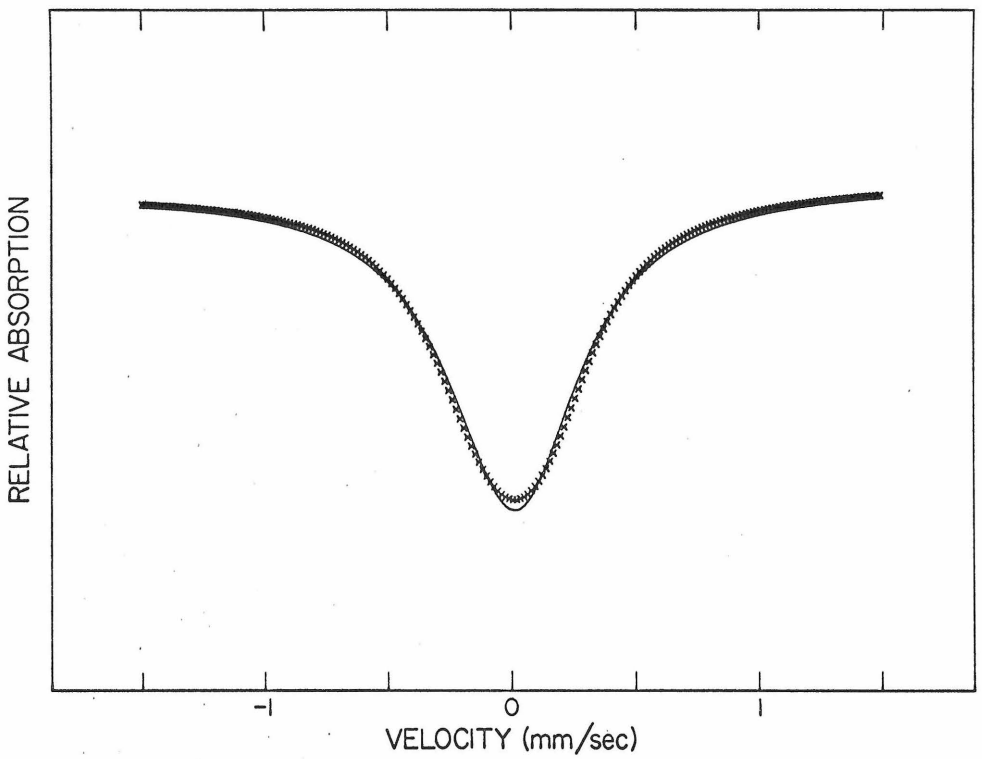

Fig. 17. Illustration of the line broadening caused by the quadrupole interaction in the Mössbauer spectra of the amorphous alloys. The solid curve is the Lorentzian line which best approximates the actual lineshape calculated from Eq. (35).

In summary, then, the effect of the quadrupole interaction on the Mössbauer spectrum of the amorphous alloys well below their transition temperature is only to broaden the peaks (all equally) of each component spectrum in the hyperfine field distribution. The spread in hyperfine fields causes further broadening which has increasing effect from inner to outer peaks.

3. Analysis of Mössbauer Data Near the Transition Temperature

As the temperature approaches the Curie point of a magnetic material, the hyperfine field drops rapidly to zero. Just above the Curie point, the absorption spectrum returns to simply two peaks. There are several reasons why the data analysis just described is not adequate in this temperature region. First of all, the spectrum from a distribution of fields approaches a single peak instead of a quadrupole type spectrum as all fields go to zero. This means that even above the Curie point a finite hyperfine field will be obtained as the analysis attempts to fit the two peaks. The temperature dependence of the hyperfine field in the transition region will therefore be incorrect. Secondly, the hyperfine field is a very nonlinear function of temperature near the Curie point. In this temperature region even the high field distribution is likely to be skewed toward low fields rather than a simple Gaussian distribution. The most important reason for using a different approach is that certain

quantities of interest relating to the nature of the phase transition are not available from the previous analysis. For example, it is well known that in any alloy, the phase transition is never perfectly well defined in temperature due to inhomogenities and other effects. In the amorphous alloys, a very pronounced effect of this type might be expected.

The approach to be followed here is similar to that used by Dunlap and Dash[39] in their analysis of Co Pd alloys by a thermal scanning technique. In their experiments the full Mössbauer spectrum was not measured, but only the transmission rate with fixed source and absorber as a function of temperature near the Curie point. The problem here is complicated by the fact that a distribution of hyperfine fields exists even at $T = 0^{o}K$, and by the lack of cubic symmetry.

For simplicity in the analysis, the average value of hyperfine field obtained at $4.2^{o}K$ (well below all Curie points) is assigned to each Fe atom as its saturation value. Around each Fe atom we consider a cell in which the magnetization is determined by the local concentration of Fe atoms and the temperature. The Fe atoms are assumed to be distributed throughout the material in a random fashion. If the cell has N atoms altogether then the probability of finding n Fe atoms is

$$P(n) = \binom{N}{n} x^n \ (1-x)^{N-n} \tag{36}$$

For a reasonable size cell (more than 50 atoms) we can write to an excellent approximation

$$P(n) \cong \frac{1}{\sqrt{2\pi \bar{n}(1-x)}} \exp\left[-\frac{(n-\bar{n})^2}{2\bar{n}(1-x)}\right] \tag{37}$$

where $\bar{n} = xN$ is the average number of Fe atoms per cell.

The local Curie temperature is assumed to be a function of n. Since the experimental results indicate a fairly well defined transition, the transition temperature of a cell does not vary too rapidly with n. Thus

$$T_c(n) \cong T_c(\bar{n}) + \left(\frac{dT_c}{dn}\right)_{n=\bar{n}} (n-\bar{n}) + \ldots \tag{38}$$

Letting $T_c(\bar{n}) = \bar{T}_c$ and $\left(\frac{dT_c}{dn}\right)_{n=\bar{n}} = \alpha$ we obtain

$$P(T_c) = \frac{1}{\sqrt{2\pi (\Delta T_c)^2}} \exp\left[-\frac{(T_c-\bar{T}_c)^2}{2(\Delta T_c)^2}\right] \tag{39}$$

where $(\Delta T_c)^2 = \alpha^2 \bar{n}(1-x)$. ΔT_c is a direct measure of the width of the transition.

To calculate the hyperfine field distribution we further assume that $H(T)/H(0)$ and $M(T)/M(0)$ for each cell vary with temperature according to the molecular field approximation:

$$\frac{H(T)}{H(0)} = \frac{M(T)}{M(0)} = B_s\left[\frac{3S}{S+1}\ \frac{M(T)/M(0)}{T/T_c}\right] \qquad (40)$$

where

$$B_s(x) = \frac{2S+1}{2S}\ \coth\left(\frac{2S+1}{2S}\ x\right) - \frac{1}{2S}\ \coth\frac{x}{2S}$$

is the Brillouin function for spin S. From the temperature of the experiment, the average Curie temperature $\bar{T}_c$, and ΔT_c, it is possible to calculate the hyperfine field distribution and the resulting Mössbauer spectrum. To analyze the experimental data, $\bar{T}_c$ and ΔT_c are treated as parameters to be varied to best fit the data. Once they have been determined, the average hyperfine field can also be calculated. Table V gives the parameter values obtained from the experimental data.

By combining this method of analysis with the one previously described, the spectra can be fitted over the complete temperature range. Several examples are shown in Figs. 18-24.

B. Variation of Transition Temperature with Fe Concentration

The Mössbauer results just described give several transition temperatures directly, and place upper and lower bounds on the rest. To give a more precise value to these intermediate points, the inductance measurements described in section II were used. For those alloys with $x \geq 28$ ($T_c > 77^{\circ}K$), the results obtained are in

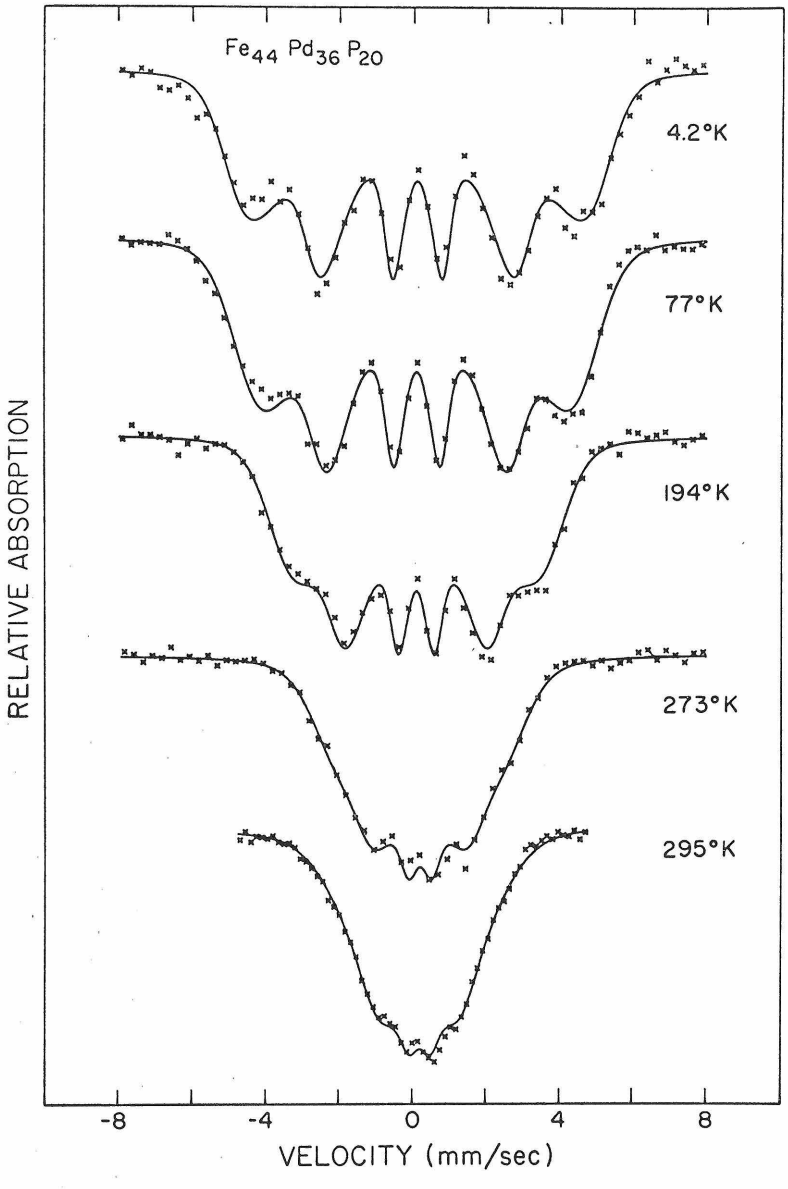

Fig. 18. Temperature dependence of the Mössbauer spectrum for the amorphous $Fe_{44}Pd_{36}P_{20}$ alloy. The solid curves are the fittings based on Eq. (32).

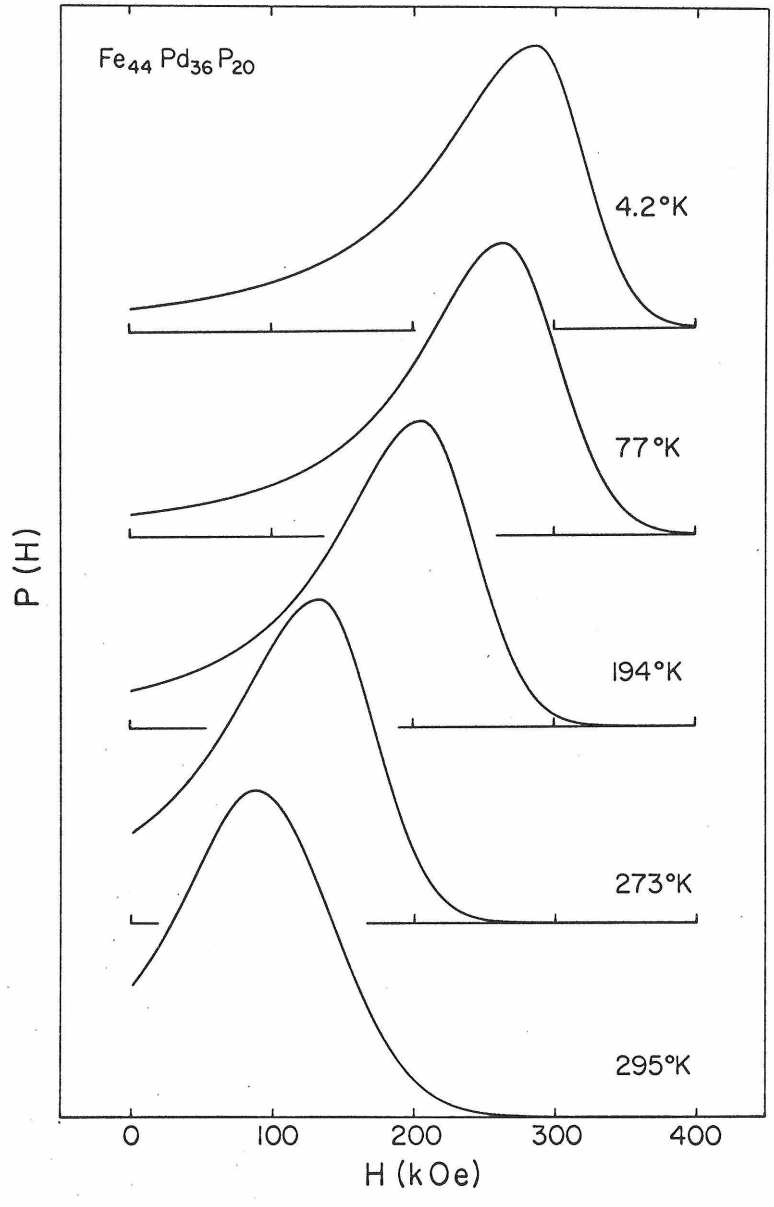

Fig. 19. Temperature dependence of the hyperfine field distribution for the amorphous $Fe_{44}Pd_{36}P_{20}$ alloy.

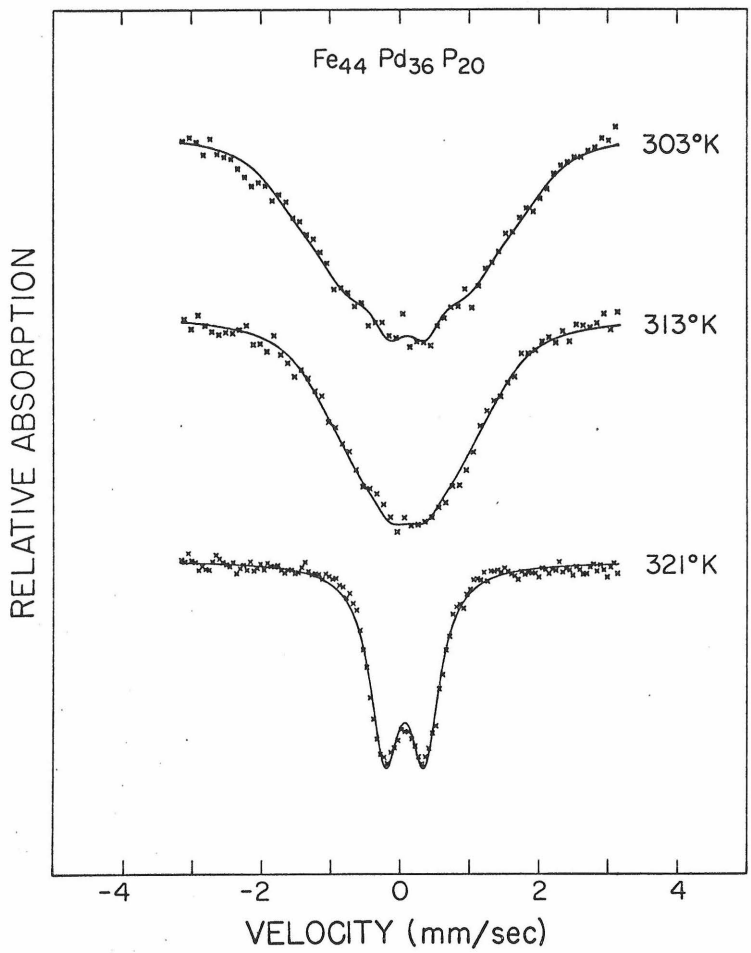

Fig. 20. Mössbauer spectra of the $Fe_{44}Pd_{36}P_{20}$ alloy near the transition temperature.

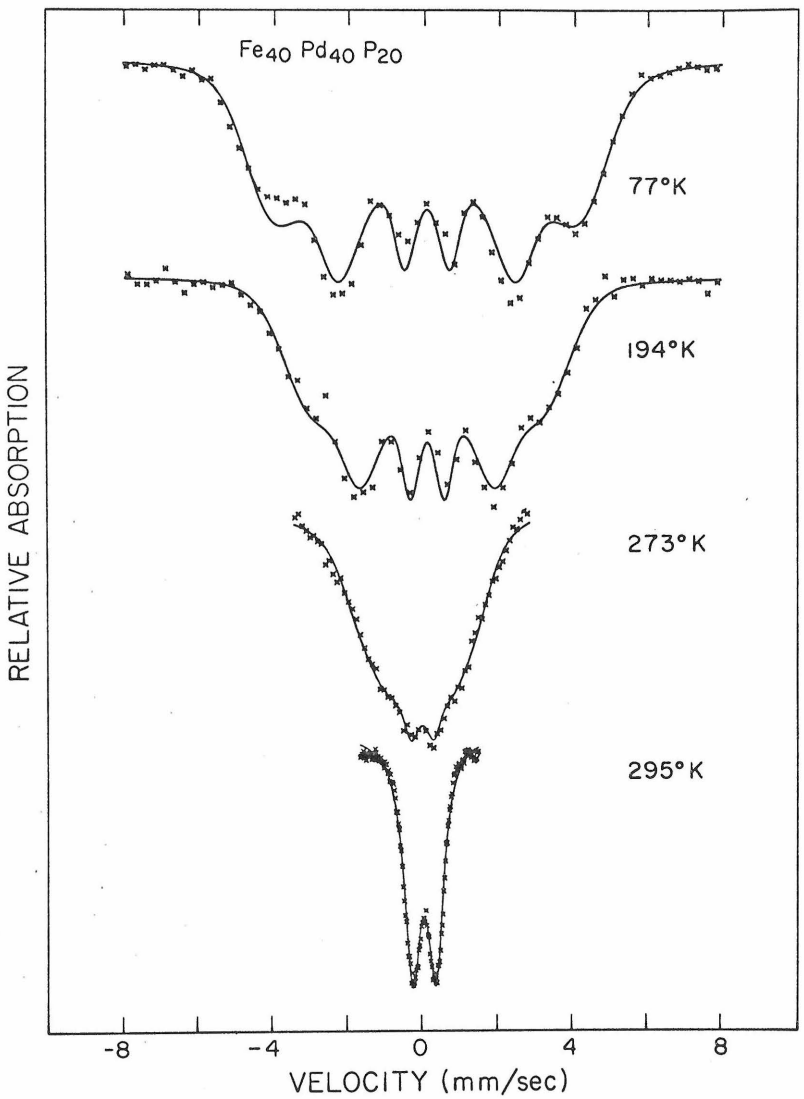

Fig. 21. Temperature dependence of the Mössbauer spectrum for the $Fe_{40}Pd_{40}P_{20}$ alloy.

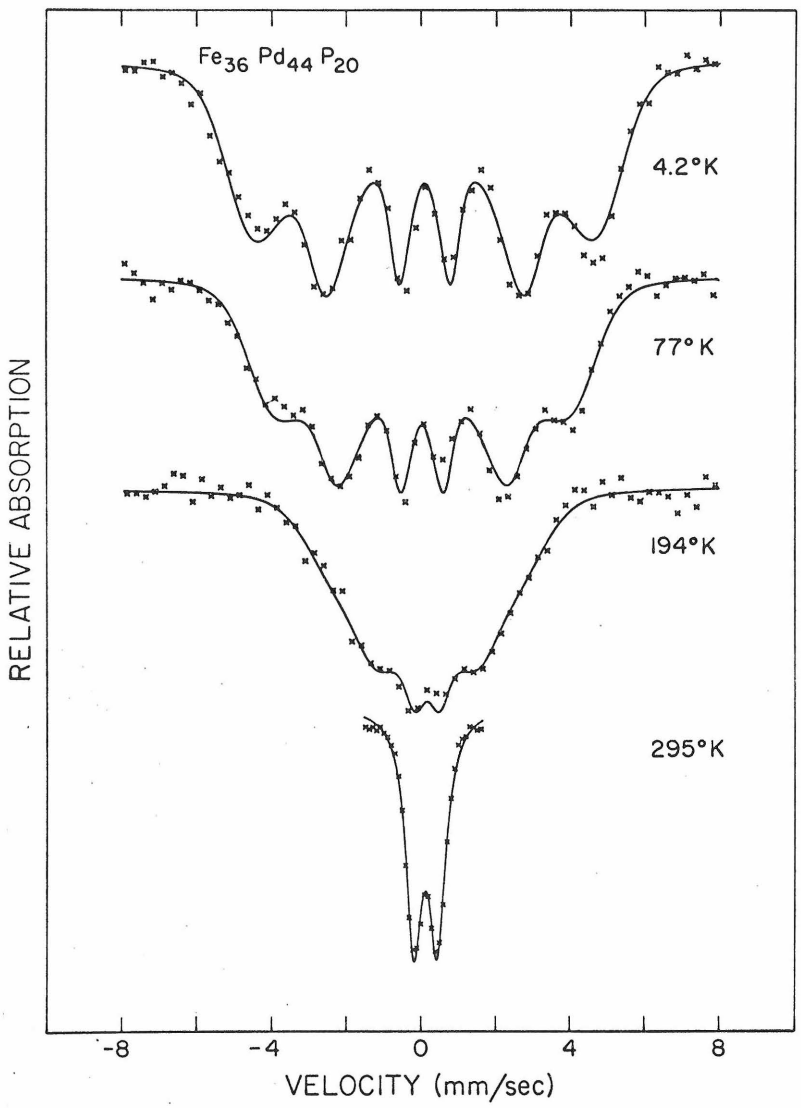

Fig. 22. Temperature dependence of the Mössbauer spectrum for the $Fe_{36}Pd_{44}P_{20}$ alloy.

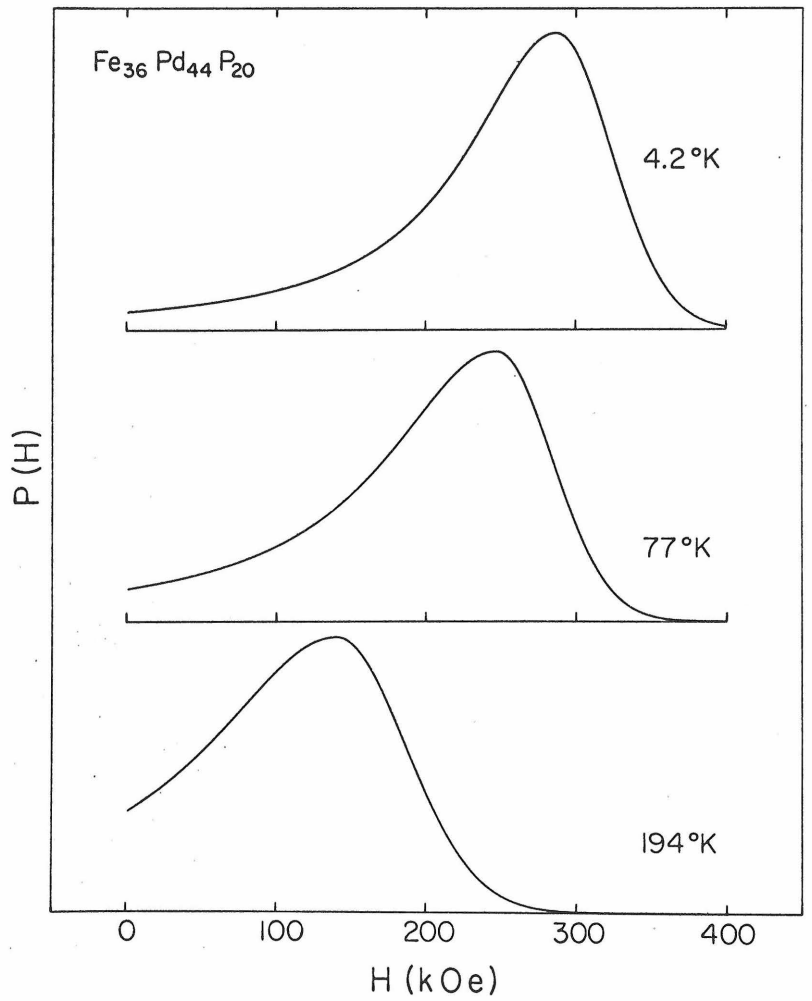

Fig. 23. Temperature dependence of the hyperfine field distribution for the $Fe_{36}Pd_{44}P_{20}$ alloy.

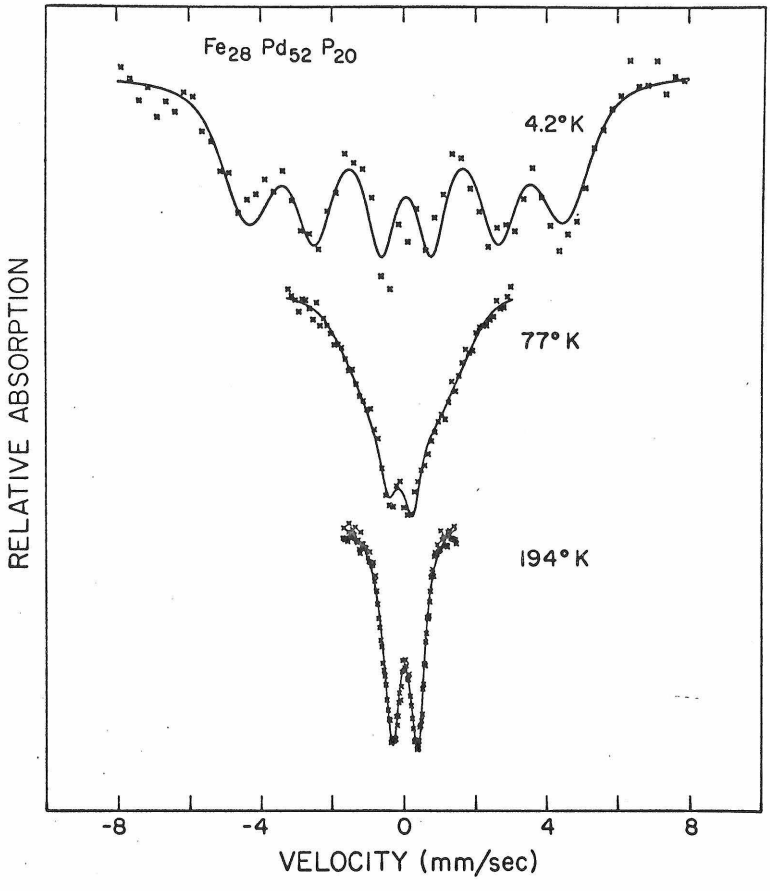

Fig. 24. Temperature dependence of the Mössbauer spectrum for the $Fe_{28}Pd_{52}P_{20}$ alloy.

TABLE V

Parameters obtained from analysis of Mössbauer Spectra near the transition temperature.

Composition	Temperature (^{o}K)	$\bar{T}_c$ (^{o}K)	ΔT_c (^{o}K)	$\bar{H}$(kOe)
$Fe_{44}Pd_{36}P_{20}$	303	317.7	7.98	63.4
$Fe_{44}Pd_{36}P_{20}$	313	319.3	3.71	46.0
$Fe_{44}Pd_{36}P_{20}$	316	319.7	2.25	33.6
$Fe_{40}Pd_{40}P_{20}$	273	284.1	6.10	72.5
$Fe_{28}Pd_{52}P_{20}$	77	79.3	2.28	60.2

agreement with Mössbauer effect results, in view of the experimental uncertainty in the exact composition of the foils. Results of the frequency measurements for two foils in this range are shown in Figs. 25 and 26. These curves are typical of a ferromagnetic material, in which a large and sudden decrease in inductance at the Curie point is observed. This change occurs over a temperature interval of a few degrees, in agreement with Mössbauer results.

For the alloys of composition $x \leq 24$, a dramatic change in the nature of the effect is seen. The change in frequency or inductance shown in Fig. 27 is exceedingly small compared to the sample with only 4% more Fe. For the alloys with even less Fe, the frequency change is so small it is difficult to accurately determine the transition point. Alloys with $x = 13$, 14 and 20 were measured with the inductance bridge described in section II. Approximately 100 mg of each sample was used. Typical results are shown in Fig. 28 for the $Fe_{14}Pd_{66}P_{20}$ alloy. The curve shown is a reproduction of the tracing of an X-Y recorder, in which the vertical scale is the bridge output and the horizontal scale the resistance of a calibrated Germanium crystal which measures the temperature. The bridge was operated at maximum sensitivity by using the lock-in amplifier in the phase mode at the maximum gain feasable. In the region 22-25°K, a very slight imbalance in the bridge is observed, superimposed on

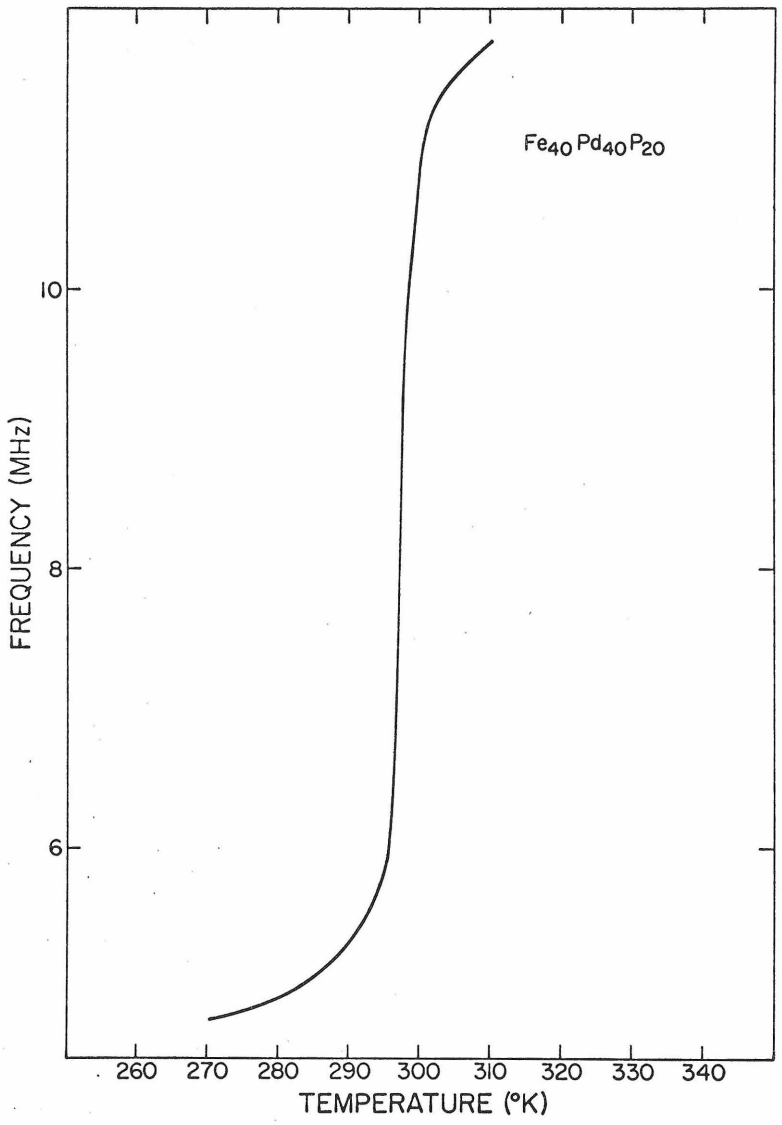

Fig. 25. Frequency measurement for the $Fe_{40}Pd_{40}P_{20}$ alloy.

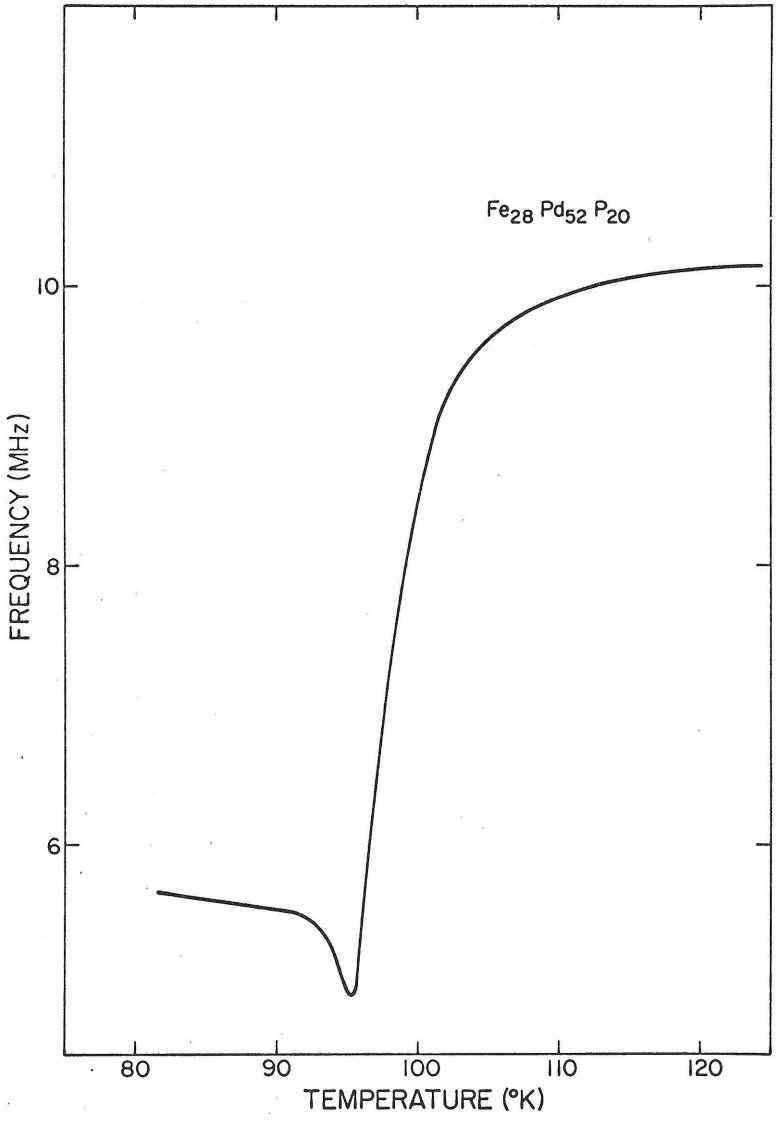

Fig. 26. Frequency measurement for the $Fe_{28}Pd_{52}P_{20}$ alloy.

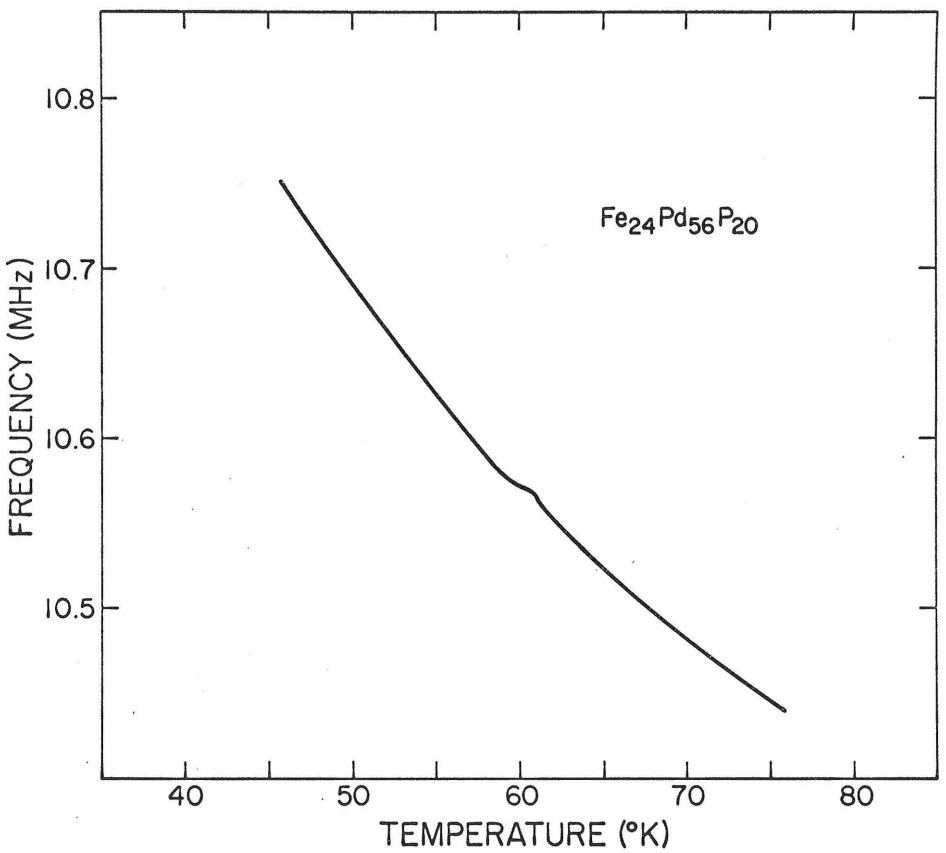

Fig. 27. Frequency measurement for the $Fe_{24}Pd_{56}P_{20}$ alloy.

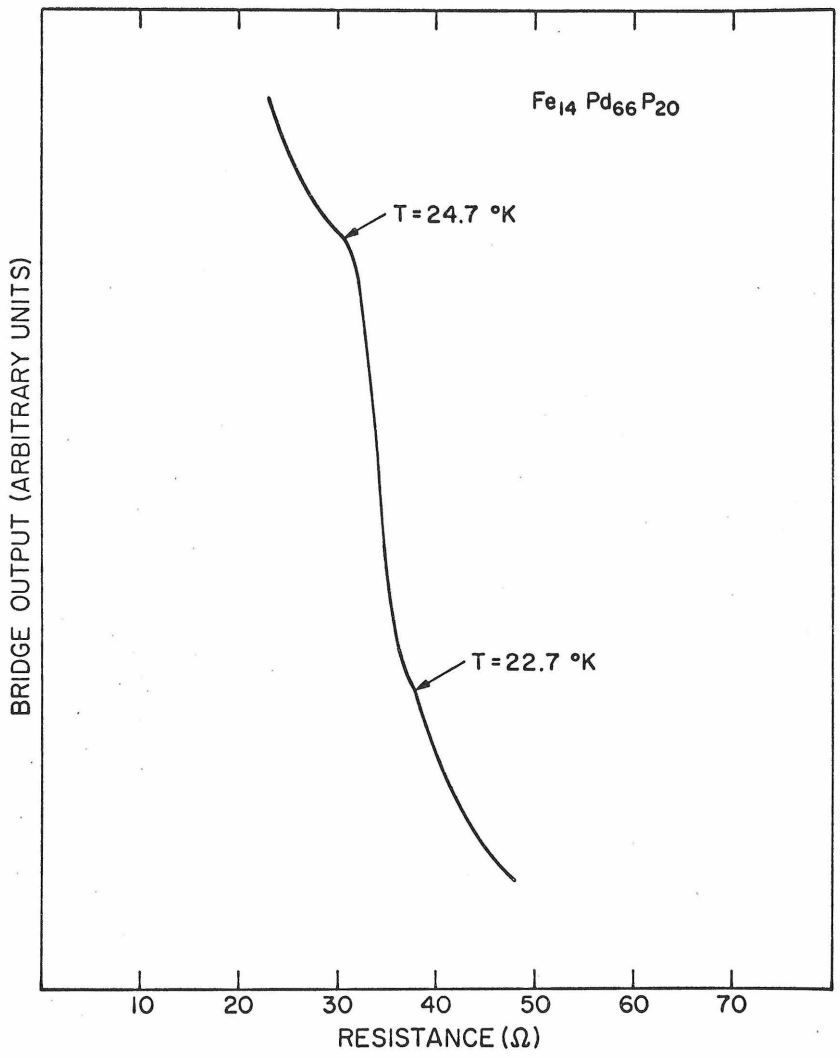

Fig. 28. Output of inductance bridge vs. temperature for the $Fe_{14}Pd_{66}P_{20}$ alloy.

the normal slowly varying signal due to the temperature dependence of the other elements in the bridge. This latter effect is evident because of the very high sensitivity used. A similar effect was seen for the $Fe_{13}Pd_{67}P_{20}$ alloy at a slightly lower temperature, but no effect in the temperature range $4.2^{o}K$ - $30^{o}K$ was observed for the $Fe_{20}Pd_{60}P_{20}$ alloy.

The transition temperatures determined by these three methods are shown in Fig. 29. The most significant feature of the variation with Fe concentration is the sharp change in slope at about $x \simeq 26$. If the upper portion of the curve were extrapolated, it would appear that there would be no magnetic transition below approximately 25% Fe.

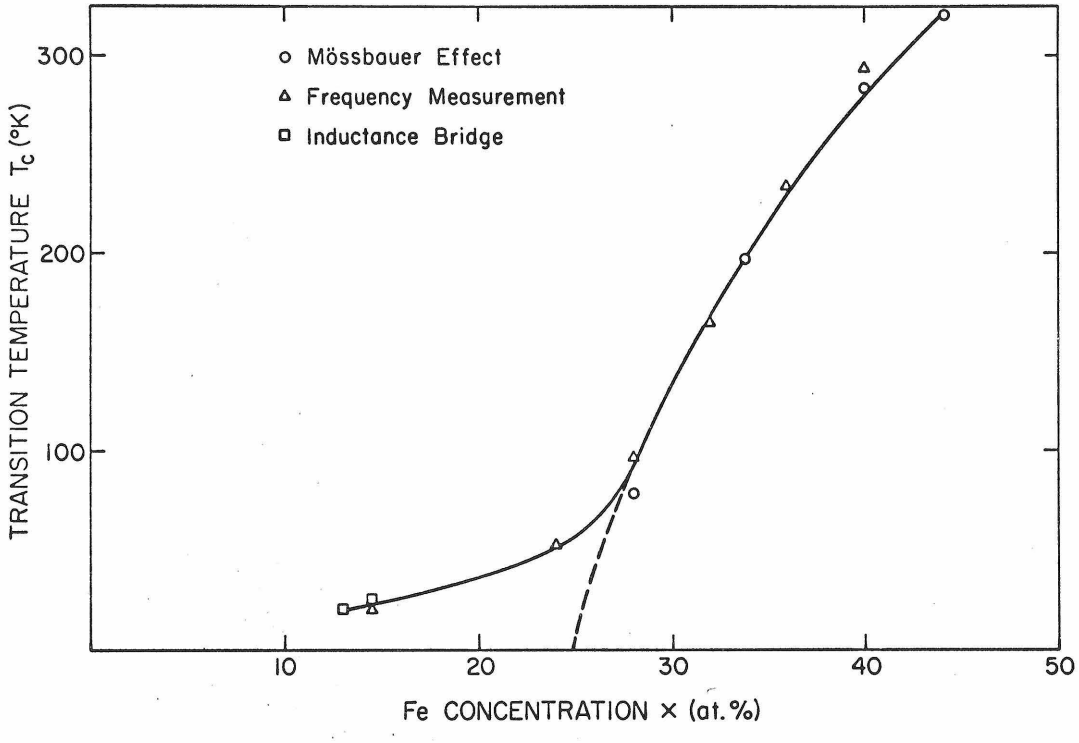

Fig. 29. Magnetic transition temperature vs. iron concentration for the amorphous $Fe_xPd_{80-x}P_{20}$ alloys.

V. DISCUSSION

A. Mössbauer Effect

1. Electronic Configuration of Fe in the Fe-Pd-P Amorphous Alloys

The isomer shift and hyperfine field found from Mössbauer effect are valuable indications of the electronic state of the Fe atoms. As can be seen from Fig. 6, the average isomer shift is almost independent of concentration, with a value of $0.125 \pm .005$ mm/sec relative to Fe Pd. Furthermore, the spread in isomer shifts is not too large, since the Mössbauer data can be fitted well by assuming all Fe atoms have identical isomer shifts. The fact that a positive value relative to Fe Pd is obtained means that the total electronic density at the nucleus is less than in these alloys. It is useful to place this value of isomer shift on the diagram of Walker et al.[41] Using Hartree-Fock wave functions for the core electrons and the Fermi-Segré-Goudsmit formula to estimate the 4s electron contribution to the electronic density at the nucleus, Walker et al have proposed a calibration of isomer shift for Fe compounds. On the vertical axis of Fig. 30 the total electronic density at the nucleus is plotted from these calculations for several different atomic configurations. This is calibrated against isomer shift by measuring the most ionic compounds corresponding to divalent $Fe^{+2}(3d^6)$

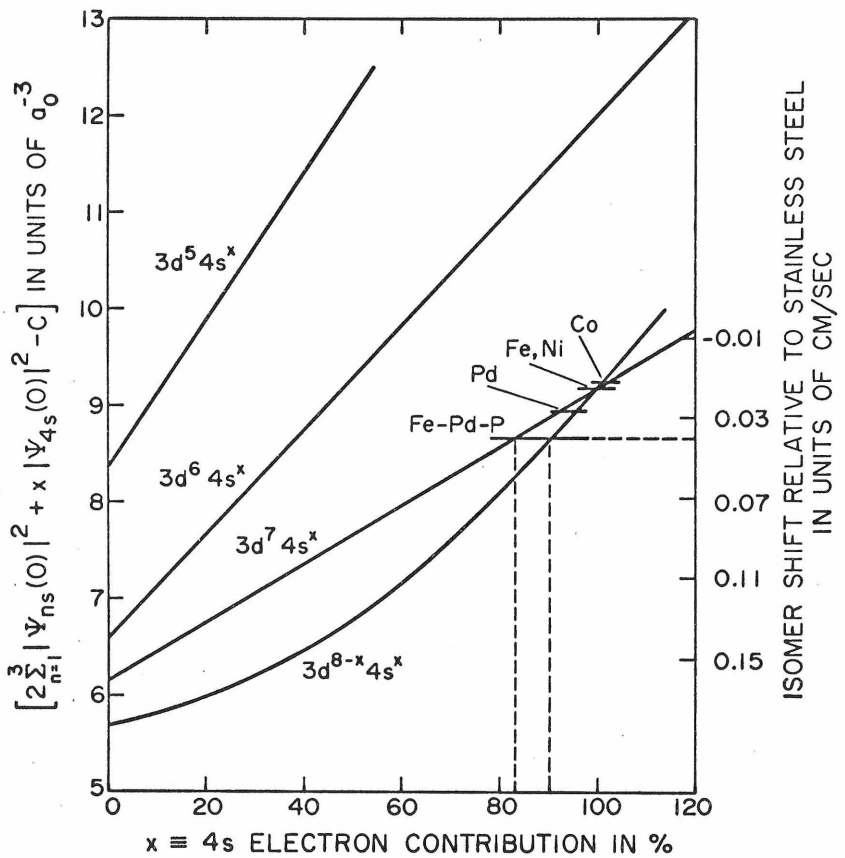

Fig. 30. Isomer shift of Fe^{57} in various configurations. (Ref. 41)

and trivalent $Fe^{+3}(3d^5)$. These values are compared with Watson's Hartree-Fock calculations of $2\sum_{n=1}^{3}|\Psi_{ns}(0)|^2$ for the $3d^6$ and $3d^5$ configurations. The contribution from the 4s conduction electrons is estimated from $x|\Psi_{4s}(0)|^2$, the value obtained from the Segrè-Goudsmit formula for one 4s electron outside the $3d^n$ configuration. For the Fe-Pd-P amorphous alloys, the value of isomer shift (relative to stainless steel) is drawn as a horizontal line at + 0.40 mm/sec. (To convert from a Pd source to a stainless steel source, we use the fact[42] that the Fe^{57} gamma ray in Pd has +0.275 mm/sec more energy than in stainless steel). Provided we know the 3d electron configuration we can determine the 4s contribution, and vice versa.

Since the Fe-Pd-P alloys are metallic, it is probably a good approximation to assume that the Fe atom is not far from being electrically neutral. It is well known that in most alloys transition metals can be assigned a valence of zero. This means that the appropriate electronic configuration would be $3d^{7.1}4s^{0.9}$. On this same diagram pure Fe or Fe in Fe Pd would correspond to a configuration of roughly $3d^74s^1$. For pure Fe, this assignment agrees well with band structure calculations[43].

The other plausible configuration $3d^74s^x$ yields a configuration $3d^74s^{0.83}$. It seems unlikely,however, that in the presence of the

electron donor phosphorus the total electronic charge would decrease. It is interesting to note that the value of isomer shift falls in the range assumed by Fe in most transition metals, as indicated in Fig. 30.

According to Wertheim et al[37], an increase of 0.2 electron to the 3d shell of Fe should lead to a decrease in hyperfine field of about 26 kOe. Since $H_o \sim 290$ kOe for the Fe-Pd-P alloys, as compared to 340 kOe for Fe and 295-335 kOe for Fe Pd alloys, both isomer shift and hyperfine field results are consistent with the idea that in these amorphous alloys the electronic moment has been only slightly reduced by an additional filling of the 3d shell. It is quite reasonable to suggest that the mechanism for this effect is the ability of phosphorus, with five valence electrons, to act as an electron donor. In a band picture, phosphorus contributes electrons which fill the d band of Fe (and Pd); or locally, s or p electrons from phosphorus become convalently mixed into the "magnetic" electron shells of Fe. The increased shielding due to these additional 3d electrons causes the electron density at the nucleus to be reduced, thereby increasing the isomer shift. The magnetic moment is also slightly reduced because the number of holes in the Fe 3d shell has decreased.

2. Asymmetry of Mössbauer Spectra

The electronic structure for Fe in the amorphous alloys just proposed has an interesting and quite direct verification in the fine detail of the Mössbauer spectra. As can be seen in Figs. 11 or 13, the discrepancy between experimental data and fitted curve is such that in all cases the peak at highest energy (furthest right) is slightly deeper and rises more rapidly than the peak at lowest energy (furthest left). These results are consistent with the model just proposed. In fitting the experimental data, it was assumed in section IV that the isomer shift for all the Fe atoms was the same. This forced the theoretical function to be symmetric about the average isomer shift. In reality, however, it seems likely that a correlation between isomer shift and hyperfine might arise. From our previous remarks, this would come about as follows: We assume that one of the largest effects upon hyperfine field comes from covalency effects from immediate phosphorus neighbors. Because the phosphorus atoms are somewhat randomly distributed, some Fe atoms are surrounded by a higher local concentration of P atoms than others. For these atoms, the hyperfine field and charge density at the nucleus are reduced more than the average. Fe sites with larger hyperfine fields therefore have smaller isomer shifts. The net effect is a better lining up of the right hand peaks and a relative

broadening of the left hand peaks.

To include this effect in the calculations to a first approximation one can assume a dependence of isomer shift on hyperfine field as follows:

$$\delta(H) = \delta(H_o) + \gamma(H-H_o) \qquad (41)$$

In terms of the model just proposed, γ should be negative. Sites with larger than average hyperfine fields should have smaller than average isomer shifts.

The additional parameter γ can be included in the least squares analysis described earlier. There is a noticeable improvement in the fitting of the outer peaks, as can be seen in Fig. 31. The other parameters remained essentially unchanged. As predicted, the coefficient γ is negative and increases in magnitude with decreasing Fe concentration. This is evident in Fig. 31, since the asymmetry effect is more pronounced in the lower Fe concentration samples. This result may suggest that the charge disturbance near the phosphorus atoms tends to increase in the less concentrated alloys, a topic which will be discussed in detail later.

3. Variation of Hyperfine Field Distribution with Fe Concentration

a. Discussion of possible Pd d band polarization

The nature of the hyperfine field distribution in the amorphous

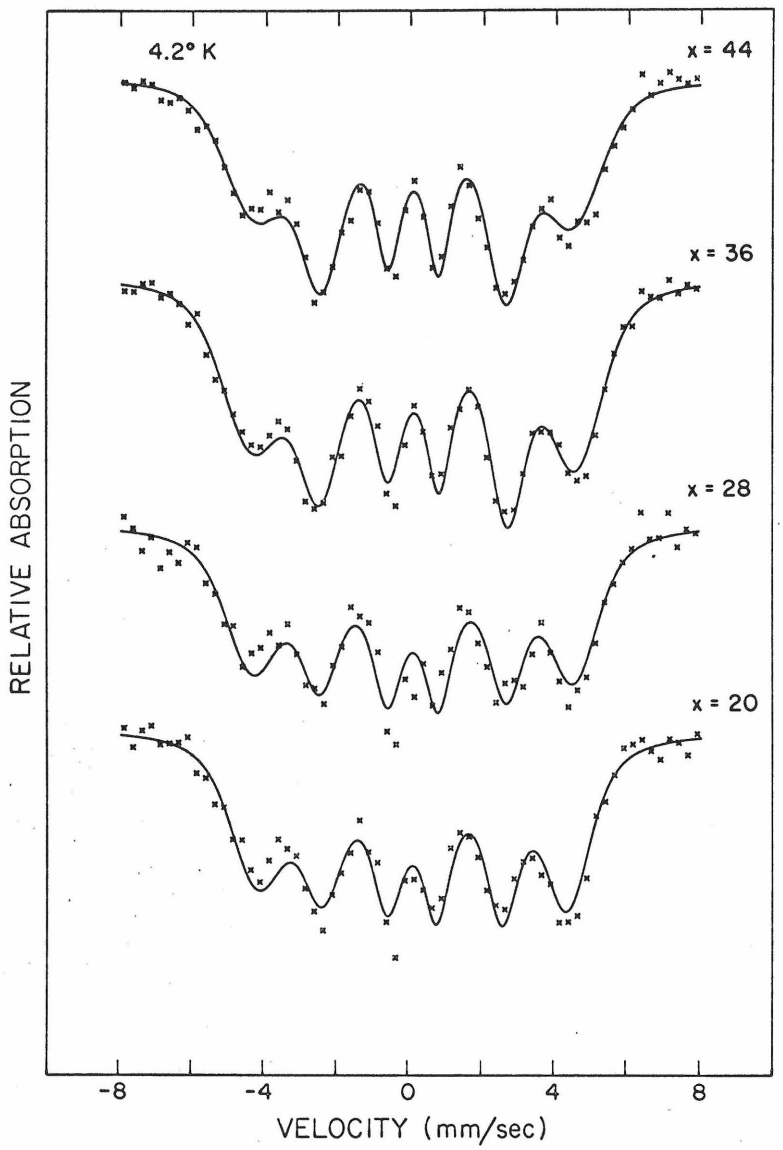

Fig. 31. Illustration of the correlation between isomer shift and hyperfine field described by Eq. (41).

Fe-Pd-P alloys is quite different from that observed in crystalline Fe Pd alloys[38, 44]. In a series of such alloys ranging in composition from $Fe_{0.4}Pd_{99.6}$ to $Fe_{43}Pd_{57}$, measurements of the Mössbauer spectrum at 4.2°K (well below all Curie points) showed that the hyperfine field was essentially unique - that is, all six lines in the spectrum had essentially equal linewidth, which was the same as that observed above the Curie point. A rapid increase in the magnitude of the hyperfine field was observed in the range 0-12% Fe, after which the value leveled off at approximately 335 kOe. These observations were shown to be consistent with a long range polarization of the Pd conduction band. This polarization varies extremely slowly over distances compared to the average spacing between Fe atoms (thus giving a unique field), and does not oscillate in sign. From neutron diffraction experiments Low[45] has estimated the range of this spin polarization to exceed 10Å in $Fe_{0.25}Pd_{99.75}$. Although a very large moment per Fe atom is observed ($\sim 10\ \mu_B$), the moment of the Fe atom itself is only about $3\mu_B$. The remainder resides on the polarized Pd atoms. The maximum value of moment per Pd atom is only about $0.06\ \mu_B$, but the extremely long range interaction encompasses many Pd atoms (~ 100).[45]

These results are pertinent to the discussion here because the possibility of this type of polarization has been suggested to explain

the high value of μ_{eff} in the Fe-Pd-P alloys[9] and also in related amorphous Pd-Si alloys with dilute Fe[7] or Co[46] impurities. Since $\mu_{eff} \sim 6\mu_B$ in the $Fe_xPd_{80-x}P_{20}$ alloys with $x \gtrsim 25$, it is inconsistent to assume such a large moment could exist on the Fe atom itself.

To contrast the Fe Pd results with those obtained here for the amorphous Fe-Pd-P alloys, the most obvious difference is the very broad distribution of hyperfine fields which exists in the amorphous material. On the scale of Fig. 12, the distribution function for a typical Fe Pd alloy would be essentially a delta function in comparison with those shown. Secondly, there is a pronounced increase in the width of this distribution with increasing Fe concentration for the amorphous alloys. The simple model presented in section IV showed that a finite width was expected, merely because of the random fluctuations in local atomic arrangement. It was also suggested that one of the dominant effects to be considered in the distribution of hyperfine fields was the electron transfer effect from phosphorus. Since the P content remains constant, this effect alone cannot explain the increased width observed in the higher Fe concentration alloys.

As mentioned in section III, there are also contributions to the hyperfine field from the conduction electrons, which may become

polarized through the RKKY[47-49] interaction and contribute to the observed hyperfine field. In Fe Pd alloys, this polarization, which normally oscillates in sign with distance from the magnetic moment, becomes so enhanced by the exchange interaction that it no longer oscillates and acquires a very large range[50]. For a long range interaction of this type, the hyperfine field distribution remains very narrow and merely changes its position with varying concentration.

The broad hyperfine field distributions shown in Fig. 12 argue strongly against a long range polarization of this type. There are also several other reasons for thinking that polarization of the Pd matrix does not play a large role in these amorphous alloys. First of all, the presence of phosphorus as an electron donor should greatly reduce the polarizability of the Pd matrix. It is a well documented fact that Pd tends to assume a diamagnetic state in alloys[51]. Pd often acts in alloying as if 0.6 holes per Pd atom existed in its 4d band. In the Pd H system, for example, at a ratio H/Pd = 0.6 the Pd 4d band appears to be completely full, and the material is diamagnetic[52]. This effect is also observed when many other higher valence elements are substituted into Pd[51]. Specific heat measurements indicate a low density of states in these alloys. One can also substitute Fe for Pd in Pd H, up to approximately 10% Fe[52]

A Mössbauer study[53] of two such alloys showed a considerably reduced transition temperature relative to an Fe Pd alloy of the same percentage Fe. Hyperfine field and isomer shift results showed that the Fe atoms retained approximately their same state as in Fe Pd, however. It is quite interesting to note that the μ_{eff} obtained from susceptibility measurements was essentially constant in the range 0-9% Fe with the large value of 5.7-5.9 μ_B [52], although it was clear that the Pd d band is completely full.

A similar band filling effect of this type might be expected for the Fe-Pd-P alloys, and it is unfortunate that the amorphous range does not extend to lower Fe concentrations. Amorphous $Fe_xPd_{80-x}Si_{20}$ alloys can be made in the dilute range (0-7% Fe), however, and show magnetic properties quite similar to the low Fe concentration Fe-Pd-P alloys (incomplete saturation, high μ_{eff}, diffuse magnetic transition from magnetization measurements). The host $Pd_{80}Si_{20}$ has a very low susceptibility ($\chi \sim 10^{-7}$-10^{-8} emu/g)[54], indicating a filled d-band.

A recent Mössbauer effect study[55] of these $Fe_xPd_{80-x}Si_{20}$ amorphous alloys reaffirmed several of the conclusions reached in section IV. First, a quite symmetric six peak spectrum appeared with no evidence of any quadrupole splitting in the magnetic state. Above the transition temperature, the quadrupole splitting reappeared

(Fig. 32). As a function of temperature, the transition was also found to be relatively sharp.

The width of the hyperfine field distribution was 30-40 kOe, and a simple Gaussian distribution of fields fits the data quite well. Thus in these alloys, the narrowing trend shown in Fig. 12 continues until a point is reached where the width is caused only by the kind of effects outlined in section IV.

b. Nature of the hyperfine field distribution: relation to Kondo effect

In an attempt to put the discussion of P(H) on a more quantitative basis, we can use the following model: considering the hyperfine field H as a random variable, we separate the contributions to H into two categories:

$$H = H_1 + H_2 \tag{42}$$

where H_1 represents contributions which are approximately independent of the Fe concentration x, and H_2 the factors which may change appreciably with x. Since the Fe moment appears to be almost constant in magnitude over the composition range, the second group comprises basically contributions from the conduction electrons.

Included in H_1 are the dominant core polarization term[26]

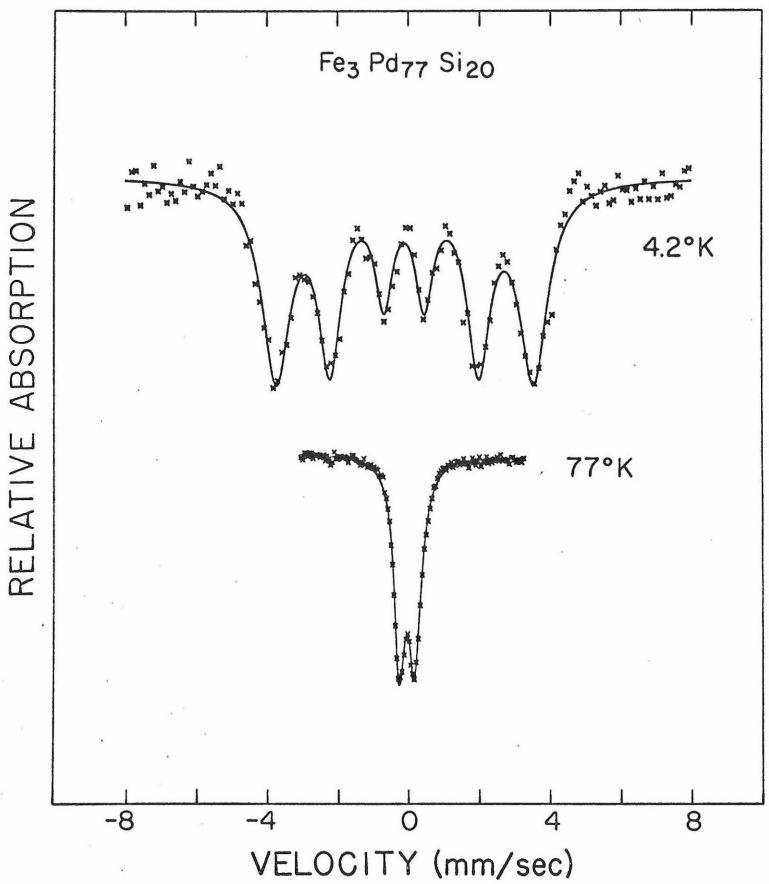

Fig. 32. Mössbauer spectrum of an amorphous $Fe_3Pd_{77}Si_{20}$ alloy.

and the smaller effects due to possible orbital and dipolar contributions. The latter should not depend greatly on x. Also in this category are the electron transfer effects from phosphorus discussed in section IV. It was argued there that the probability distribution from these contributions should have the approximate form

$$P_1(H_1) = \frac{1}{\sqrt{2\pi\Delta_1^2}} \exp\left[-\frac{(H_1-\bar{H}_1)^2}{2\Delta_1^2}\right] \tag{43}$$

To calculate $P_2(H_2)$ we need a model which represents the most relevant interactions in producing conduction electron spin polarization. One mechanism is the RKKY interaction[47-49] between the Fe moments and the conduction electrons. Since the arrangement of the Fe atoms is governed by the radial distribution function, H_2 should be statistically independent of H_1. In such a case the probability distribution for $H = H_1 + H_2$ can be obtained from a convolution of the separate probability distribution functions:

$$P(H) = \int P_1(H')\, P_2(H-H')\, dH' \tag{44}$$

The response of a free electron gas to a point magnetic moment leads to an oscillatory spin polarization (RKKY interaction):

$$\Phi_{RKKY}(r) = \rho_\uparrow(r) - \rho_\downarrow(r) = \rho_o \left[\frac{\cos 2k_F r}{(2k_F r)^3} - \frac{\sin 2k_F r}{(2k_F r)^4}\right] \tag{45}$$

where r is the distance from the magnetic moment and k_F is the Fermi wave vector. The RKKY interaction produces a spatially nonuniform spin polarization, and therefore from Eq. (25) leads to a broadening of the hyperfine field distribution. This effect is quite evident in NMR studies, and was first observed in dilute Cu Mn alloys[56].

In Fig. 12 the width of the central peak in P(H) increases by roughly a factor of two, which means that broadening effects due to conduction electron polarization are comparable to those from other factors. The RKKY interaction is capable of effects of this magnitude, as was shown in Mössbauer experiments by Stearns and Wilson[57]. By introducing impurities in the Fe lattice, they were able to verify the oscillatory nature of the conduction electron spin polarization, although the magnitude was roughly seven times that predicted by Eq. (45). This was presumably due to the neglect of electron-electron interactions in the analysis which leads to the RKKY form factor. It was found that the spin polarization from one Fe atom at a nearest neighbor Fe nucleus leads to a hyperfine field (through Eq. (25)) of approximately 26 kOe. It is clear, therefore, that in the concentration range of the Fe-Pd-P alloys these effects can produce a broadening of sufficient magnitude to agree with experimental results.

A calculation of $P(H_2)$ would then proceed as follows: knowing ρ_o, k_F, and the Fe arrangement, we can calculate $P(H_2)$ using Eq. (45). Only the average distribution of Fe atoms can be obtained from the radial distribution function, so the actual calculation would have to consider all possible Fe arrangements weighted with the appropriate probability. This type problem is well suited to numerical methods such as Monte Carlo techniques.

There is one other factor to be considered before embarking on such an approach - the short mean free path of the conduction electrons in a disordered structure. It is known that the amplitude of the magnetization oscillations decreases with decreasing mean free path. This effect can be described qualitatively by the intuitive formula:[58]

$$\Phi(r) = \Phi_{RKKY}(r) \exp(-r/\Lambda) \qquad (46)$$

where Λ is the mean free path for conduction electrons. This effect was verified by Heeger et al[59], who observed a decrease in NMR linewidth when nonmagnetic impurities (which decrease the mean free path) were introduced into the Cu Mn system. In amorphous materials, the mean free path must be extremely short. It can be estimated from the simple conductivity formula

$$\sigma = \frac{n e^2 \tau}{m} \qquad (47)$$

(The measured resistivity of the Fe-Pd-P alloys is in the range 160-180 $\mu\Omega$ -cm). The mean free path Λ is simply $v_F \tau$. Assuming that n and v_F are characteristic of a noble metal such as Cu, we find that $\Lambda \sim 3\,\text{Å}$ (on the order of the interatomic spacing). The range of the RKKY polarization should be drastically reduced in such a situation, and should not extend appreciably beyond nearest and next nearest neighbors.

The complicated numerical approach outlined above, therefore, is not necessary. The arguments of section IV can be applied immediately, with the only difference being that α in Eq. (28) comes from the RKKY spin polarization, and n is now the number of Fe nearest neighbors. Again the probability distribution should have a form similar to the Gaussian distribution, with average value $\bar{H}_2$ and standard deviation Δ_2.

In the convolution of $P_1(H_1)$ and $P_2(H_2)$ according to Eq. (44), the resulting shape will again be approximately Gaussian with $\bar{H} = \bar{H}_1 + \bar{H}_2$, $\Delta = \Delta_1 + \Delta_2$. If the RKKY polarization is basically limited to nearest neighbors, $\Delta_2 \alpha \sqrt{x(.8-x)}$ for the $Fe_xPd_{80-x}P_{20}$ alloys (from the binomial distribution). Therefore,

$$\Delta H = \Delta_1 + \Delta_2 \sqrt{x(.8-x)} \qquad (48)$$

The trend in ΔH shown in table IV can be well approximated by such a formula with $\Delta_1 = 20$ kOe and $\Delta_2 = 145$ kOe.

One feature of the probability distributions in Fig. 12 which cannot be explained by this simple model is the large "tail" effect seen at low fields. The reason for this discrepancy can be understood as follows: The calculation just outlined would predict the distribution of saturation fields which exist in the material. To get the actual P(H) distribution, we must consider the effective fields (dynamical effects) which act on the magnetic moments. For example, in an effective field theory, the actual hyperfine field measured corresponding to a given magnetic moment μ is

$$H = H_{sat} \quad B_s\left(\frac{\mu h}{kT}\right) \qquad (49)$$

where h is the effective(Weiss)field at that site. Our model just proposed has really been concerned with $P(H_{sat})$. In order to obtain P(H), we must in addition know P(h).

In the amorphous Fe-Pd-P alloys the existence of a Kondo type resistivity minimum implies that there are spins in low effective fields, even in the concentrated alloys. It has been shown theoretically that the effect of spin-spin correlations is to produce an internal

field which suppresses the Kondo effect. If the spins are locked into parallel alignment, the spin-flip scattering process (which gives rise to the resistivity minimum) cannot occur. The appearance of the "tail" on the observed low field P(H) distribution is a confirmation of the possibility of a Kondo effect in these amorphous alloys. These smaller hyperfine fields come from Fe atoms which reside in low effective fields and are weakly coupled. These moments are quasi-free and can participate in the spin-flip scattering.

4. Variation of Hyperfine Field Distribution with Temperature

According to the discussion of section III, the average hyperfine field should be proportional to the zero field magnetization of the sample. The complications which sometimes arise from differences in host-impurity and host-host exchange interactions should not enter here, since only the Fe atoms appear to have moments and are exchange coupled. In Figs. 33 and 34 the reduced (average) hyperfine field is plotted versus the reduced temperature for two compositions, along with the molecular field predictions for several values of S. No special significance should be attached to the fact that the classical result ($S = \infty$) best agrees with the data. The value $S = 1$ should actually be used in the comparison, since the moment per Fe atom is about $2\,\mu_B$. The molecular field theory results are of

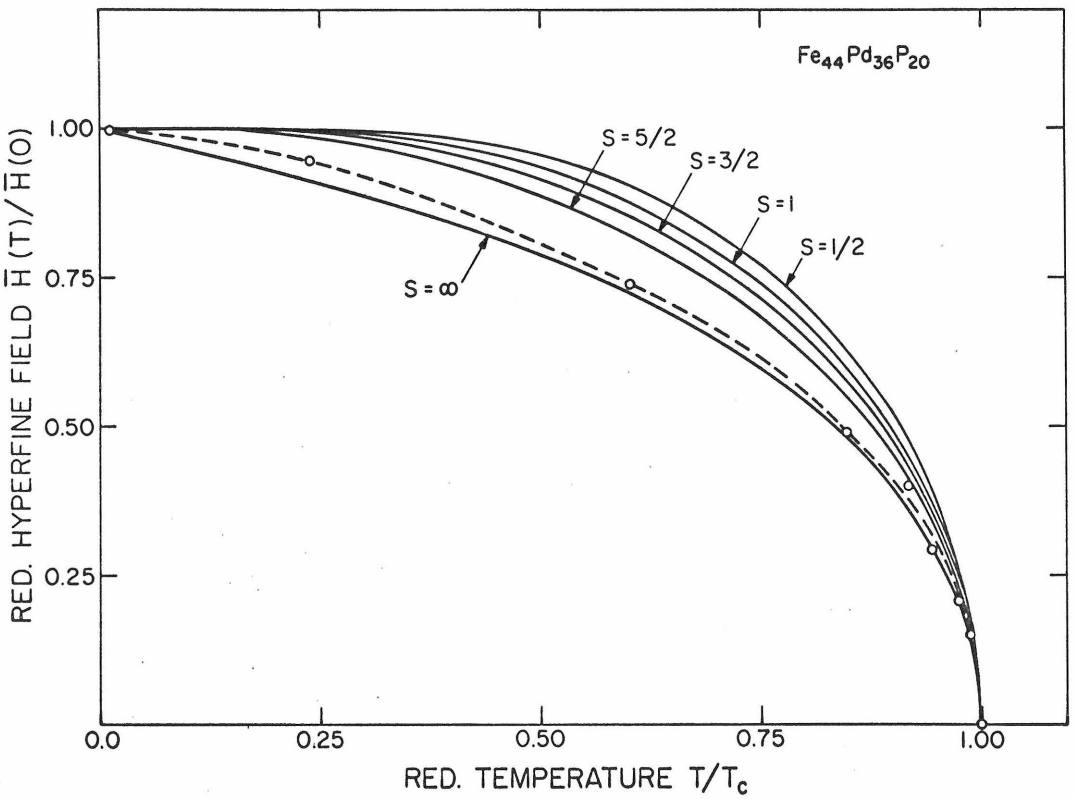

Fig. 33. Reduced (average) hyperfine field vs. temperature for the $Fe_{44}Pd_{36}P_{20}$ alloy (dashed line). The solid curves are the molecular field approximation results for different spin values.

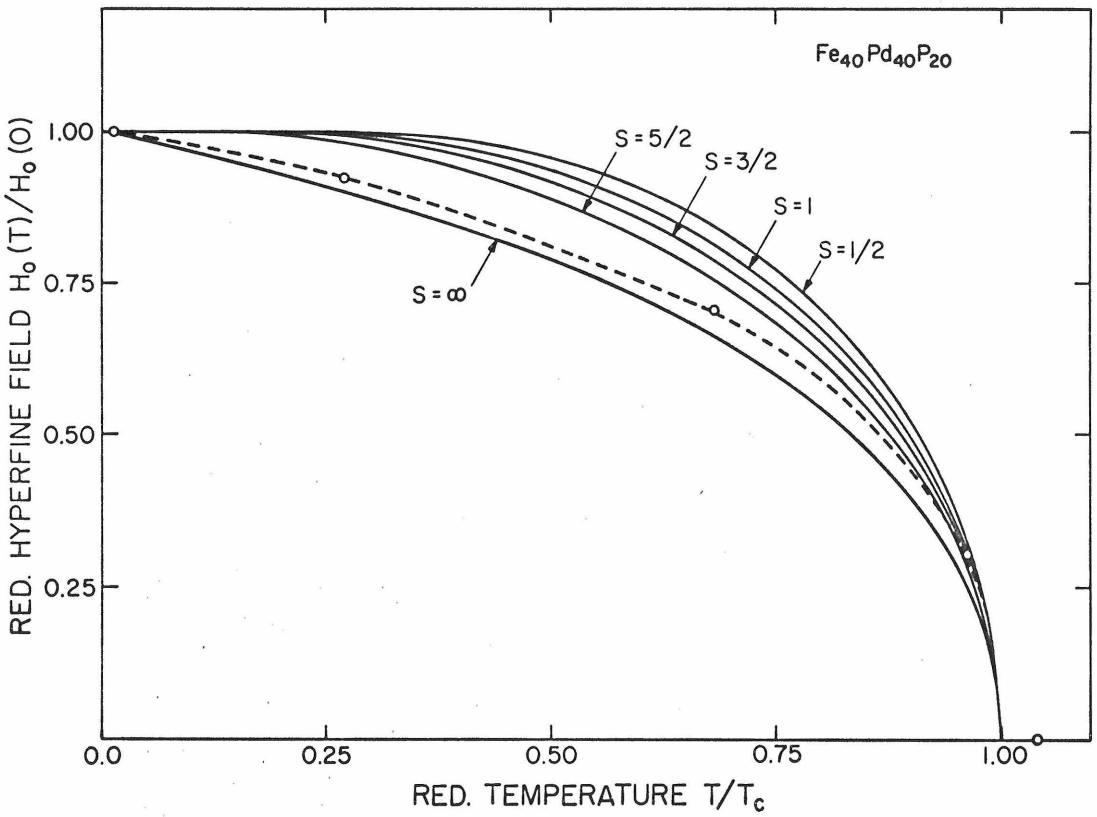

Fig. 34. Reduced (average) hyperfine field vs. temperature for the $Fe_{40}Pd_{40}P_{20}$ alloy (dashed line).

interest because Fe follows qualitatively the theoretical curve for $S = \frac{1}{2}$ [60], while the magnetization in Fe Pd alloys is in fair quantitative agreement for $S = 1$ for all but the lowest temperatures [29]. The main point of interest in the experimental data is the sharp decrease in hyperfine field near T_c.

If the hyperfine field at each Fe site followed exactly the same temperature dependence, then the quantity $\Delta H(T)/\bar{H}(T)$ would be independent of temperature. As shown in Fig. 35, this statement is true only for sufficiently low temperatures $(T/T_c \lesssim 0.5)$. As the temperature approaches T_c, $\Delta H/\bar{H}$ increases rapidly. The nature of this effect is not unique to amorphous materials. Although $\Delta H \sim 0$ for crystalline Fe Pd alloys at temperatures well below T_c, a gradual broadening of the outer peaks is noted as the temperature increases. Near the Curie point, the spectrum is smeared into one broadened Lorentzian whose excess linewidth is proportional to the average hyperfine field [61]. In contrast, the six peaks in Mossbauer spectrum of a high purity Fe foil remain sharp right up to T_c. There are two possible explanations for this effect: Due to the Fe concentration fluctuations across the sample, there may exist a range of Curie temperatures in the material. This would result in a "tail" effect when the hyperfine field is plotted near T_c; or it may arise

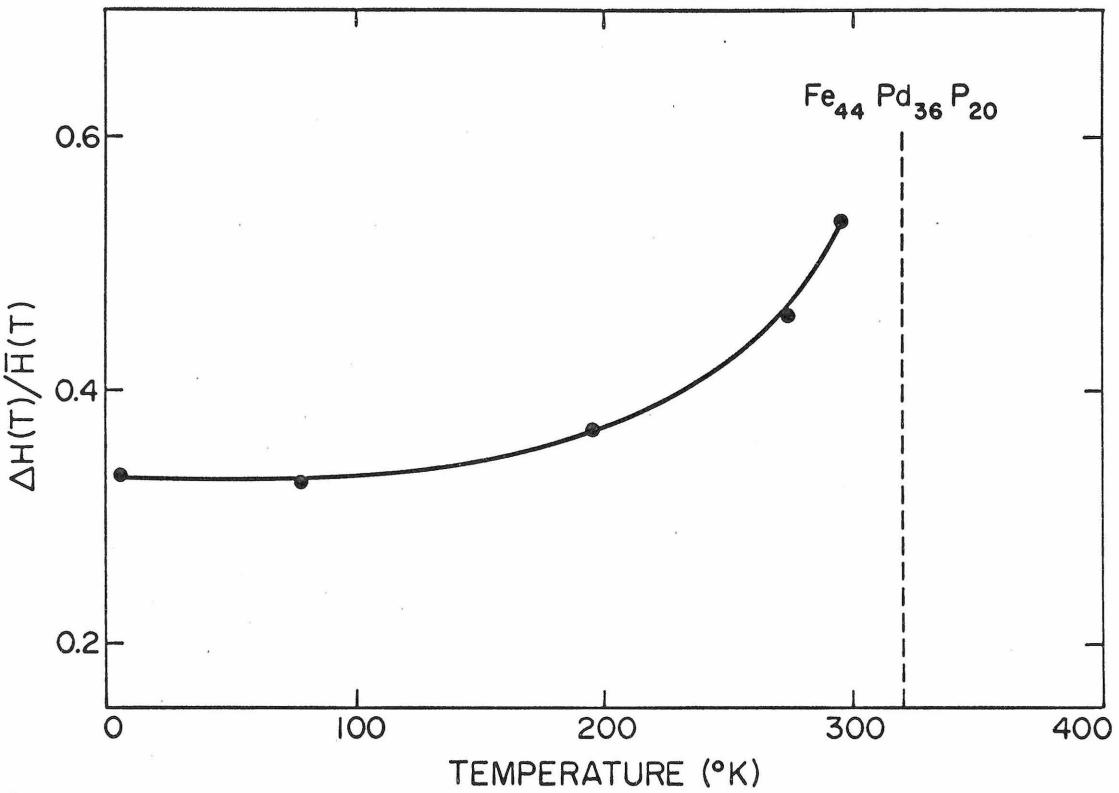

Fig. 35. Temperature dependence of $\Delta H(T)/\bar{H}(T)$ for the $Fe_{44}Pd_{36}P_{20}$ alloy. The transition temperature is indicated by the dashed line (320°K).

in completely homogeneous, well annealed samples if the temperature dependence of the hyperfine field is site dependent. By this we mean that Fe atoms which are more tightly coupled by exchange interactions (those which happen to have more Fe neighbors than others) exhibit a slower decrease in hyperfine field with temperature. The latter explanation seems to hold in Fe Pd alloys, since Craig et al[29] have shown that the transition is quite sharp - no "tail" effect is seen.

In the amorphous Fe-Pd-P alloys, the calculations near T_c of section IV indicate a width of only a few degrees for the data of Fig. 35. This cannot account for the increase in $\Delta H/\bar{H}$ beginning at approximately $T/T_c \sim 0.5$. Hence it must also be true for the amorphous alloys that the magnetization is site dependent.

Along this line, Trousdale et al[61] have discussed this effect for a $Fe_{13}Pd_{87}$ alloy in terms of a cell model in which the statistical fluctuations in Fe concentration are taken into account. The exchange interactions in a cell as well as between neighboring cells are treated within a molecular field approximation. This approach could possibly be extended to the amorphous alloys, but the lack of cubic symmetry and detailed structive information would make such an approach quite difficult.

5. Variation of Quadrupole Splitting with Fe Concentration

At first thought it is difficult to assess the meaning of the increase

in quadrupole splitting with decreasing Fe concentration shown in Fig. 7. Assuming that the short range order remains constant, the only change is to gradually replace Pd by Fe. Since the main electrostatic effects are due to phosphorus (because of its large charge contrast), and its concentration is fixed, this variation may seem quite puzzling. The discussions of the previous sections show how a possible resolution of this question may be achieved. From the isomer shift and hyperfine field results, the electronic state of the Fe atoms remains roughly unchanged throughout the composition range. However, it seems reasonable to assume that the 4d shell of Pd is full. If we think of phosphorus as an electron donor to palladium, then the electron transfer depends only on the concentration of Pd. Hence the local charge perturbation should be proportional to (.8-x). Since electric field effects are proportional to this quantity, $q(x) \alpha (.8-x)$. Actually this predicts that the quadrupole splitting would vanish at $x = .8$, whereas in reality we would undoubtedly have a small quadrupole splitting even in an amorphous $Fe_{80}P_{20}$ alloy. Thus we should write

$$\left| \tfrac{1}{2} e^2 q Q \right| = Q_o(.8-x) + Q_1 \qquad (50)$$

Fig. 36 shows the curve for $Q_o = 1.0$ mm/sec, and $Q_1 = 0.2$ mm/sec.

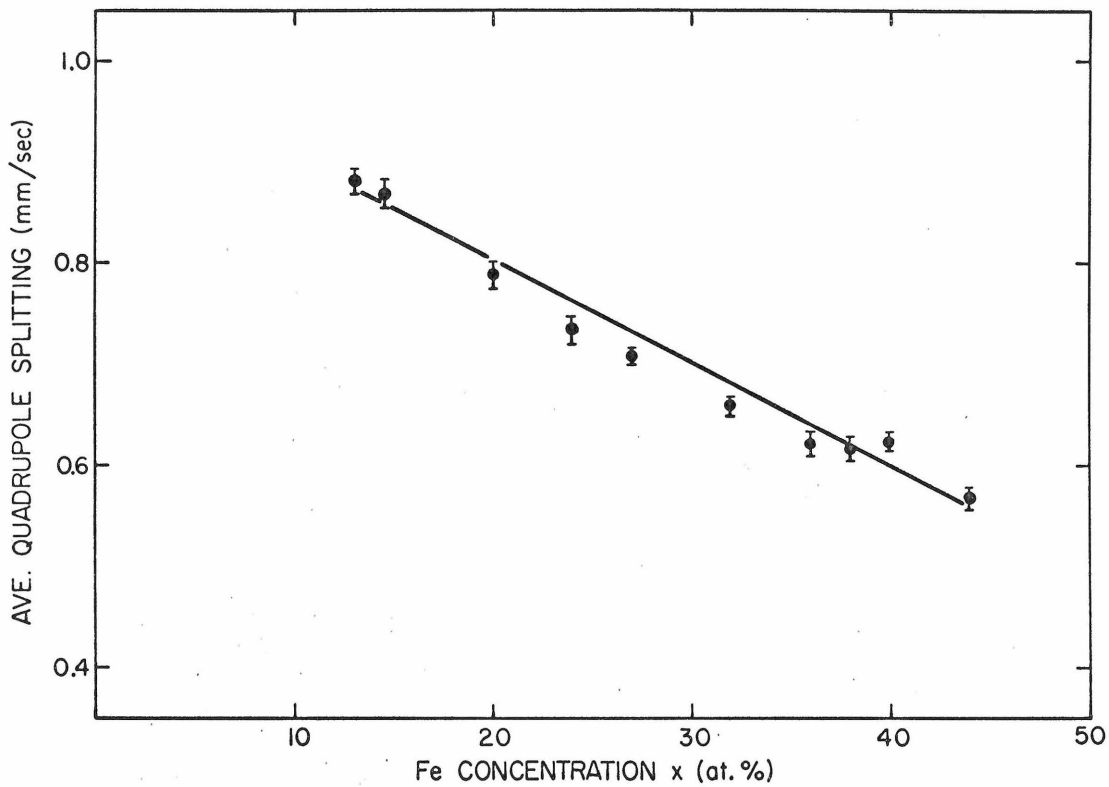

Fig. 36. Quadrupole splitting vs. iron concentration according to Eq. (50).

Any numerical agreement with such a simple model is clearly in part fortuitous. However, the model is consistent with the earlier discussion and accounts for an effect which seems quite mysterious otherwise.

6. Structural Considerations

Up to this point the model used to discuss the properties of the Fe - Pd - P alloys has been based on a continuous random type structure, rather than a microcrystalline viewpoint. From x-ray diffraction studies, it is known that if such microcrystals existed, they would be exceedingly small ($\lesssim 20$ Å) [9]. However, x-ray diffraction results are not completely convincing since there are many possible complicating factors in their interpretation. The Mössbauer results presented thus far should be helpful in deciding which is the better point of view, since there is no interference effect from neighboring atoms or crystallites as in diffraction. In the composition range of the Fe-Pd-P amorphous alloys, the equilibrium compounds would contain numerous intermediate phases (the complete ternary phase diagram is not known). Any attempt to fit the Mössbauer data by a superposition of varying amounts of these phases is doomed to failure, however, for several reasons. First of all, the complete lack of quadrupole splitting and near symmetry of the pattern for the magnetic spectra are inconsistent with such a superposition of spectra

corresponding to these individual phases. Fe_3P, for example, has a very complicated and asymetrical pattern with three Fe sites per unit cell. More than 13 peaks can be distinguished in the Mössbauer spectrum of this alloy, which would be expected to be one of the constituent phases in a microcrystalline model. It would be especially difficult to reconcile such a model with the spectrum shown in Fig. 32, which shows that there is essentially only one hyperfine field in the material.

Secondly, the sharp magnetic transition shows that even if microcrystallites of several phases were present, they retain none of the magnetic properties (in particular a characteristic Curie temperature) of the bulk material. It is clear that microcrystallites completely lose their meaning in such a case. Therefore, the model based on a continuous random type structure (with a degree of short range order) that has been used seems to be justified.

B. Magnetic Properties

1. High Fe Concentration Alloys: $x \gtrsim 25$

a. Discussion of magnetization results

From the experimental data presented in section IV, in particular the transition temperature curve of Fig. 27, it seems appropriate to divide the discussion of the magnetic properties of the amorphous

Fe-Pd-P alloys into two sections. In this section we will discuss the alloys with $25 < x \leq 44$. In this range the alloys appear to be good examples of amorphous ferromagnets. Hence they are good candidates for evaluating several recent theories of the magnetization in this type of material. The magnetization measurements of Maitrepierre[9] on two alloys ($Fe_{44}Pd_{36}P_{20}$ and $Fe_{32}Pd_{48}P_{20}$) in this range gave saturation moments of $2.1\mu_B$ and $1.7\mu_B$, respectively. The magnetic transitions were described as not well defined in temperature, with a noticeable "tail" on the magnetization curve covering several tens of degrees. These results are in conflict with Mössbauer effect results which indicate an unchanged moment and a sharp transition.

Both the large "tail" effect and the decreasing moment are now clearly seen to be the result of the fact that large magnetic fields must be applied to saturate the sample. In magnetization measurements, to obtain meaningful results, the sample must be subjected to a large enough field so that it is one single magnetic domain. The magnetization measurements are then made for several values of field, all sufficiently large to achieve the single domain condition. A zero field magnetization can then be determined by extrapolation[60]. It was noted that the Fe-Pd-P alloys were magnetically "hard", and that they did not appear to be saturated in a field of 8.4 kOe.

Nevertheless, conventional extrapolation procedures were used to obtain the saturation moment[9]. If one extrapolates to zero field from a series of unsaturated domain conditions, the moment/atom value obtained will be low. Apparently this is in part the reason for the decrease in moment/Fe atom observed for the $Fe_{32}Pd_{48}P_{20}$ alloy.

The large "tail" effect observed is also an artifact of the method of measurement. Mössbauer results indicate the transition width is on the order of a few degrees. The magnetization results in a field of 8.4 kOe indicate a much more poorly defined transition. To give a quantitative value to the width from the magnetization results, the following calculation was performed: It was assumed that different regions of the sample had different Curie temperatures. These fluctuations were characterized by an average value $\bar{T}_c$ and a standard deviation ΔT_c. A normal or Gaussian distribution of Curie temperatures was assumed, as in section IV.

For each Curie temperature, the reduced magnetization should vary with temperature (according to the molecular field approximation) as [40]

$$\sigma = B_s \left[\frac{3S}{S+1} \frac{\sigma}{\tau} + \frac{g\mu_B H}{kT} \right] \qquad (51)$$

where $\tau = T/T_c$ is the reduced temperature, g is the g-factor which can be taken equal to approximately 2, and H is the applied field (8.4 kOe).

The average (reduced) magnetization per Fe atom is then given by

$$\sigma(T) = \int_0^\infty P(T_c)\, \sigma_{MFA}(T/T_c)dT_c \qquad (52)$$

where $P(T_c)$ is given by Eq. (39). These calculations for the magnetization data of a $Fe_{32}Pd_{48}P_{20}$ alloy in a field of 8.4 kOe yield values of $\Delta T_c \cong 60^\circ K$ and $\bar{T}_c = 180^\circ K$, whereas Mössbauer and frequency measurements (also a zero measurement) yield $\Delta T_c = 2^\circ K$, $\bar{T}_c = 165^\circ K$. Thus the result of the large magnetic field is a tremendous "smearing out" effect on the transition. This result was also noted by Craig et al,[29] who observed that for a $Fe_{2.65}Pd_{97.35}$ alloy, even a small external field (0.5 kOe) considerably smeared out the Curie point, while a field of 20 kOe entirely obscured the transition.

b. Comparison with theoretical treatments

As mentioned previously, the average hyperfine field is a measure of the zero field magnetization of the sample. Hence we can compare directly the experimentally obtained magnetization with that predicted theoretically.

Handrich[62] has recently given a treatment of the amorphous ferromagnet on the basis of the molecular field approximation. Starting from the Heisenberg-Dirac Hamiltonian,

$$\hat{H} = - \sum J_{ij} \bar{S}_i \cdot \bar{S}_j \qquad (53)$$

the amorphous nature of the material is taken into account by allowing random fluctuations in the exchange integrals J_{ij}. It is found that the effect of these fluctuations is to produce the following equation of state for the (reduced) magnetization:

$$\sigma = \tfrac{1}{2} \left\{ B_s \left[(1+\delta)x \right] + B_s \left[(1-\delta)x \right] \right\} \qquad (54)$$

where $x = \frac{3S}{S+1} \frac{\sigma}{\tau}$, $\tau = T/T_c$, and δ is a measure of the fluctuations. For $\delta > 1$ no ferromagnetism exists at any temperature.

A numerical calculation was performed for various values of δ, and is compared with the experimental data in Figs. 37 and 38. The effect of increasing structure fluctuations is a decrease in the hyperfine field, while the Curie point remains unchanged. The magnetization has infinite slope at $T = T_c$. The failure of the theory to account for the low temperature behavior is a characteristic of all molecular field theories, and results from the inability to predict the low temperature excitations (spin waves). Qualitatively, however,

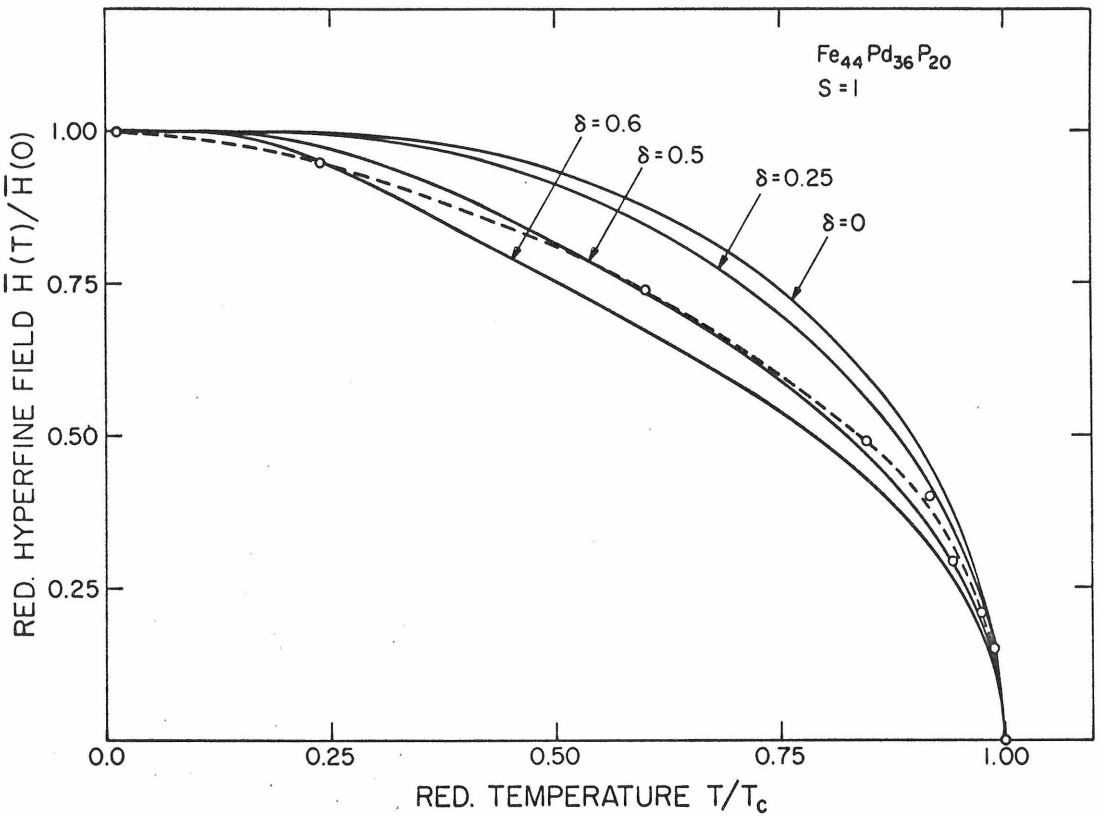

Fig. 37. Comparison of experimental results (dashed line) with Eq. (54) for the $Fe_{44}Pd_{36}P_{20}$ alloy.

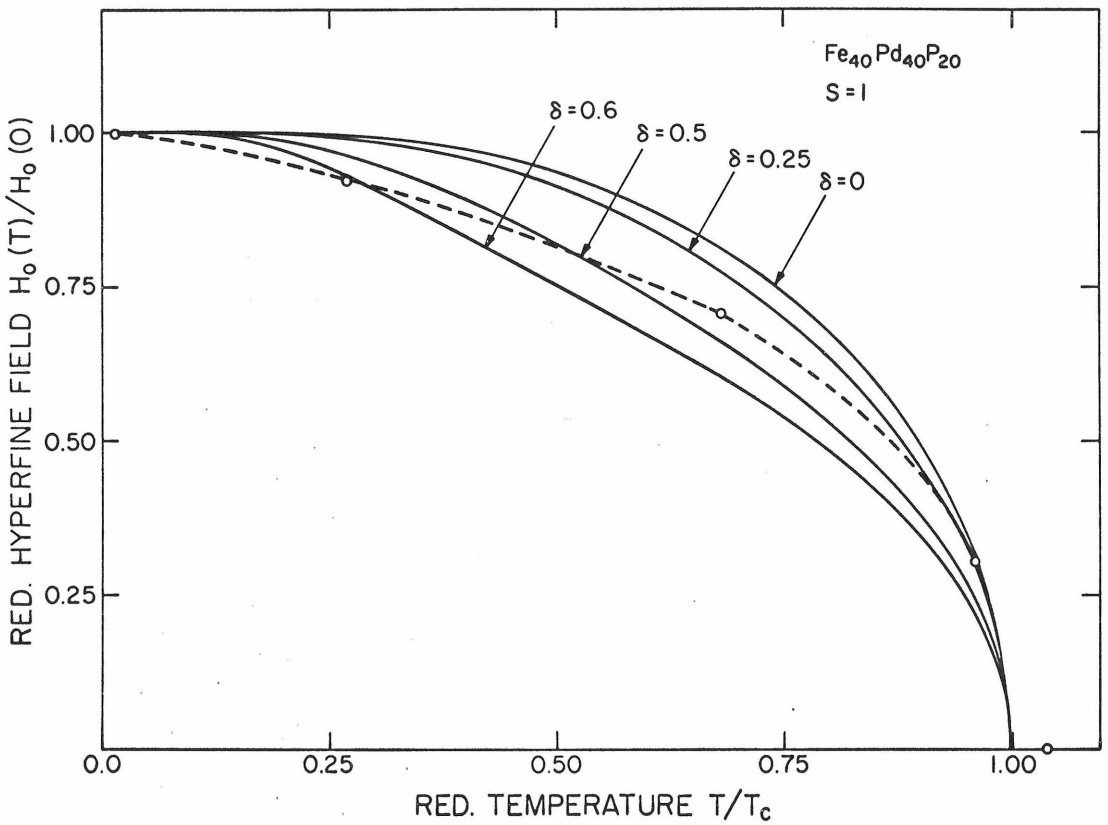

Fig. 38. Comparison of experimental results (dashed line) with Eq. (54) for the $Fe_{40}Pd_{40}P_{20}$ alloy.

the prediction that the fluctuations have reduced the magnetization relative to the ordered state ($\delta = 0$) seems to be verified.

A recent calculation by Montgomery et al[63] treats the disordered Heisenberg ferromagnet by a Green's function technique. Although this theory is not strictly applicable to an amorphous material but rather a disordered alloy, the general conclusions are expected to remain valid. The density of spin wave states, the ferromagnetic Curie temperature, and the magnetization were found as a function of disorder. The randomness of the alloy was taken into account by defining a parameter P such that

$$P = \frac{j^2}{3J_0^2}$$

where j^2 is the mean square deviation in exchange integrals from the average value J_0. The parameter P thus defined is a measure of the disorder analogous to δ in Handrich's molecular field theory. It was found that the density of spin wave states changes markedly with disorder. The main effect of increasing P is to introduce a low energy peak in the density of states, which results in the reduction in Curie temperature according to

$$T_c = T_o \left(1 - \frac{6}{Z} P \right) \qquad (55)$$

where T_0 is the transition temperature for the ordered case and Z is the number of nearest neighbors. The magnetization curves retain their characteristic shape and are merely flattened slightly from the perfect crystal case.

It is difficult to quantitatively assess the agreement of this approach with the amorphous case, since the numerical calculations involved must be made for a specific type of lattice. Nevertheless, the general conclusion that the magnetization is flattened relative to the perfect crystal case is seemingly valid. For example, in crystalline Fe at $T/T_c = 0.25$, the magnetization has dropped only 2%, while for the amorphous alloys shown in Figs. 37 and 38 it is reduced $\sim$5-6%. The Green's function method also predicts infinite slope at $T = T_c$, but throughout the calculation assumes that the magnetization is site-independent. From the experimental results shown in Fig. 35 it is clear that this assumption is not valid. Thus the question remains as to whether the small tail effect actually observed near T_c is an intrinsic property of an amorphous or disordered ferromagnet, or whether it is due to possible Fe concentration gradients or fluctuations in the degree of disorder across the sample, which from Eq. (51) would produce a spread in Curie temperatures. It is obvious that in the process of rapid quenching, the

interior portions of the material must cool more slowly than the surface which makes contact with a metallic conductor. The fact that the ΔT_c observed is as small as it is must mean that throughout the foil the rate of cooling is sufficiently fast to produce a very uniform scale of disorder.

2. Low Fe Concentration Alloys: $x \lesssim 25$

a. Evidence against superparamagnetism

A dramatic change in the magnetic properties is observed between the Fe-Pd-P alloys corresponding to $x = 24$ and $x = 28$. This is quite surprising, since the Fe concentration differs by only a few percent. The response of these lower Fe concentration alloys ($x < 25$) to an external field is greatly reduced, as discussed in section IV. Also the susceptibility results[9] yield a value of $\mu_{eff} \simeq 6\mu_B$ per Fe atom in this composition range. However, the saturation moment in a field of 8.4 kOe is significantly less than $2\mu_B$ per Fe atom ($1.07\mu_B$ for $Fe_{23}Pd_{57}P_{20}$), and decreases with decreasing Fe concentration. The hyperfine field results at 4.2°K, on the other hand, indicate that the moment per Fe atom is roughly constant over the entire composition range. Certainly a factor of 2 or more difference in the moment per Fe atom would produce a large change in hyperfine field.

From the magnetization results, Maitrepierre suggested that these alloys may be "superparamagnetic" [9]. The requirements for superparamagnetism are that no hysteresis effects such as remanence or coercive force are present. This is due to the fact that the thermal fluctuations of the single domain particles are so rapid that the associated relaxation time is small compared to the measurement time[25]. Without an external field, the average magnetization is therefore zero. By applying an external field, a net moment in the direction of the field is induced, just as for paramagnetic atoms. Because the magnetic atoms within a cluster are tightly coupled by exchange interactions, an increased susceptibility (relative to the uncoupled atoms) is obtained. In a superparamagnetic system, there always exists a distribution of cluster sizes and therefore the magnetization does not follow a simple Langevin function for a given magnetic moment μ. Nevertheless, the magnetization curves should superimpose when plotted versus H/T.

The concept of superparamagnetism is appealing as an explanation for the magnetic properties of these amorphous alloys, because the small saturation moment and large value of μ_{eff} are explained naturally. However, the results of section IV, coupled with a careful reexamination of the magnetization data, offer convincing evidence that this simple explanation is inadequate.

It was noted that a hyperfine field appears at $4.2^{o}K$ in the spectrum of the lowest Fe concentration alloy used ($Fe_{14}Pd_{66}P_{20}$). There is no evidence of a central peak due to particles with no average hyperfine fields over the Larmor period ($\sim 10^{-7}$sec). From the μ_{eff} value obtained in Ref. 9, we can estimate the average size of the superparamagnetic particles and the number of Fe atoms they contain. In the paramagnetic region,

$$\chi = \frac{N\mu^2}{3k(T-\theta)} \tag{56}$$

where N is the number of clusters per unit volume, and μ is the moment per cluster. Assuming there are n Fe atoms per unit volume and z Fe atoms per cluster, then $N = \frac{n}{z}$ and $\mu \cong z\,\mu_{Fe}$. In this situation

$$\chi = \frac{n}{z}\,\frac{(z\,\mu_{Fe})^2}{3k(T-\theta)} = z\,\frac{n\mu_{Fe}^{\,2}}{3k(T-\theta)} = z\,\chi_{indep} \tag{57}$$

Thus by grouping into clusters of z atoms each, the susceptibility is increased by a factor of z, or the effective moment by a factor $\sqrt{z}$. Since $\mu_{eff} \cong 6$ for the amorphous Fe-Pd-P alloys and $\mu_{Fe} \cong 3$, there are only about 4 Fe atoms per cluster on the average. If Pd contributed to the net moment, this value would be even smaller. In the composition range $13 \leq x \leq 25$, the clusters

would contain 16-32 atoms on the average. Since the RDF indicates an atomic radius of 1.4 - 1.5 Å[9], 20 atoms would occupy a volume V of only $\sim 3 \times 10^{-22}$ cm^3.

If the clusters are noninteracting, thermal fluctuations will occur at a rate

$$f_{relax} = f_0 \exp -\left(\frac{KV}{kT}\right) \cong 10^9 \exp -\left(\frac{KV}{kT}\right) \text{sec}^{-1} \qquad (58)$$

In order to observe a hyperfine field, $f_{relax} < f_{Larmor}$. For Fe^{57}, $f_{Larmor} \cong 10^7$ sec^{-1}. To be consistent with the result that a hyperfine field is observed at 4.2°K, we find from Eq. (58) that the condition on the anisotropy energy constant K is $K \gtrsim 10^{-7}$ erg /cm^3. This is greater than an order of magnitude larger than Fe[60]. It would be difficult to explain such a large value for the amorphous alloys, where there would seem to be no crystallographic axis to even define a preferred direction. One would expect the anisotropy energy to be much lower than in the crystalline case. In fact, amorphous Fe-P-C alloys exhibit magneto-elastic properties which indicate this is the case[64].

Another characteristic effect seen in superparamagnetic materials is noticeably absent in the amorphous Fe-Pd-P alloys with $x < 25$. Because of the distribution of cluster sizes, there are always a wide range of transition temperatures evident in the

Mössbauer spectrum. If the $Fe_{24}Pd_{56}P_{20}$ alloy were superparamagnetic, we would expect to see some evidence of hyperfine splitting at 77°K, since its transition temperature is just below this temperature ($T_c \sim 60°K$). Similarly, for $Fe_{14}Pd_{66}P_{20}$ at 4.2°K, some quadrupole component should be seen from paramagnetic Fe atoms which happen to be in an uncoupled state. Furthermore, the frequency and inductance bridge results indicate a rather well defined transition temperature, which seems to correspond to the value extrapolated from Mössbauer effect. If the alloys were superparamagnetic, the transition temperature obtained from the two different techniques would vary greatly because of the difference in measurement time. In the Mössbauer effect, the average hyperfine field is obtained over a Larmor period ($\sim 10^{-7}$ sec), while the inductance bridge is essentially a static measurement (oscillator frequency = 1 kHz). For example, small particles of nickel ferrite ($Ni\ Fe_2O_4$) of average size 168 Å show paramagnetic behavior in magnetization measurements at all temperatures, but exhibit a stable hyperfine field pattern in Mössbauer experiments up to 628°K, where a gradual narrowing of the pattern sets in[34]. The corresponding Curie point of the bulk material is 858°K.

Figure 39 shows the Mössbauer spectra of a series of amorphous

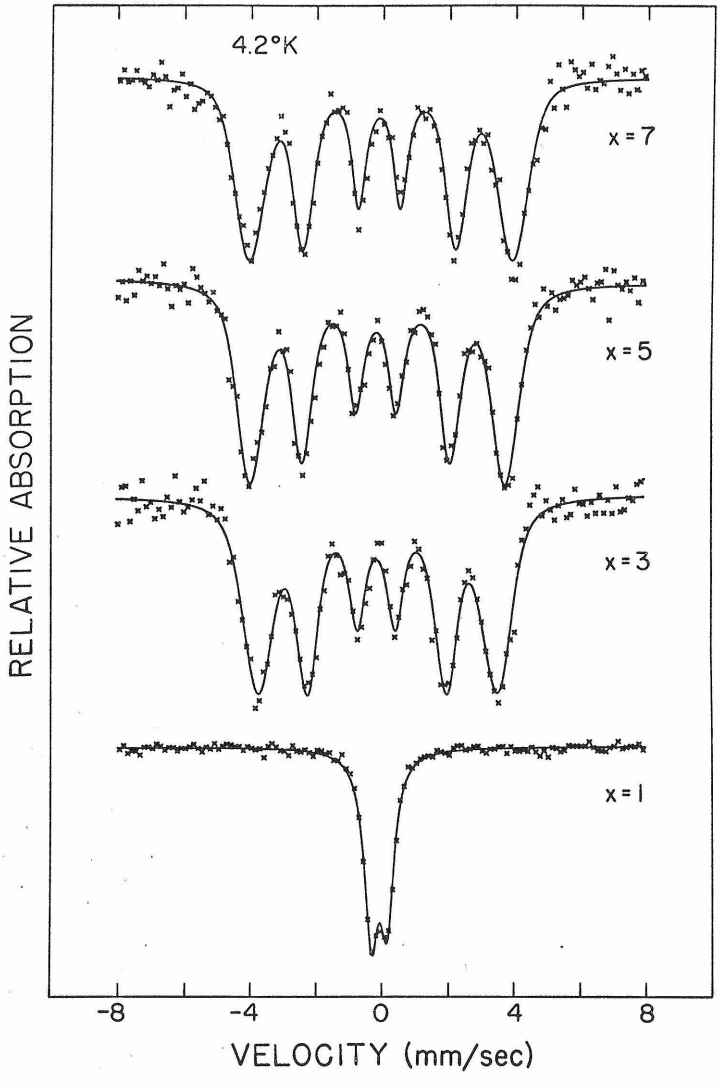

Fig. 39. Mössbauer spectra of amorphous $Fe_xPd_{80-x}Si_{20}$ alloys at 4.2°K.

$Fe_xPd_{80-x}Si_{20}$ alloys[55]. As noted earlier, these materials show very similar magnetic properties to the low Fe concentration Fe-Pd-P alloys. Hasegawa[7] has suggested that each Fe atom and its immediate Pd neighbors form a single magnetic domain, and the collection of these constitute a superparamagnetic system. It is evident from Fig. 39 and the arguments just presented that this description is inadequate.

A close examination of the magnetization data at low temperatures for the Fe-Pd-P alloys shows that the magnetization curves do not superimpose when plotted versus H/T. Instead, a saturating behavior at a considerably reduced moment is observed. For example, in the $Fe_{23}Pd_{57}P_{20}$ sample measured by Maitrepierre[9], at 6.5°K and 4 kOe the magnetization is approximately 10 emu/g. At 93.5°K, therefore, to reach an equivalent magnetization one should require a field of 93.5/6.5 x 4 kOe $\simeq$ 57.5 kOe. However, experimentally this magnetization is reached at only 8.3 kOe. Thus the superposition requirement at low temperatures does not hold. Naturally the magnetization data will superimpose versus H/T if only temperatures above the magnetic transition are used[7,46].

The second criterion of zero remanence was not demonstrated either. Hence we conclude that the concept of superparamagnetization fails to explain the magnetic properties of the low Fe concentration

amorphous Fe-Pd-P alloys.

In addition to providing an inadequate description of the magnetic properties of these alloys, the concept of superparamagnetism in these alloys meets two other objections. First of all, in the composition range $13 \leq x \leq 25$, the exchange interactions which presumably couple the Fe atoms together in a cluster (ferromagnetically) would appear to be unable to produce a nonzero transition temperature for the "bulk" material in these clusters. From extrapolation of the transition temperature versus Fe concentration curve of Fig. 29, one would conclude that ferromagnetism inside each cluster should not exist. Secondly, the use of the term "particles" or "clusters" seems somewhat misleading, since the clusters as such would actually be overlapping in this Fe concentration range.

b. Critical concentration effects

The transition temperature versus Fe concentration curve of Fig. 29, together with the sharp change in bulk magnetic properties for alloys with $x < 25$, strongly suggest a breakdown of the long range ferromagnetic order present in the higher Fe concentration alloys. Actually this result is not too unexpected, for the following reasons. In an amorphous material, the short range interactions are expected to dominate. Thus as the direct exchange interactions

between Fe atoms become less effective, the long range magnetic state is unable to maintain itself. Below a certain critical concentration x_c of the magnetic element, the long range magnetic order therefore becomes disconnected and a more local type of ordering may set in.

For crystalline lattices, there have been several calculations of this effect based on the Heisenberg model of ferromagnetism (Eq. 53). Elliot et al[65] have showed that this critical concentration is independent of the spin S or the strength of exchange coupling J, and depends only on the topology of the lattice. Moreover, x_c is the same for both the Heisenberg and Ising models. To show this, the high temperature susceptibility χ was expanded in a power series of x, the concentration. The critical concentration x_c is obtained fron an analysis of the radius of convergence of this power series. The following values were found for the simple cubic (sc), body centered cubic (bcc), and face centered cubic (fcc) lattices: x_c = 0.28, 0.22, and 0.18 respectively.

Sato et al[66] have also discussed critical concentration effects based on other approximations to the Heisenberg Hamiltonian. They find that the molecular field approximation, which predicts $T_c \alpha x$ (and therefore has no critical concentration), is completely inadequate in treating the case of dilute magnetic alloys with short range inter-

actions. This failure of the MFA is due to the averaging technique adopted. One can show, in fact, that the molecular field theory is exact only in the limit of Z (the number of nearest neighbors) becoming infinite. The neglect of short range order effects in the MFA is manifested in its inability to predict the curvature in $1/\chi$ versus T plots just above T_c, and also in the prediction that the magnetic contribution to the specific heat drops abruptly to zero above T_c. Several other effective field theories, which do attempt to treat short range order effects, are considerable improvements in accounting for these effects[40]. It appears that the longer the range of the interaction, the more applicable the MFA may be. This may be the reason for its semiquantitative success in Fe Pd, where there are extremely long range interactions. In amorphous materials, where short range interactions are dominant, the MFA is not expected to be a good approximation.

Two such predictions for critical concentrations are given by the average coordination number (ACN) method and the Cluster Variation (CV) theory[66]. The ACN treatment is essentially a generalization of Bethe's method for dealing with order-disorder phenomena in alloys. It is found that a critical concentration is reached when $xZ = 2$. The other method (CV) gives $x_c = 1/(Z-1)$. Table VI gives a summary and comparison of these estimates for the

TABLE VI

Critical Concentration for nearest neighbor interactions. (Z is the coordination number of the lattice).

Lattice	Expansion Method	Average Coordination Number	Cluster Variation
sc (Z = 6)	0.28	0.333	0.20
bcc (Z = 8)	0.22	0.25	0.143
fcc (Z = 12)	0.18	0.166	0.091

three different methods.

In the amorphous Fe-Pd-P alloys there is no lattice on which to count nearest neighbors. However, it is known from the RDF that the metal-metal coordination number is about 10-11. With this value for Z, the predicted critical concentration would be in the range of 10-20%. Since only 0.8 of the atoms are metallic, x_c should be between 8-16% Fe. Experimentally $x_c \tilde{=} 25\%$. It is reasonable that x_c for an amorphous structure should be greater than the ordered case, since all theories predict that the Curie point of the amorphous structure is reduced relative to the ordered case.

c. Nature of the magnetic state: comparison with the Au Fe system

Below the critical concentration, there is no long range ferromagnetism. This does not mean that no magnetic order of any kind exists, however. In the Au Fe system, for example, the magnetic susceptibility measurements of Kaufmann et al[67] showed that the onset of ferromagnetism was reached at a finite Fe concentration ($\sim$ 16 at.% Fe). Above this concentration, the Au Fe alloys are ferromagnetic with a moment per Fe atom of about $2\mu_B$. At 16% Fe, there is a sharp change in slope of the transition temperature versus Fe concentration curve. Below this value, the alloys respond only weakly to an external field. The measured saturation moment

of an $Au_{95}Fe_5$ alloy in an applied field of 95 kOe at 4.2°K was only $0.6\mu_B$/Fe atom[68]. The Mössbauer spectrum of an alloy of the same composition was unchanged in an applied field of 30 kOe[69]. These results suggest antiferromagnetic ordering between Fe atoms, but the observed broadening of the absorption lines was not consistent with the picture of a simple antiferromagnet. Gonser et al[70] showed that this same behavior was observed in an alloy of 15.7% Fe, but at 19.5% Fe the intensity of the second and fifth lines were affected. This indicates a ferromagnetic alignment parallel to the field.

The magnetic susceptibility results[67] for this composition range (< 16% Fe) are also quite puzzling, and inconsistent with a simple antiferromagnetic model. A large value of μ_{eff} is obtained from the slope of the $\chi^{-1}(T)$ curve by applying the Curie Weiss law. The Weiss constant θ also is positive for $x > 5\%$ Fe, which usually indicates ferromagnetic interactions. With increasing Fe concentration the effective moment approaches the value corresponding to $S = 5/2$ ($\mu_{eff} \cong 6\mu_B$). These results are shown in Fig. 40.

The puzzling magnetic susceptibility results led to several Mössbauer effect studies of these alloys in an attempt to clarify the nature of the magnetic ordering. It was established that magnetic ordering was present at low temperatures for Fe concentrations as

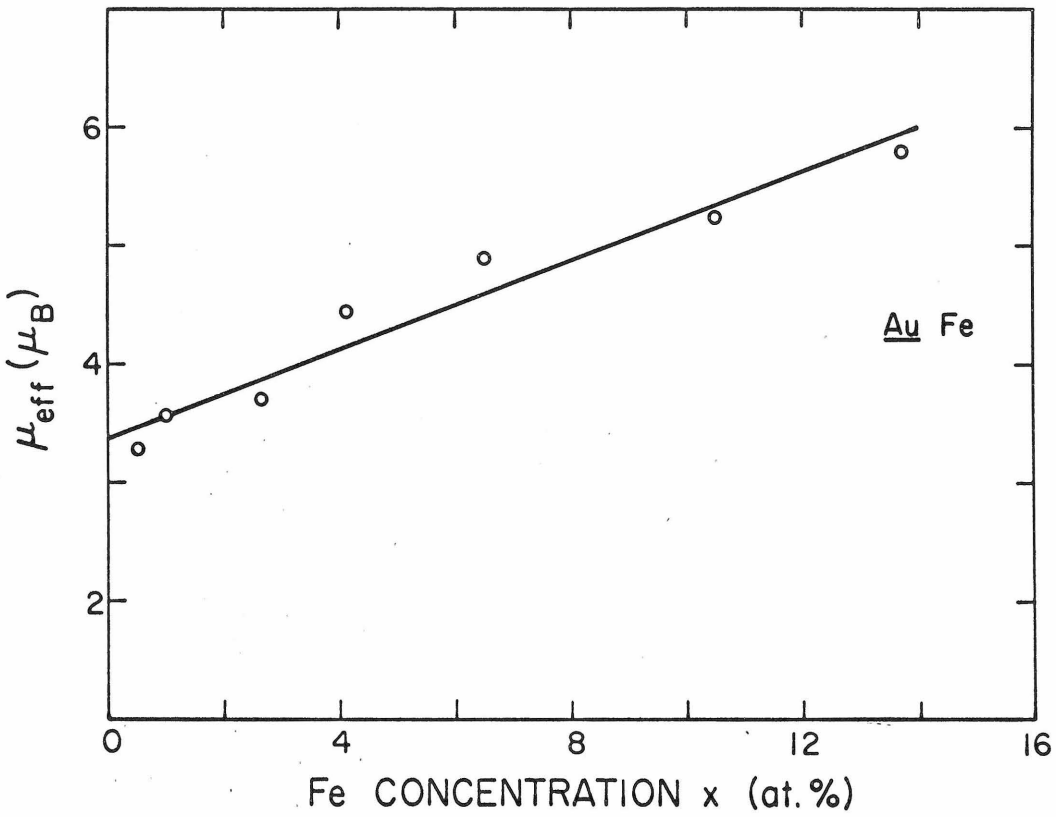

Fig. 40. Effective magnetic moment per Fe atom from susceptibility measurements in $Au_{1-x}Fe_x$ alloys. (Ref. 66)

low as 0.84% [71,72]. The essential results of these studies are that (1) the hyperfine field has a fairly well defined value (field width of approximately 10%) and has a magnitude about 66-75% of pure Fe. (2) The temperature dependence of the hyperfine is very similar to α-Fe, and vanishes at a well defined transition temperature (3) For low Fe concentrations, the transition temperature is approximately proportional to the square root of the concentration.

The transition temperature versus Fe concentration curve of Fig. 41 summarizes the results of several experiments. There is good agreement between Mössbauer effect results and those obtained from magnetic susceptibility measurements[73-75].

The parallel between the behavior of the Au Fe alloys and the Fe - Pd - P alloys is by now obvious. The reason for the apparent similarity between the two systems is not obvious at first sight. However, the model for the magnetism in these alloys proposed in section V. A showswhy the analogy may be expected. In that discussion it was argued that the effects of Pd 4d electron polarization are neglible because of electron transfer from phosphous. If the 4d shell of Pd is filled, it has the same electronic configuration as Ag, except for a slight difference in s electron density. In this model phosphorus plays no direct role in the magnetism except to fill the 4d shell of Pd and provide possible conduction electrons to the

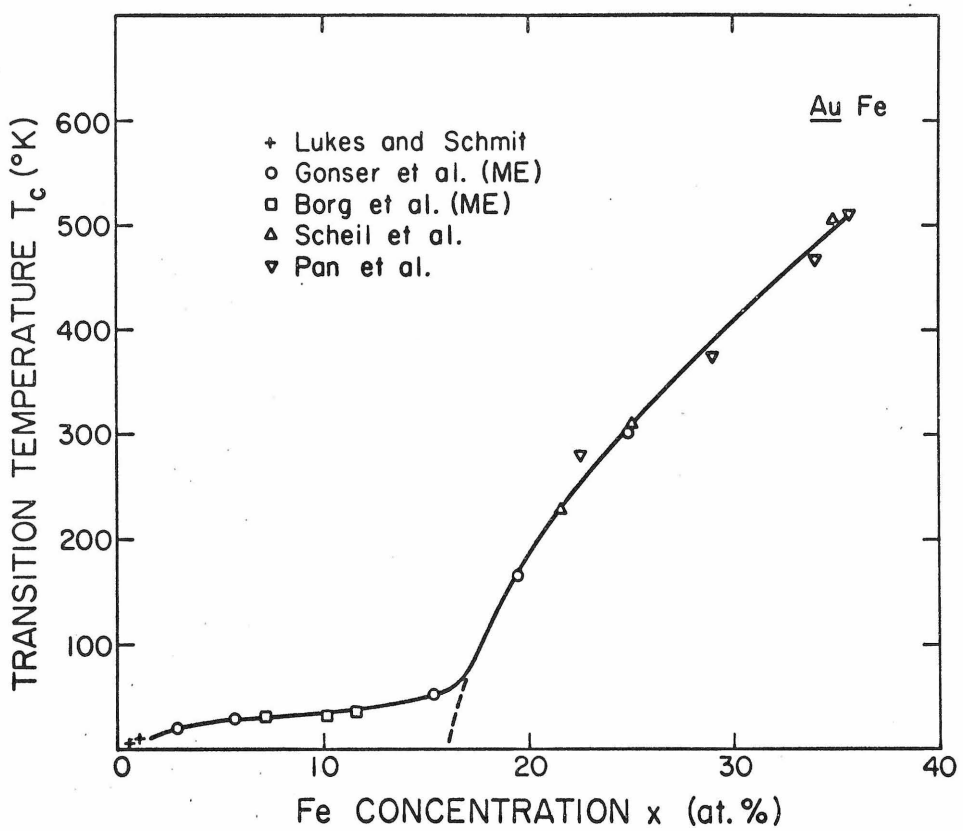

Fig. 41. Magnetic transition temperature vs. iron concentration in $Au_{1-x}Fe_x$ alloys.

system. It is well established that alloys of 3d transition metals (Fe, Co, ...Cr) in elements of the IB group (Cu, Ag, Au) all show anomalous magnetic properties[76]. The systems Cu Fe and Au Fe are good examples of this effect. It would be interesting to compare the magnetic properties of the amorphous Fe-Pd-P alloys with Ag Fe alloys. Unfortunately, Fe is only very slightly soluble in Ag (~.0004% Fe)[77]. Therefore a direct comparison is impossible.

One final note of interest regarding the Au Fe system is that some of the Mössbauer experiments were done in response to the suggestion of Crangle and Scott[78] that the alloys with less than 11% Fe were superparamagnetic , since no magnetic transition was evident from their susceptibility results.

d. Mechanism for magnetic ordering

From the present experimental data it is impossible to determine the exact nature of the magnetic ordering in this concentration range. Mössbauer experiments in external fields are needed to see if the ordering is possibly antiferromagnetic as in Au Fe. Nevertheless, it is possible to speculate on several mechanisms which may produce a magnetic state with such weak macroscopic magnetic properties. It is clear that the conduction electrons are the intermediary for the exchange between Fe atoms in these alloys. Klein and Brout[79] have discussed a statistical model for random alloys in which the

magnetic atoms interact via a Ruderman-Kittel interaction. In this model there are about 3-4 strongly correlated Fe atoms but no long range order. This explains the large value for μ_{eff}. Unfortunately this model does not have a well defined transition temperature T_c.

Much of the theoretical work in this area was done to describe the strange magnetic properties of the Cu Mn system[76]. Anderson[80] has recently proposed the concept of "spin glasses" to describe the strange properties of this system. In this model below a certain concentration the nature of the eigenfunctions of the Heisenberg Hamiltonian becomes localized instead of describing long range order. In this case there is no real ordering transition, but only a range of local transition temperatures. Anderson notes that this type of ordering should be more likely in a random lattice. Presumably an amorphous system would be ideal. However, since the experimental results seem to indicate a sharp transition, this model would seem to fail.

It was noted that there is a noticeable resistivity minimum effect (Kondo effect) for alloys in this range. Liang[81] has suggested that the magnetic ordering observed in certain related amorphous alloys containing Fe is due to the overlap to the spin polarization clouds about each magnetic impurity.

In these dilute alloys (0-4% Fe), the oscillatory nature of the RKKY interaction and its short range ($\sim r^{-3}$) make it unlikely that this mechanism can produce a well defined transition temperature[72]. The spin polarization arising from the Kondo effect, on the other hand, varies as only the inverse square at the distance from the impurity, and always has the same sign. This should be more favorable to the formation of the ferromagnetic state observed in these alloys. Such a mechanism should be considered as the cause of the magnetic ordering observed in the low Fe concentration Fe-Pd-P alloys. This could possibly explain the weak effect of magnetic fields, since a magnitude of several hundred kOe is required to break up this quasi-bound state. In this model also it is unclear whether there is a well defined phase transition.

3. Relation of Amorphous Fe-Pd-P Alloys to Related Systems

Since the short range order in the amorphous Fe-Pd-P alloys appears to be based on the transition metal phosphides (which are quite abundant) it is expected that there will be many related systems corresponding to different metal and non-metal atoms. For example, the structure of the transition metal borides, carbides, and silicates are closely related[12]. In all these structures the metal atoms form a connected lattice of polyhedra joined together at their verticies.

The smaller non-metal phosphorus atoms tend to be located in the holes inside this structure. In a sense, there is a strong relation to interstitial compounds (hydrides, for example) but the larger size of the phosphorus atoms makes the actual structure more complicated. An interesting example of the correlation between these crystalline and amorphous alloys is shown by the isostructural Pd series Pd_3B, Pd_3Si, and Pd_3P[12]. Pd_3P has a wide range of homogeniety on either side of the exact stoichiometric compound. For the metal rich alloys, the structure is based on Pd_3P with P vacancies, and can be extended to "Pd_4P" (or $Pd_{80}P_{20}$). By rapid quenching from the liquid state one can form in certain composition ranges amorphous alloys of the form $Pd_{80}Si_{20}$, $(Fe\text{-}Pd)_{80}P_{20}$, $(Ni\text{-}Pd)_{80}P_{20}$, $(Fe\text{-}Pd)_{80}Si_{20}$, $(Ni\text{-}Pd)_{80}Si_{20}$, and $(Ni\text{-}Pd)_{80}B_{20}$, to mention just a few. The RDF's of Ni-Pd-P and Ni-Pd-B are very similar, indicating the short range in these alloys probably only differ by a replacement of P by B.

The mechanism of Pd d-band filling just proposed for the Fe-Pd-P alloys has several interesting correlations with these related systems. Consider first the closely related $Ni_xPd_{80-x}P_{20}$ series studied by Maitrepierre[9]. It is found that none of these alloys are ferromagnetic, but in fact show only a weak paramagnetism which

is relatively temperature independent. These alloys can be formed over a very wide composition range ($13 \leq x \leq 73$), as if Ni and Pd have very similar properties. There are many indications of this in crystalline alloys. Ni and Pd both act as if 0.6 holes per atom existed in their d bands, when alloying or when forming a hydride phase. Both Ni $H_{0.6}$[25] and Pd $H_{0.6}$[52] have completely filled d bands. In Ni-Pd alloys, using Stoner's band theory of magnetism[60], one finds that the introduction of Ni into Pd leaves the number of holes in the d bands unchanged, although the susceptibility is enhanced. Fe and Co, on the other hand, increase the number of d holes[51]. The magnetic properties of the amorphous Ni-Pd-P alloys are completely understandable if P acts as an electron donor to Ni and well as Pd, and fills its d shell also. This is consistent with the experimental results, and would predict that the state of phosphorus should be relatively constant over the entire composition range. This could be checked by introducing dilute Fe^{57} impurities ($\lesssim 1\%$) and measuring the quadrupole splitting as a function of composition. $Ni_xPd_{80-x}Si_{20}$ alloys are also non-magnetic over the range $0 \leq x < 15$. This also fits into the picture since $Pd_{80}Si_{20}$ is almost diamagnetic, but Fe-Pd-Si and Co-Pd-Si form magnetically ordered states at low temperatures.

Ni-Pd-B alloys, on the other hand, are relatively strongly

paramagnetic[81]. The introduction of a few at. % Fe produces a true ferromagnetic state (T_c = 28°K for 2.5% Fe). The resistivity in these alloys shows a "kink" effect at T_c characteristic of a ferromagnetic material and only a very weak Kondo type effect. This indicates that the d spins are well coupled together as opposed to Fe-Pd-Si and Fe-Pd-P alloys where a sizeable resistivity minimum is observed. Using the inductance bridge described in section III, these alloys show an enormous effect at T_c. In the Ni-Pd-B alloys, note that B has only 3 valence electrons to contribute to d band filling. Apparently this results in only a partially filled d band in the Ni-Pd-B alloys, which therefore retain a high density of states and are quite polarizable.

In a certain sense, therefore, all these related alloys seem to follow some sort of rigid band model. This is indeed surprising due to the complexity of the alloys. We now suggest two possible reasons for this effect. First, the short range order in all these amorphous systems is undoubtedly similar. Since the metallic atoms are responsible for the magnetic properties, the only function of the non-metal atoms is to allow the formation of the amorphous structure and to possibly change the electronic state of the metal atoms which continue to form a coherent lattice. Electron transfer to the d shell of the transition metal atoms seems to be an important feature of

this state.

If one introduces magnetic impurities into such a system, for example Fe in $Pd_{80}P_{20}$, there is a simple substitution of Fe for Pd except that now the state of phosphorus is indirectly changed because Fe maintains its own electronic configuration. It may be that the reason for this is that it is energetically unfavorable to transfer electrons to the 3d spin up shell which is split off from the spin down shell by a considerable intratomic exchange (Coulomb) energy. The tendency for Fe to maintain its electronic state in a variety of alloys is well documented. In Ni Cu alloys, for example, Wertheim and Wernick[82] have shown that dilute Fe impurities retain their electronic configuration despite the fact that the Ni d shell is being filled with increasing Cu concentration and is full at $Ni_{40}Cu_{60}$. It has already been mentioned that in Fe Pd H alloys the H electrons fill the d shell of Pd, but the electronic state of Fe remains constant.

The amorphous alloys based on this structure show a range of compositions in which the amorphous structure can be easily formed. This effect, although due in part to size considerations, must also be an electronic effect to some extent. In amorphous $(T\text{-}Pd)_{80}Si_{20}$ alloys were T = Fe, Co, or Ni, it is found that the maximum amount of 3d transition metal corresponds approximately to 7% Fe, 11% Co, and 15% Ni. Since the size of Fe, Co, and Ni are almost identical,

this clearly is an effect relating to the formation of moments and the number of holes in the d shell of the impurity atom. In the Fe-Pd-P alloys, for example, it was shown that in the more Fe rich alloys, the phosphorus atoms are much less ionized as reflected in the quadrupole splitting. The increased size due to this larger charge cloud may then possibly be unfavorable to the formation of this type of amorphous structure.

Secondly, there has been a suggestion that atoms in an amorphous material tend to retain their individual characteristics much more than in a crystalline material, where band structure effects are quite important. In amorphous semiconductors, for example, the existence of an energy gap is a sign that each atom somehow fulfills its own valency requirements locally. This may be a possible reason for the fact that Ni in Ni-Pd-Si seems to behave in the same way as Ni in Ni-Pd-P.

VI. SUMMARY AND CONCLUSIONS

The subject of this investigation is the magnetism in an amorphous Fe-Pd-P alloy system. Alloys of the form $Fe_xPd_{80-x}P_{20}$ ($13 \leq x \leq 44$) can be quenched from the liquid state into an amorphous structure using the "piston and anvil" technique. Mössbauer effect measurements have been used to determine the distribution of hyperfine fields in these materials as a function of composition and temperature. Despite the presence of a combined electric quadrupole and magnetic interaction in the magnetically ordered alloys, the Mössbauer spectra can be analyzed in terms of a hyperfine field distribution alone. This simplification arises from the fact that structure fluctuations in the amorphous alloys lead to a completely random angle between the magnetic field direction and the principal axis of the electric field gradient at the nucleus. The only effect of the electric quadrupole interaction is therefore to broaden the observed six peak spectrum resulting from the magnetic hyperfine interaction. The hyperfine field distributions in the amorphous Fe-Pd-P alloys are found to extremely broad (width $\sim$ 100 kOe), with a maximum at approximately 290 kOe which is relatively independent of concentration. The increased width observed in the higher Fe concentration alloys results from the spin polarization of

the conduction electrons. From these results it has been concluded that the electronic configuration of Fe remains approximately constant throughout the entire composition range. The magnetic moment per Fe atom is about $2\,\mu_B$. The Pd atoms appear to play little role in the magnetism, since the Pd 4d shell has been filled due to electron transfer from phosphorus. The quadrupole splitting observed above the transition temperature is consistent with this model. Phosphorus thus plays a dual role in affecting the Pd d band and also in allowing the formation of the amorphous structure.

On a macroscopic scale, there is a drastic change in the magnetic properties of the Fe-Pd-P alloys at approximately 26% Fe. The transition temperature versus Fe concentration curve shows a sharp change in slope in this region. Above this critical concentration, the alloys are amorphous ferromagnets. The temperature dependence of the magnetization for these alloys agrees fairly well with recent theoretical predictions. Below the critical concentrations, the short range exchange interactions which produce the ferromagnetism are unable to establish a long range magnetic order. The local magnetic ordering which occurs must be due to some indirect exchange interactions through the conduction electrons. In many respects, the behavior of the Fe-Pd-P amorphous alloys parallels that observed in the Au Fe system. This might be expected,

since the electronic configuration of Pd is the same as the noble metal Ag if its d shell is filled.

One of the most significant features of the amorphous state is the fact that correlations between neighboring spins in such a material are greatly reduced. This makes possible the existence of Kondo spin flip scattering even in quite concentrated alloys. Only those spins which are in weak effective fields can contribute to the Kondo effect. The hyperfine field distributions obtained experimentally confirm the existence of such weakly coupled spins.

This model of Fe atoms interacting on a random lattice can explain the observed magnetic properties without introducing any concepts such as superparamagnetism or concentration dependent magnetic moments for the Fe atoms. It also shows the connection between the magnetism in such apparently dissimilar amorphous alloys as ferromagnetic $Fe_{80}P_{13}C_7$ and $Fe_xPd_{80-x}Si_{20}$ $(0 < x \leq 7)$. The large critical concentration observed in the Fe-Pd-P alloys provides further support for the statement that spin-spin correlations are greatly reduced in the amorphous state. This seems to be more than just a question of a short mean free path for the conduction electrons, since the alloys can be magnetically ordered in the dilute region.

To investigate the magnetic ordering in the less concentrated alloys ($x < 25$), Mössbauer experiments in large external fields should be quite useful. Specific heat measurements at low temperatures should also show a large contribution from the quasi-free spins in weak effective fields. The detailed analysis may be quite complicated, however, since there is no base alloy ($Pd_{80}P_{20}$) to use in the subtraction of the nonmagnetic contributions.

Finally it should be noted that the Mössbauer effect is at present the only technique by which one can determine the complete distribution of hyperfine fields in these materials. The enormous widths of the distributions would make an NMR absorption, for example, so broadened that no useful information could be obtained. Thus it represents a unique tool in the study of magnetism in amorphous materials, and should become even more important in future developments in this field.

REFERENCES

1. A.I. Gubanov, Fiz. Tverd. Tela 2, 502 (1960) (English Transl.: Soviet Phys. Solid State 2, 468 (1961)).
2. S. Mader and S. Nowick, Appl. Phys. Letters 7, 57 (1965).
3. C. C. Tsuei and Pol Duwez, J. Appl. Phys. 37, 435 (1966).
4. Pol Duwez and S. C. H. Lin, J. Appl. Phys. 38, 4096 (1967).
5. K. Tanura and H. Endo, Phys. Letters 29A, 52 (1969).
6. C. C. Tsuei, G. Longworth, and S. C. H. Lin, Phys. Rev. 170, 603 (1968).
7. R. Hasegawa, J. Appl. Phys. 41, 4096 (1970).
8. A. K. Sinha, J. Appl. Phys. 42, 338 (1971).
9. P. L. Maitrepierre, Ph.D Thesis, California Institute of Technology, 1969 (unpublished).
10. P. L. Maitrepierre, J. Appl. Phys. 40, 4826 (1969).
11. P. Pietrokowsky, Rev. Sci. Instr. 34, 445 (1962).
12. S. Rundqvist, Arkiv Kemi 20, 67 (1963).
13. W. L. Trousdale, C. J. Song, and G. Longworth, in Mössbauer Effect Methodology (Plenum, New York, 1966), Vol. 2, pp.77-83.
14. R. M. Bozorth, Ferromagnetism (Van Nostrand, New York, 1951).
15. E. Kankeleit, in Mössbauer Effect Methodology (Plenum,

New York, 1965), Vol. 1, pp. 47-66.

16. R. S. Preston, S. S. Hanna, and J. Heberle, Phys. Rev. 128, 2207 (1962).

17. L. R. Newkirk, Ph.D. Thesis, California Institute of Technology 1970 (unpublished).

18. O. C. Kistner and A. W. Sunyar, Phys. Rev. 139 B, 295 (1965).

19. J. D. Jackson, Classical Electrodynamics (John Wiley and Sons, New York, 1962), p. 101.

20. H. Wegener, Der Mössbauer-Effektund Seine Anwendungen in Physik und Chemie (Bibliographisches Institut AG, Manheim, 1965).

21. R. L. Collins and J. C. Travis, in Mössbauer Effect Methodology (Plenum, New York, 1967), Vol. 3, pp. 123-161.

22. R. S. Preston, D. J. Lam, M. V. Nevitt, D. O. Van Ostenburg, and C. W. Kimball, Phys. Rev. 149, 440 (1966).

23. G. K. Wertheim, Mössbauer Effect: Principles and Application (Academic Press, New York, 1964).

24. W. Marshall, Phys. Rev. 110, 1280 (1958).

25. V. G. Bhide, in Physics of the Solid State (Academic Press, London, 1968), Chap. 13.

26. V. I. Gol'danskii and E. F. Makarov, in Chemical Applications of Mössbauer Spectroscopy (Academic Press, New York, 1968), Chap. 1.

27. W. Marshall, Rev. Mod. Phys. 36, 399 (1964).

28. G. B. Benedek and J. Armstrong, J. Appl. Phys. 32, 1065 (1961).

29. P. P. Craig, R. C. Perisho, R. Segnan, and W. A. Steyert, Phys. Rev. 138 A, 1460 (1965).

30. G. K. Wertheimand J. P. Remeika, Phys. Letters 10, 14 (1964).

31. C. P. Bean and J. D. Livingston, J. Appl. Phys. 30, 120 S (1959).

32. L. Neel, Compt. Rend. 228, 664 (1949).

33. T. Nakamura, T. Shinjo, Y. Endoh, N. Yamamato, M. Shiga, and Y. Nakamura, Phys. Letters 12, 178 (1964).

34. W. J. Schuele, S. Shtrikman, and D. Treves, J. Appl. Phys. 36, 1010 (1965).

35. W. Kundig, H. Bommel, G. Constabaris, and R. H. Lindquist, Phys. Rev. 142, 327 (1966).

36. D. W. Collins, J. T. Dehn, and L. N. Mulay, in Mössbauer Effect Methodology (Plenum, New York, 1967), Vol. 3, pp. 103-122.

37. G. K. Wertheim, V. Jaccarino, J. H. Wernick, and D.N.E. Buchanan, Phys. Rev. Letters 12, 24 (1964).

38. P. P. Craig, B. Mozer, and R. Segnan, Phys. Rev. Letters 14, 895 (1965).

39. B. D. Dunlap and J. G. Dash, Phys. Rev. 155, 460 (1966).

40. J. S. Smart, Effective Field Theories of Magnetism (W. B. Saunders Co., Philadelphia, 1966).

41. L. R. Walker, G. K. Wertheim, and V. Jaccarino, Phys. Rev. Letters 6, 98 (1961).

42. A. H. Muir, Jr., K. J. Ando, and H. M. Coogan, Mössbauer-Effect Data Index 1958-1965 (Interscience, New York, 1966), p. 26.

43. J. H. Wood, Phys. Rev. 126, 517 (1962).

44. T. A. Kitchens and W. L. Trousdale, Phys. Rev. 174, 606 (1968).

45. G. Low, in Proceedings of the International Conference on Magnetism, Nottingham, England, 1964 (The Institute of Physics and the Physical Society, University of Redding, Berkshire, England, 1965).

46. M. E. Weiner, Ph.D. Thesis, California Institute of Technology, 1968 (unpublished).

47. M. A. Ruderman and C. Kittel, Phys. Rev. 96, 99 (1954).

48. T. Kasuya, Progr. Theoret. Phys. (Kyoto), 16, 45 (1956).

49. K. Yosida, Phys. Rev. 106, 893 (1957).

50. B. Giovanni, M. Peter, and J. R. Schrieffer, Phys. Rev. Letters 12, 736 (1964).

51. E. Vogt, in Magnetism and Metallurgy, Vol. I, (Academic Press, New York, 1969), Chap. VI.

52. J. P. Burger, Ann. Phys. (Paris) 9, 345 (1964).

53. W. C. Phillips and C. W. Kimball, Phys. Rev. 165, 401 (1968).

54. R. Hasegawa and C. C. Tsuei, Phys. Rev. 2B, 1631 (1970).

55. T. E. Sharon (to be published).

56. J. Owen, M. Browne, W. D. Knight, and C. Kittel, Phys. Rev. 102, 1501 (1956).

57. M. B. Stearns and S. S. Wilson, Phys. Rev. Letters 13, 313 (1964).

58. P. G. de Gennes, J. Phys. Radium 23, 630 (1962).

59. A. J. Heeger, A. P. Klein, and P. Tu, Phys. Rev. Letters 17, 803 (1966).

60. D. H. Martin, Magnetism in Solids (M.I.T. Press, Cambridge, 1967).

61. W. L. Trousdale, G. Longworth, and T. A. Kitchens, J. Appl. Phys. 38, 922 (1967).

62. K. Handrich, Phys. Stat. Solidi 32, K55 (1969).

63. C. G. Montgomery, J. I. Kruger, and R. M. Stubbs, Phys. Rev. Letters 25, 669 (1970).

64. Pol Duwez, private communication.

65. R. J. Elliot, B. R. Heap, D. J. Morgan, and G. S. Rushbrooke, Phys. Rev. Letters 5, 366 (1960).

66. H. Sato, A. Arrott, and R. Kikuchi, J. Phys. Chem. Solids 10, 19 (1959).

67. A. R. Kaufmann, S. T. Pan, and J. R. Clark, Rev. Mod. Phys. 17, 87 (1945).

68. W. E. Henry, Phys. Rev. Letters 11, 468 (1963).

69. P. P. Craig and W. A. Steyert, Phys. Rev. Letters 13, 802 (1969).

70. U. Gonser, R. W. Grant, C. J. Meecham A. H. Muir, Jr., and H. Wiedersich, J. Appl. Phys. 36, 2124 (1965).

71. R. J. Borg, R. Booth, and C. E. Violet, Phys. Rev. Letters 11, 464 (1963).

72. C. E. Violet and R. J. Borg, Phys. Rev. 149, 540 (1966).

73. O. S. Lutes and J. L. Schmidt, Phys. Rev. 134 A, 676 (1964).

74. E. Scheil, H. Specht, and E. Wachtel, Z. Metallk, 49, 590 (1958).

75. S. T. Pan, A. R. Kaufman, and F. Bitter, J. Chem, Phys. 10, 318 (1942).

76. A. N. Gerritsen, Physica 25, 489 (1959).

77. M. Hansen, Constitution of Binary Alloys (McGraw-Hill, New York, 1966), p. 20.

78. J. Crangle and W. R. Scott, Phys. Rev. Letters 12, 126 (1964).

79. M. W. Klein and R. Brout, Phys. Rev. 132, 2412 (1963).

80. P. W. Anderson, Mat. Res. Bull. 5, 549 (1970).

81. V. K. C. Liang, Ph.D. Thesis, California Institute of Technology, 1971 (unpublished).

82. G. K. Wertheim and J. H. Wernick, Phys. Rev. 123, 755 (1961).